Technische Universität München
Institut für Energietechnik

Lehrstuhl für Thermodynamik

Large Eddy Simulation of Autoignition in Turbulent Flows

Rohit Madhukar Kulkarni

Vollständiger Abdruck der von der Fakultät für Maschinenwesen der Technischen Universität München zur Erlangung des akademischen Grades eines

DOKTOR – INGENIEURS

genehmigten Dissertation.

Vorsitzender:
Univ.-Prof. Dr.-Ing. Hartmut Spliethoff
Prüfer der Dissertation:
1. Univ.-Prof. Wolfgang Polifke Ph.D. (CCNY)
2. Univ.-Prof. Dr. rer. nat. Michael Pfitzner
Universität der Bundeswehr München

Die Dissertation wurde am 30.10.2012 bei der Technischen Universität München eingereicht und durch die Fakultät für Maschinenwesen am 04.03.2013 angenommen.

Acknowledgments

The present work was accomplished at the Lehrstuhl für Thermodynamik, TU München from September 2008 to March 2012 under the supervision of Prof. Wolfgang Polifke. First and foremost, I offer my sincerest gratitude to Prof. Polifke, who with his constant motivation and patience played a crucial role in guiding the research work in a proper direction. His ability to elucidate complex matters whilst allowing me the freedom to work was the principal factor in the success of the work.

The work was financially supported by Alstom Power, Switzerland. I would like to thank Dr. Birute Bunkute, Dr. Uwe Rüdel, Michael Düsing and Fernando Biagioli from Alstom, whos support made the work and my stay in Switzerland interesting and enjoyable.

I would like to thank Prof. Dr. rer. nat. Michael Pfitzner for being the co-examiner, and Prof. Dr.-Ing. Hartmut Spliethoff for being the chairman of the thesis committee.

I would like to thank all my colleagues to make my stay in Munich enjoyable. My special thank goes to Mathieu Zellhuber, who has played a prominent role in the project right from the initial stages of the work to the submission of the dissertation. His friendly nature and ability to see things unbiasedly helped me to improve the quality of the work. Frederic Collonval was the most closest companion during the entire work. No day was fulfilling without an interesting discussion with him. I wish that these discussions continue in the future. I also want to thank Luis Tay Wo Chong Hilares for taking the time to solve many of my technical and nontechnical problems. I would also like to thank Marco Konle, Robert Leandro, and Florian Ettner for their support.

I would like to thank my wife Sonja for her understanding and patience during the entire work. I thank all family members for their support and faith in me. I cannot express my gratitude to my father whos thirst for knowledge always inspires me.

Munich, October 2012 Rohit Kulkarni

Kurzfassung

In dieser Dissertation wird die Selbstzündung in turbulenten Strömungen numerisch untersucht. Dafür wurde ein neuartiges Verbrennungsmodell für die Grobstruktursimulation (LES) konzipiert. Es basiert auf tabellierter Chemie und beschreibt die Turbulenz-Chemie-Interaktion mittels der Verwendung stochastischer Felder. Die Chemie wird anhand einer Fortschrittsvariable sowie eines Mischungsbruchs tabelliert. Die gewählte Fortschrittsvariable beinhaltet sowohl Zwischenspezies als auch Verbrennungsprodukte. Die wichtigsten Vorteile des Modells sind dessen geringe Komplexität, sowie die Möglichkeit, es für die Untersuchung komplexer, industrieller Mehrstromanwendungen zu verwenden. Der Rechenaufwand in LES ist dabei vergleichsweise niedrig und unabhängig von der Art des Brennstoffs sowie vom Reaktionsmechanismus, steigt jedoch linear mit der Anzahl der Ströme an. Das turbulente Selbstzündungsmodell wurde in einem kommerziellen CFD-Code (Fluent 12) implementiert und für drei Experimente mit unterschiedlichen Kraftstoffen (Wasserstoff, n-Heptan und Methan) und einem Direct Numerical Simulation Testfall validiert. Das Modell erlaubt die korrekte Vorhersage der Zündlänge sowie der unterschiedlichen Selbstzündungsregimes. Das Modell kann nach Anpassung der Tabellierungsmethoden auch für die Berechnung von Vormisch- und Diffusionsflammen verwendet werden. Mit dieser Simulationsmethode wurde der Einfluss von Turbulenz auf Mischung und Selbstzündung in einer „Jet-in-Coflow“ Anordnung mittels einer systematischen Variation der Turbulenzparameter der Co-Flow-Strömung untersucht. Dabei konnte eine nicht-monotone Abhängigkeit der Zündlänge von der turbulenten Zeitskala beobachtet werden. Für industrielle Anwendungen, bei denen die turbulenten Zeitskalen kleiner als die Zündverzugszeiten sind, führt eine weitere Erhöhung der Turbulenzintensität demnach zu einer überproportionalen Verzögerung des Selbstzündvorgangs.

Abstract

Autoignition in turbulent flows is numerically investigated in the dissertation. A novel combustion model is conceptualized for Large Eddy Simulation (LES) context. The model is based on a progress variable approach for chemistry tabulation and stochastic fields model for turbulence chemistry interaction. The chemistry is tabulated using a "composite progress variable", which constitutes intermediate species and combustion products. The major advantage of the model is the capability of its extension to complex industrial multi-stream mixing applications at low computational cost and modeling complexity. The computational cost in LES is independent of the type of fuel or size of the chemical mechanism, but scales linearly with the number of streams. The turbulent autoignition model is implemented in a commercial CFD code (Fluent v12) and validated against three laboratory scale experiments with various fuels (hydrogen, n-heptane and methane) and a Direct Numerical Simulation (DNS) test case. The model captures autoignition lengths and regimes satisfactorily. The model also shows potential to be applicable for premixed and diffusion flames with suitable tabulation methods. The impact of turbulence on mixing and autoignition in a jet-in-coflow arrangement is studied by varying coflow turbulent characteristics (time scale). The parametric study predicts a non-trivial dependence of autoignition length on turbulent time scale. For industrial applications, where the turbulent time scales are smaller than the ignition delays, increased turbulence intensity is expected to result in disproportionately delayed autoignition.

Contents

Nomenclature

Latin Characters

dW	Wiener process $[s^{-1/2}]$
f_α	One point probability density function [-]
h	Enthalpy [J]
l_t	Integral length scale [m]
u	Velocity [m/s]
Da	Damköhler number [-]
Da_I	Ignition Damköhler number [-]
Da_q	Quenching Damköhler number [-]
D	Molecular Diffusivity $[m^2/s]$
D_{sgs}	Turbulent Diffusivity $[m^2/s]$
P	Pressure $[N/m^2]$
Q_α	Mass fraction conditioned on mixture fraction [-]
Re	Reynolds number [-]
T	Temperature [K]
Y_α	Mass fraction of species α [-]
Y_c	Mass fraction of composite progress variable [-]
Z	Mixture fraction [-]

Greek Characters

χ	Scalar dissipation rate $[s^{-1}]$
Δ	LES filter length [m]

μ	Dynamic viscosity [kg/ms]
μ_{sgs}	Turbulent dynamic eddy / sub-grid viscosity [kg/ms]
η	Kolmogorov length scale [m]
ν	Kinematic viscosity [m^2/s]
$\nu_{t,\text{eff}}$	Effective (laminar + eddy) Kinematic viscosity [m^2/s]
ρ	Density [kg/m^3]
τ_{ign}	Ignition delay [s]
τ_{SGS}	Sub-grid time scale [s]
τ_t	Turbulent time scale [s]
$\dot{\omega}_\alpha$	Chemical source term for species α [mol/s]

Abreviation

CMC	Conditional Moment Closure
$CTHC$	Confined Turbulent Hot Co-flow
CVA	Cold Vitiated Air
DNS	Direct Numerical Simulation
FDF	Filtered Density Function
$HCCI$	Homogeneous Charge Compression Ignition
HVA	Hot Vitiated Air
$ILDM$	Intrinsic Low Dimensional Manifold
LES	Large Eddy Simulation
$MILD$	Mild of Intensely Low oxygen Dilution
PV	Progress Variable
$RANS$	Reynolds Averaged Navier Stokes
PDF	Probability Density Function
SDR	Scalar Dissipation Rate
SF	Stochastic Fields
SGS	Sub Grid Scale
$SLFM$	Steady Laminar Flamelet Model
$SPDE$	Stochastic Partial Differential Equation
TI	Turbulence Intensity
$TPDF$	Transported Probability Density Function

1 Introduction

The modern industrialized world is largely dependent on combustion of fossil fuels to satisfy its ever growing demand for energy. Automobiles with combustion engines are the most common means of transportation, whereas power plants using fossil fuels are the principal suppliers of electric power. According to the IEA (International Energy Association), the global energy demand will increase by about 40 % in the next 20 years. The share of the energy provided by fossil fuels will be more than 80 %. At least in the next few decades, the use of combustion for electric power generation and transportation will play a dominant role.

Global warming, which is one of the undesired consequences of combustion, has alarmed the world in last few decades. Combustion of fossil fuels produces carbon-dioxide, NOx (NO_2 and NO), carbon-monoxide, and other products that are malicious to the human health and the environment. NOx contributes to the problem of smog and acid rain. CO_2 is a green house gas responsible for the global warming. From the total greenhouse gases from various sources, the share CO_2 from fossil fuel combustion is about 60%. CO_2 emissions are expected to increase by about 28 %. CO is a poisonous gas that can cause cardiovascular diseases, damage the nervous system, and in extreme cases, cause death. The CO_2 emissions can be reduced by either capturing the CO_2 before releasing the exhaust gases into the atmosphere (carbon capture and storage) or increasing the efficiency of combustion systems. Other pollutants can be reduced by improving the combustion process. Apart from the hazardous effects of the combustion products, the fossil fuel supplies are limited.

In a quest to increase efficiency and reduce pollutant emissions, new combustion technologies were explored in last few years. HCCI (Homogeneous Charge Compression Ignition) gasoline engines, PCCI (Premixed Charged Compression Ignition) diesel engines, and reheat/after-heat combustors (gas

turbine applications) are some of the examples. All these applications operate in an efficient combustion mode called 'MILD (Moderate or Intensely Low Oxygen Dilution)' or 'flameless combustion'. In HCCI engines, combustion takes place homogeneously in the combustion chamber. The distributed heat release in this mode leads to low peak temperatures attained in the combustion process, resulting in low NOx emissions. Radiative losses decrease as a result of lower peak temperatures. The exhaust heat recovery and reduced radiation losses increase the efficiency. In reheat combustors or afterburners, like ALSTOM's GT24/GT26 gas turbines, fuel is injected into hot gases coming from the first stage of a gas turbine power plant. Fuel mixes with hot gas and reactions initiate due to high temperature and pressure conditions. The reduced amount of oxygen (consumed in the first stage) and lean fuel air mixtures at the location of the flame result into more gradual heat release and lower peak temperatures. In most of these applications based on MILD combustion, the combustion process is stabilized by autoignition. Understanding autoignition in those applications is indispensable in the design process to ensure their stable operation.

For the development of these industrial applications, numerical simulation of flow and combustion is proving to be a valuable tool. Numerical simulations reduce the overall product development cycle time. The flow in most of the industrial combustion applications is turbulent. Models are necessary for turbulent reacting flow simulations, as the cost of computing the entire range of flow and chemical time scales is impractical. There are two main approaches for turbulence modeling: RANS (Reynolds Averaged Navier Stokes) and LES (Large Eddy Simulation). RANS averages the flow equations temporally, whereas LES averages them spatially up to a certain scale called the filter length. RANS simulations, due to their steadiness (no time dimension), are computationally cheap but the entire range of scales are modeled. LES solves the large scales and models the smaller ones assuming their universal behavior. The computational cost of LES is more than RANS due to its inherent transientness, but with the reduced degree of modeling, LES captures flow and mixing reliably. Moreover, LES captures transient phenomena like autoignition and extinction. In addition, the computational capability has been increasing day by day, which promotes the use of LES for industrial applications

in the near future. This work concentrates on LES turbulence modeling. Combustion takes place at scales smaller than those resolved in LES. Thus, modeling combustion is necessary in LES.

Most of the flames in the MILD combustion regime are stabilized by autoignition, due to the high temperature of the recirculation gases. Modeling autoignition is challenging as it does not allow for scale separation assumption (assuming chemistry faster than mixing). Additionally, many of the industrial reacting flows feature multi-stream mixing. For example, in HCCI engines, fuel is injected into a mixture of inhomogeneously mixed air and hot recirculation gases. Another example is the reheat combustors or afterburners, where fuel along with cold shielding air is injected into hot gases and combustor wall cooling air. Most of the computationally efficient combustion models are developed for elementary binary (two stream mixing) configurations. Their extension to multi-stream mixing introduces unavoidable modeling complexities and errors.

The necessity of a combustion model for multi-stream mixing and autoignition and understanding the impact of turbulence on mixing and autoignition is the motivation behind this work.

1.1 Contribution of the thesis

The present work introduces a novel LES turbulent combustion model for autoignition that is suitable for industrial applications with multi-stream mixing. The model is based on tabulated chemistry and the ”stochastic fields” turbulence chemistry interaction model. Although both the elements of the combustion model are not new, their combination is the novelty of the model. The chemistry is tabulated using a ”composite progress variable”, which constitutes an intermediate species and a combustion product. Homogeneous plug-flow reactors are used for the tabulation purpose. The major advantage of the model is its capability of being extended to multi-stream mixing problems at low computational cost and modeling complexity. The computational cost of the model increases linearly with the number of streams. The model is

validated in this work against autoignition experiments with various fuels (hydrogen, vaporized n-heptane and methane) and hydrogen autoignition DNS (Direct Numerical Simulation).

This thesis also throws light on the impact of turbulence on mixing and autoignition, which to the point of time is disputed in the combustion community. The present work attempts to investigate into the complex problem using the validated LES combustion model. The LES simulations predict an enhancing effect of turbulence on mixing, but a non-trivial effect on autoignition length. Turbulence-chemistry interaction mechanisms are analyzed in order to explain these observations.

1.2 Thesis Outline

The following chapter describes the fundamentals of autoignition. In the first sections, turbulent flows and characteristic variables to quantify them are introduced. A short overview on the autoignition phenomenon for gaseous fuels is given in the subsequent section. The interaction between the two (turbulent flows and autoignition) is an active topic of research. A brief overview of the current state of knowledge on the impact of turbulence on mixing and autoignition is presented. Chapter 3 reviews LES combustion models from the literature. The models are qualitatively compared with respect to their degree of assumptions and computational cost. This comparison highlights the necessary design objectives for a computationally efficient turbulent autoignition model for for industrial applications in LES.

The model proposed in the present work is described in chapter 4. The extension of the model to multi-stream mixing is demonstrated for a ternary (three stream) mixing case. Chapter 5 compiles the validation work on the LES combustion model. Four laboratory scale autoignition cases (three experiments and a DNS) are selected for the validation. All the test cases feature a fuel jet in a turbulent vitiated hot coflows. One of the test cases (Delft flame) is a ternary mixing case with MILD combustion mode, which is a challenge to combustion models.

Chapter 6 describes the parameter study on the impact of turbulence on mixing and autoignition. The DNS test case, validated in chapter 5, is used for the parameter study. LES are performed by independently varying the turbulent intensity and integral length scale in the coflow. This chapter explains various mechanisms that lead to a non-monotonous dependence of autoignition on turbulence.

2 Fundamentals of autoignition in turbulent flows

This chapter gives a short introduction to the fundamentals of autoignition, turbulent flows and the interaction between these phenomena. The chapter introduces the key parameters and quantities used later in this work. The first section describes different types of flames and regimes of combustion. Autoignition, which covers a broad range of the combustion regime diagram, is categorized into different regimes that describe the behavior of the autoignition kernels. The second section describes the basics of autoignition in homogeneous reactors and attempts to explain the interaction between flow (convection and diffusion) and autoignition chemistry. The basic description and parameters to quantify turbulent flows are included in section 3. The final section shows the current state of knowledge on the impact of turbulence on autoignition.

2.1 Types of flames

A flame, irrespective of the type of flow (turbulent or laminar), is categorized into premixed, non-premixed, and partially premixed. This categorization depends on the state of mixedness between the fuel and oxidizer streams before entering the combustion zone [82]. In premixed combustion, fuel and oxidizer are perfectly mixed at the molecular level. In non-premixed combustion, they enter the combustion zone through separate inlets. Partially premixed flames can occur in many ways. The most common configuration is a non-premixed one with fuel and oxidizer entering separately, but the flame is located further downstream of the injector. Partially premixed flames seem to be a subset of non-premixed flame configuration, but the physical interaction between flow

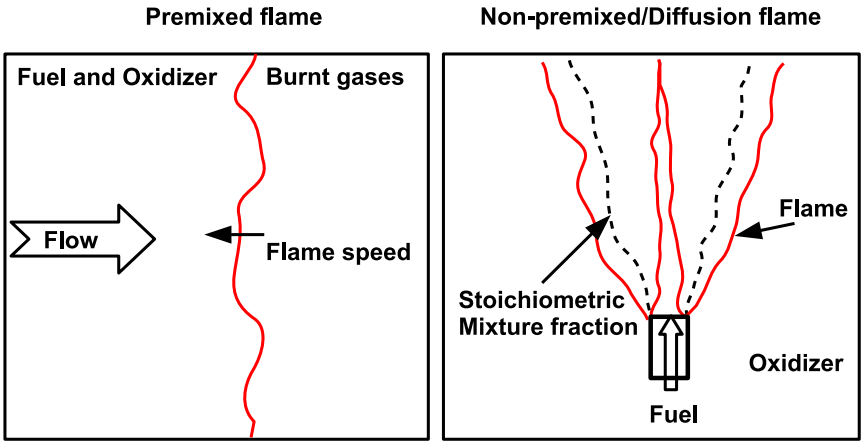

Figure 2.1: Schematics of flame types.

and chemistry is fundamentally different. This difference will be highlighted later in this chapter. Combustion in partially premixed flame takes place in stratified fuel-air mixtures. Figure 2.1 shows schematics of the premixed and the non-premixed flames.

In premixed flames, fuel and oxidizer are mixed at the molecular level before entering the combustor. A premixed flame is stabilized by a balance between the flame propagation speed and the flow velocity. In most of the industrial applications, the flow velocity is much higher than the flame propagation speed. To stabilize the flame in the combustor methods like recirculation or bluff body are used. Perfect premixing between fuel and oxidizer is difficult to attain in technical applications. Practically, the mixtures are either imperfectly premixed (temporal variation) or inhomogeneously premixed (spatially inhomogeneous), or both.

In non-premixed flames, fuel and oxidizer enter the combustion chamber separately. Reactions are controlled by the diffusion that transport the combustion products out of the reaction zone and replace them with fresh reactants. Thus non-premixed flames are also called ”diffusion flames”. The chemical reactions are faster than mixing, and the combustion process is mixing controlled. Diffusive-reactive structures are found in these flames. The disad-

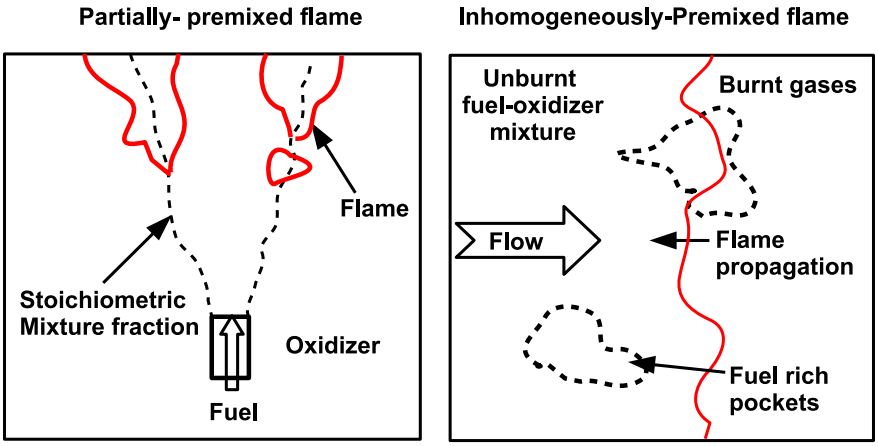

Figure 2.2: Schematics of partially premixed flames.

vantage of the diffusion flames is that the flame is attached to the injector, which increases its temperature. Also, higher amount of pollutants are emitted.

Partially premixed flames combine the advantages of the premixed and the non-premixed (diffusion) flames. Partially premixed flames are those, in which the flame is located in stratified fuel-oxidizer mixture. Figure 2.2 schematically shows a partially premixed flame. The main difference to the diffusion flame is that, although fuel and oxidizer are mixed after injection, the flame is stabilized downstream. Figure 2.2 on the right shows the so-called "inhomogeneously-premixed", which are found in practical premixed combustion applications. Perfect premixing between fuel and oxidizer is practically difficult to achieve in combustion devices. The schematic shows a premixed flame that is propagating as shown above in fig. 2.1, but some inhomogeneously mixed regions of fuel-oxidizer mixture are shown. The flame speed depends on the amount of fuel present in those regions (equivalence ratio / mixture fraction). Due to the presence of non-homogeneous mixture, the flame may also be categorized as a partially-premixed flame. The present work concentrates on the partially-premixed flames, and the "inhomogeneously-premixed" will not be considered.

Partially premixed flames have recently gained a lot of attention. Not only out of academic interests, but also due to their advantages over conventional premixed or diffusion flames. Some of the advantages of partially premixed flames are listed below:

1. The flame is far away from the combustor walls, which is desired from the component safety point of view.

2. As combustion takes place further away from the injector in stratified mixtures, where the lean air-fuel ratios are present, low pollutants are emitted.

From the brief description given above, the partially-premixed case seems to be a combination of diffusion and perfectly premixed flames, but the stabilization mechanism of the partially-premixed flames is very different and complex. There are two types of partially-premixed flames depending on whether the oxidizer is vitiated (mixed with hot combustion products) or not. In case of partially-premixed cases with non-vitiated oxidizer, the flame is stabilized by propagation of the flame in stratified fuel air mixture. A flame with tribrachial shape was observed [30, 114]. The shape of the flame is like a trident. The two side branches are premixed flames propagating against the flow. The central tail part is the diffusion flame formed by the mixing between remaining fuel from the rich branch and oxidizer from the lean branch of the flame. The flame is also known as a triple flame. Triple flames are found to be more stable than diffusion flames [114].

In partially premixed flames with vitiated oxidizer, the flame can be either stabilized by autoignition or the triple flame, depending on the triple flame propagation speed and the flow velocity. If the temperature of the vitiated oxidizer is high enough to initiate the autoignition reactions and the flow velocities are higher than the triple flame propagation velocity, the flame is stabilized by autoignition, where no external source of ignition is necessary.

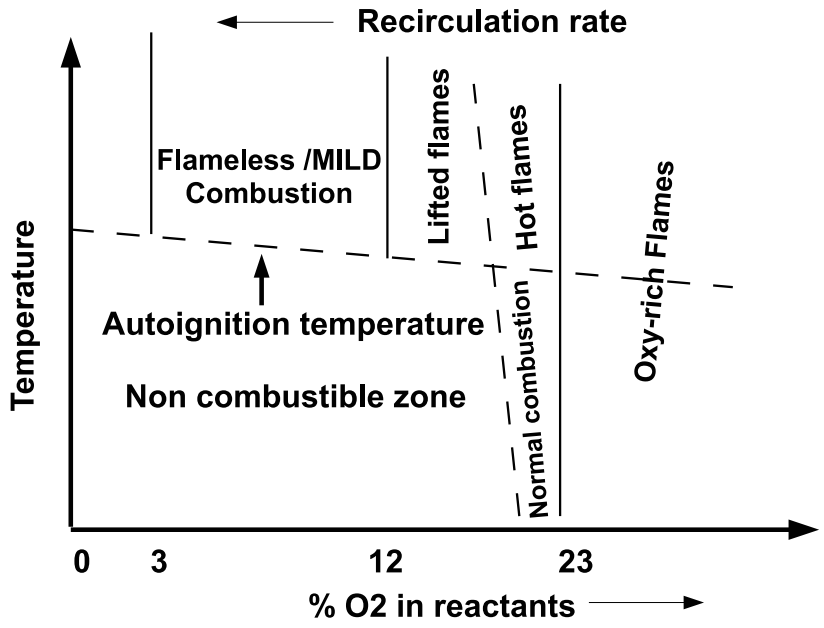

Figure 2.3: Regimes of combustion [98].

2.2 Regimes of Combustion

Depending on the oxygen content and temperatures, different regimes of combustion were marked by Rao et al. [98]. The regimes are shown schematically in Fig. 2.3. Air consists of 23% oxygen by mass. Oxy-rich flames have oxygen content higher than in air, whereas normal or hot flames have air as oxidizer. The mixtures that have oxygen content lower than that of air and temperatures below the ignition point are considered to be non-combustible. These mixtures need an external ignition zone and are difficult to stabilize due to extremely slow chemistry. The region with low oxygen content and high temperatures (above ignition temperature), called the MILD or flameless combustion, has attracted a lot of attention in recent times. The MILD regime has efficiency and low emission advantage over other regimes of combustion. The present work concentrates on autoignition stabilized flames (regimes above the ignition temperature line in Fig. 2.3), and with oxygen content equal

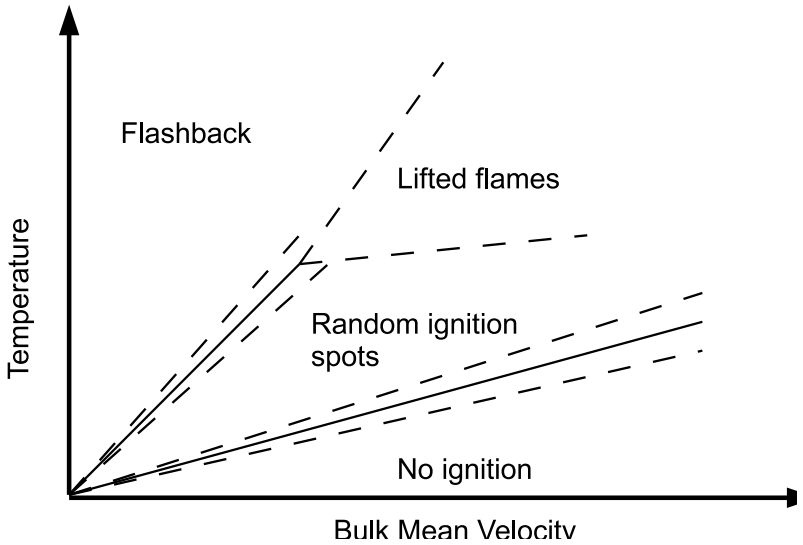

Figure 2.4: Regimes of autoignition.

to or lower than that in air. Specifically, the present work concentrates on lifted flames and flameless (MILD) combustion regimes (see Fig. 2.3). In all the cases considered in this work, the oxidizer is either vitiated (mixed with hot combustion products) or electrically heated air.

Markides et al. [71] introduced a regime diagram (see Fig. 2.4) for the stabilization of autoignition flames depending on the oxidizer temperature and the bulk mean velocity.

For a given velocity and at low temperatures no autoignition is observed, as the chemical reactions are slow and ignition time is greater than residence time. At increased temperature levels, the chemical reactions are faster, and autoignition is possible. After appearance, the ”ignition kernel” appear sporadically and grows in all directions. In the ”random ignition spots” regime, the kernel cannot propagate against the flow due to high convective transport acting downstream. At still higher temperatures, the chemical reactions and the diffusion of heat and radicals in the upstream direction may overcome the convective force. The kernel is able to propagate upstream, which is called ”flashback”. The flame stabilizes where the bulk mean velocity and

flame propagation velocities balance. A triple flame is observed in this case. If the temperature is high enough, the flame can flash back and attach to the injector, resulting into an attached flame.

In the following section, the phenomenological description of autoignition in laminar flows is described.

2.3 Autoignition in Laminar Flows

2.3.1 Homogeneous ignition

Autoignition, as the name suggests, is a phenomenon of fuel-oxidizer combustion without an external source of energy. This section describes autoignition in homogeneous conditions, i.e. premixed fuel and oxidizer. When a combustible mixture at sufficiently high pressure (p) and temperature (T_0) is contained in a homogeneous reactor, chemical reactions start on their own (chain initiation reactions), and at a certain point "thermal runaway" is attained, when heat and combustion products are released. The initial reactions that kick-off on their own are termed as "chain initiation" reactions. A pool of radicals is built up, which initiates the chain branching reactions. Chain branching reactions are those that split a molecule using a radical and in doing so produce more radicals. Chain breaking reactions act against the branching reactions, i.e. they consume radicals. If the conditions are favorable (low heat and radical loss), the branching reactions accelerate over the breaking reactions and the oxidation reactions accelerate. At some point of time, the system attains the "thermal runaway", called autoignition. At the point of autoignition, heat is released along with the formation of combustion products. The initial temperature T_0 above which autoignition is possible is called the autoignition temperature. The autoignition temperature is an important quantity to know whether a given mixture will ignite at all. Although being an important quantity, it does not help in understanding the details of the autoignition phenomenon. The time a mixture takes to auto ignite from initial conditions (the ignition delay) is a quantity of more fundamental importance. The ignition de-

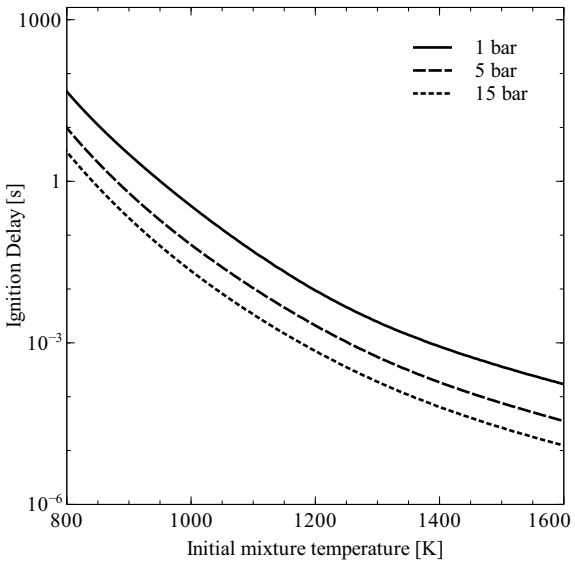

Figure 2.5: Methane ignition delays.

lay is a function of pressure, temperature T, and reactant stoichiometry. Figure 2.5 shows the ignition delays for a stoichiometric mixture of methane and air at various temperature and pressures. Higher pressure and temperature promote chain branching reactions, resulting into reduced ignition delays.

With the knowledge about the ignition delay time (τ_{ign}) and the bulk mean flow velocity (U), the location of autoignition can be determined by multiplying the two quantities, i.e $L_{ign} = U * \tau_{ign}$.

2.3.2 Inhomogeneous ignition

In inhomogeneous conditions, i.e. when fuel and oxidizer are not premixed, the ignition delay depends on the fuel-air mixture. This mixture composition is described by the mixture fraction. The mixture fraction conventionally is described by the amount of fuel present in the mixture.

$$Z = \frac{\dot{m}_1}{\dot{m}_1 + \dot{m}_2} \tag{2.1}$$

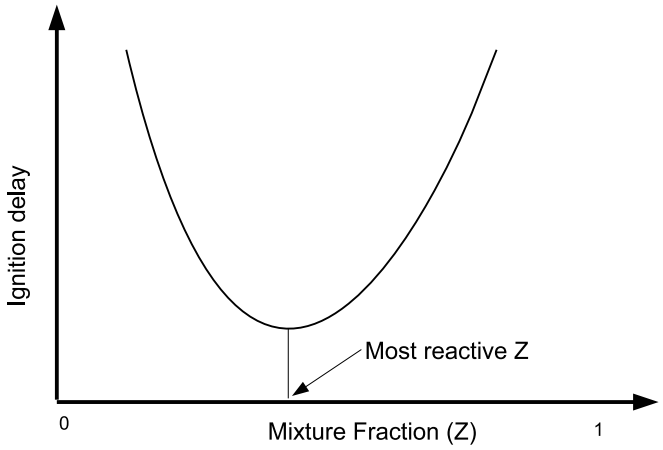

Figure 2.6: Most reactive mixture fraction.

Where $\dot{m}_1$ and $\dot{m}_2$ are the the mass flow rates of fuel and oxidizer stream, respectively. If the boundary conditions (fuel and oxidizer composition and temperature) are known, one can determine the composition and the enthalpy as they are a linear function of the mixture fraction [82, 89] ($Y_c = Z Y_{c,1} + (1 - Z) Y_{c,2}$). The relation for enthalpy is valid only in adiabatic cases. Using those initial conditions for the reactors, the ignition delays can be determined. Figure 2.6 shows schematics of ignition delay over the mixture fraction. It is interesting to observe that the curve has a minimum at a so called "most reactive mixture fraction", which must not necessarily be at the stoichiometric mixture fraction. Depending on the temperature difference between the fuel and oxidizer, the most reactive mixture fraction may shift. For a higher oxidizer temperature, the most reactive mixture fraction will be on the leaner side.

The ignition delays plotted in Fig. 2.6 can be considered as the absolute minimum ignition delays, as no radical or heat loss is taken into account. In a jet of fuel in oxidizer, there are transport effects, viz. convection and diffusion, that interact with the chemical reactions. These interactions are described using a schematic shown in Fig. 2.7 for a laminar jet of fuel in oxidizer. A line showing the most reactive mixture fraction is depicted. The chemical reactions are fastest at this mixture fraction, and autoignition is expected to take place at this location. It was observed in DNS studies [30, 45, 51, 52, 73, 101, 102] and ex-

perimental measurements [9, 10, 71] that autoignition indeed takes place on these most reactive mixture fraction surfaces.

From the bulk mean velocity (U) and the ignition delay time (τ_{ign}), a "reference" autoignition length ($L_{ref} = U * \tau_{ign}$) can be calculated. There is mixing between fuel and oxidizer simultaneously taking place with the build-up of radicals. The chemical reactions that build-up the radicals are dependent on the mixture fraction, which is evident from the figure 2.6. Due to this unequal build-up of radicals, gradients of species concentrations are formed, which lead to transport of radicals due to diffusion from faster reacting zones to slower ones. This transport reduces the overall rate of chemical reaction and increases the ignition delay of the "most reactive" mixture fractions. The location where ignition takes place will deviate from the reference ignition length L_{ref}. The actual ignition location will depend on the "history" of radicals that are built-up before ignition, which is affected by fuel-oxidizer mixing as well as the radical pool mixing. The rate of mixing is quantified by scalar dissipation rate (χ). One can define two scalar dissipation rates: based on mixture fraction (χ_Z) and the species (χ_{Y_c}).

The scalar dissipation rates based on mixture fraction and radicals are defined as:

$$\chi_Z = 2D\left(\frac{\partial Z}{\partial x}\right)^2 \tag{2.2}$$

$$\chi_{Y_c} = 2D\left(\frac{\partial Y_c}{\partial x}\right)^2 \tag{2.3}$$

The scalar dissipation rate is the rate of molecular mixing, or the inverse of the mixing time scale. The larger the gradient, the larger will be the scalar dissipation rate (faster mixing). Both scalar dissipation rates transport radicals out of the "most reactive" zones. The scalar dissipation rate is a quantity of utmost importance in non-premixed cases, which needs modeling either explicitly or implicitly.

These processes are explained below for a jet in coflow type of arrangement shown in Fig. 2.7. Due to convection, the radicals are transported downstream.

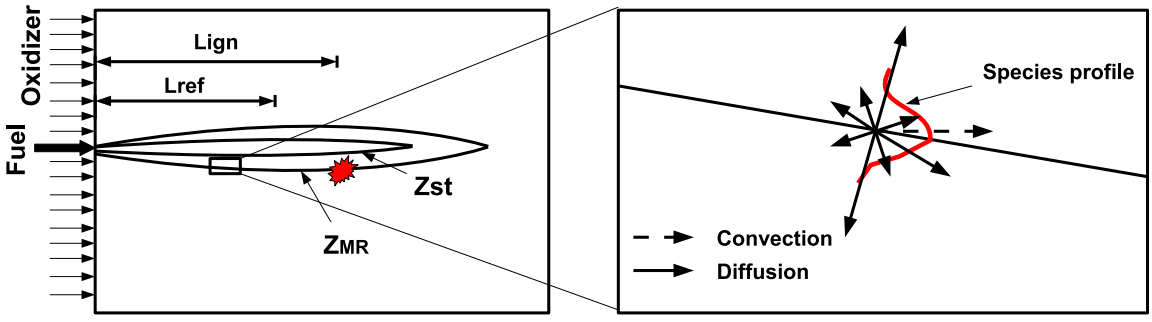

Figure 2.7: Sketch of a laminar non-premixed autoignition process.

As the chemistry is fastest at the most reactive mixture fraction, radicals are produced at the fastest rate on those surfaces. This non-uniform production creates a gradient of radical across the most reactive mixture fraction surface. The gradient of radicals results into its diffusive transport from the most-reactive mixture fraction surface, which is quantified by the SDR. This diffusive transport effect was not considered in the calculation of the reference autoignition length (L_{ref}). The diffusive transport further delays autoignition as the radicals are continuously lost to the less reactive mixture fractions. Therefore, the autoignition length will certainly be larger than the reference length.

The effect of the convective and diffusive transport can be explained from a Lagrangian point of view. Consider a particle with most reactive mixture fraction being transported downstream. In the absence of diffusion, the particle will evolve exactly like the homogeneous reactor, and will ignite at (L_{ref}). The particle looses or gains radicals to the neighboring more or less reactive particles, due to diffusive transport. This hinders or promotes the radical buildup from progressing towards the autoignition point. There is a competition between the diffusive transport (SDRs) and the chemical reactions. The diffusive transport is reduced as the mixture fraction gradient reduces (lower scalar dissipation rate). The particle will ignite at the location where the chemistry is faster than the diffusive transport effects.

In a homogeneous reactor, a pool of radicals is built up before autoignition

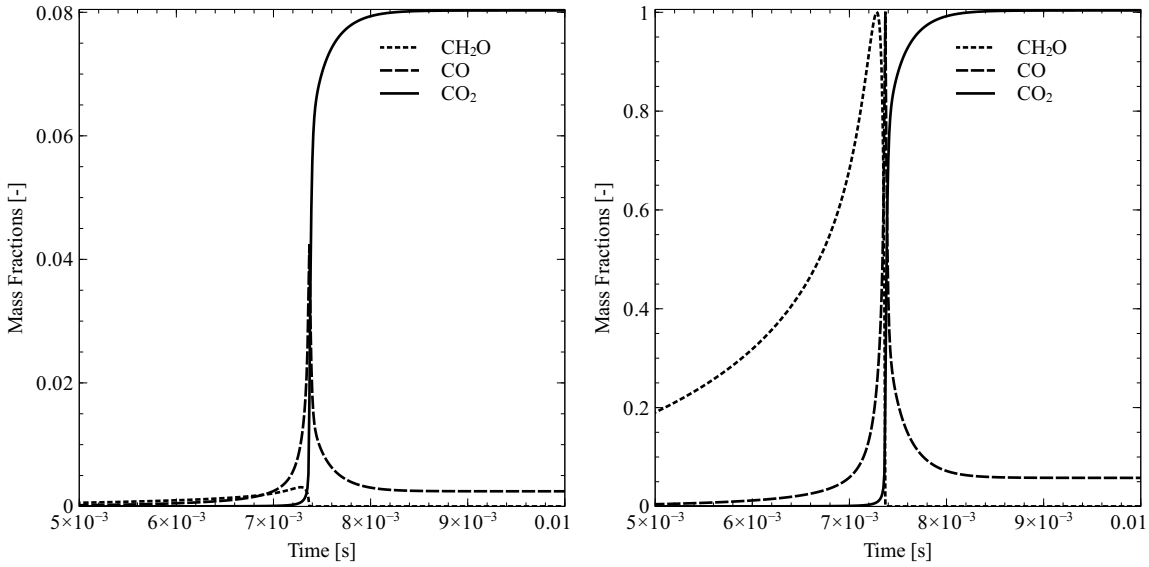

Figure 2.8: Species development in a reactor for methane.

point is attained. The pool is complex with numerous species. Some of the radicals reach a conspicuous peak before being consumed at a faster rate along with heat release and formation of combustion products. This peak of intermediate radicals can be used to determine the ignition point. Figure 2.8 shows the development of some of the major intermediates and products for methane fuel at 1300 K initial temperature and atmospheric pressure. The figure on the left shows the absolute values and on the right are the normalized curves. It is seen that the peak of CH_2O coincides with the ignition location and can be considered as a representative of the radical pool for methane combustion [39]. Brandt et al. [14] based their model for autoignition on tracking the CH_2O radical, the peak of which determined the autoignition location.

To determine the ignition location, the radical pool development history needs to be tracked. An autoignition model based on tracking of an ignition indicator species that represents the radical pool build-up was conceptualized by Brandt et al. [14, 15]. Simultaneous mixing and reaction study was performed using reactor mixing with different mixture fractions and radical pool development history. The reactors after mixing at various reactivities were compared to ”reference” reactor, which was mixed before build-up of radi-

cal. The study showed that a CH_2O was a good indicator of reaction progress towards autoignition and that the location of the indicator peak determines the location of autoignition.

In summary, for a laminar jet configuration, the autoignition length is larger than the reference ignition length that is based on the ignition delay time at the most reactive mixture fraction and the bulk mean velocity. The difference is due to the diffusive transport of radicals across the iso-mixture fraction surface. The diffusive transport, quantified by the scalar dissipation rate, transports radicals away from the most reactive mixture fraction zone, which increases the autoignition length. To determine the location of autoignition the history of radical pool development should be considered. A radical pool representative, e.g. CH_2O, can be tracked (transported) and its peak can be considered as the location of auto-ignition.

Autoignition in turbulent flows, which is the topic of this work, adds another degree of complexity: turbulence. The interaction between turbulent flows and autoignition is a topic of ongoing research and some of the recent numerical and experimental studies have thrown light on this topic. This work tries to identify key mechanisms that qualitatively predict the effect of varying turbulent flow characteristics on autoignition.

2.4 Turbulent flows

Turbulent flows occur in nature and various industrial applications. The term turbulence is synonymous to irregularity and chaos. Turbulence is difficult to define exactly; nevertheless, there are several salient characteristics that all turbulent flows possess.

Due to its presence in almost all industrial applications with combustion, turbulence and its modeling is an ongoing topic of research. As this work concentrates on autoignition in turbulent flows, the existing knowledge of turbulent flows and the parameters that are essential to describe them will be introduced in this section.

A non-dimensional number that differentiates laminar flow from turbulent is the Reynolds number, which is defined as the ratio of inertial to viscous forces and given by equation (2.4).

$$Re = \frac{\rho u d}{\mu} \tag{2.4}$$

where u is the bulk mean velocity and d is the characteristic dimension of the geometry. Flows that have Re greater than 4000 are considered as turbulent [99]. The Reynolds number in industrial applications are of the oder of several thousand. The characteristics of turbulent flows include unpredictability, rapid diffusivity, high levels of fluctuating vorticity, and dissipation of kinetic energy.

Turbulent flows consist of fluctuating 3D eddies. These eddies appear at various ranges of scales and interact with each other. The eddies are categorized into three main groups. The integral length scale (L_t) eddies constitute the large energy containing eddies. These are the energy containing eddies, which obtain energy from the mean flow. The scale of these eddies is comparable to the fluid domain. This energy is transferred to the smaller ones up to the smallest scale where the energy is dissipated at the molecular level due to viscous forces. These smallest eddies are called the Kolmogorov eddies. The intermediate scales between the integral and the Kolmogorov scales are the Taylor scales, which transfer the energy from the integral scale to the dissipative scale. Figure 2.9 summarizes the turbulent length scales.

This chaotic and irregular nature of turbulence makes it one of the major unsolved problems of classical physics. The velocity at a point in a turbulent flow will appear to an observer to be “random” or “chaotic.” The velocity is unpredictable in the sense that knowing the instantaneous velocity at some instant of time is insufficient to predict the velocity a short time later. Although the phenomenon is chaotic and irregular, there are some statistical rules that can be used to describe turbulent flows. The velocity at a point in the turbulent flow fluctuates about a certain mean value (Fig. 2.10).

The velocity will be typically described as a time-averaged value plus its fluctuation. Time-average quantities are denoted with an overbar:

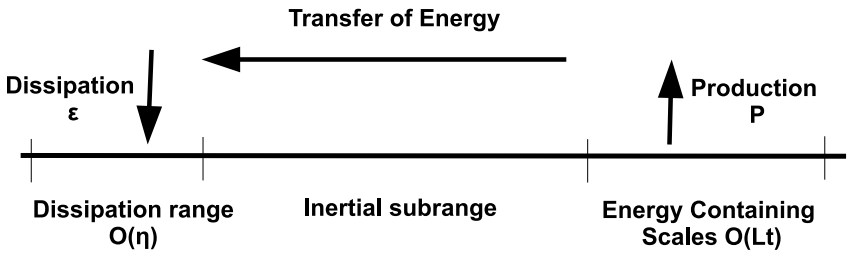

Figure 2.9: Turbulent length scales

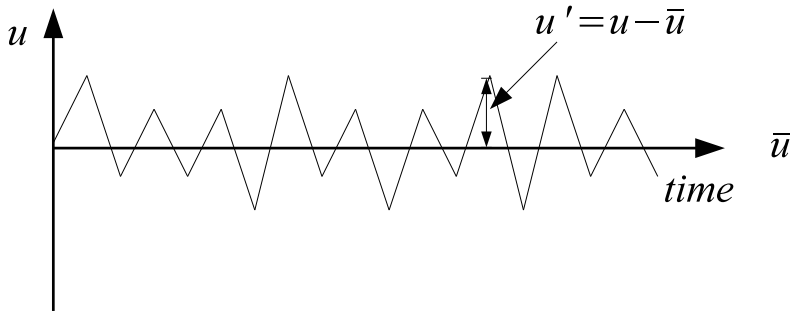

Figure 2.10: Velocity fluctuations at a location in a turbulent flow.

$$\bar{u} = \frac{1}{T}\int_0^T u\, dt \tag{2.5}$$

For a stationary velocity record, the instantaneous velocity can be decomposed into the sum of time-averaged and fluctuating contributions (called the Reynolds decomposition):

$$u = \bar{u} + u' \tag{2.6}$$

where u' is the fluctuating component (i.e. the deviation from the mean value). By definition, the time-average fluctuation is zero. Higher order statistical quantities, such as the variance, are used to describe the magnitude of the fluctuations:

$$\overline{u'^2} = \frac{1}{T}\int_0^T (u-\bar{u})^2 dt \tag{2.7}$$

These fluctuations of velocity at a point are quantified by the turbulent intensity, which is defined as the ratio of the root-mean-square of the velocity fluctuations to the mean velocity.

$$TI = \frac{\sqrt{\overline{u'^2}}}{\bar{u}} \tag{2.8}$$

In industrial applications, the turbulent intensity might range from 5 to 20 %. The integral length scale (L_t), defined above, combined with the turbulent intensity is used to describe the turbulence level. Using these two quantities the integral time scale of turbulence can be defined. A turbulent time scale, also known as the eddy turnover time can be calculated from the two quantities as shown in Eq. (2.9). This is an pivotal quantity used in the present work to quantify turbulence. Small turbulent time scale means high turbulence intensity, either due to shorter length scale or higher velocity fluctuations.

$$\tau_t = \frac{L_t}{u'} = \frac{L_t}{TI \cdot \bar{u}} \tag{2.9}$$

Using the two turbulent parameters, a turbulent Reynolds number can be defined as shown in equation (2.10). Turbulent energy is dissipated at the Kolmogorov scales, where the turbulent Reynolds number is 1, i.e. the inertial forces are equal to viscous dissipation.

$$Re_t = \frac{\rho u' L_t}{\mu} \tag{2.10}$$

The ratio of the integral length scale to the Kolmogorov scale (η) can be shown to be a function of the turbulent Reynolds number (Re_t) [89].

$$\frac{L_t}{\eta} = Re_t^{(3/4)} \tag{2.11}$$

This shows that with larger Re, a broader range of length scales are found in turbulent flows.

An important characteristic of turbulence is faster mixing. Mixing takes place at the molecular level, where molecules take random paths in the flow. The mixing of the molecules is called diffusion. Diffusion corresponds to the spreading of molecules due to the random paths they take. The velocity fluctuations efficiently transport momentum, heat, and a tracer concentration. This turbulent transport is significantly more effective than molecular diffusion. Thus, turbulence results into a high rate of diffusivity. This results in faster mixing between the molecules. Chemical reactions take place at the molecular level, where fuel and oxidizer molecules come into contact. This mixing at molecular level is of utmost importance in reactive flows and needs to be modeled in simulation of turbulent flows.

All turbulent quantities that will be encountered in this work are described in this section. For further reading, Pope [93] gives a more detailed description of turbulent flows.

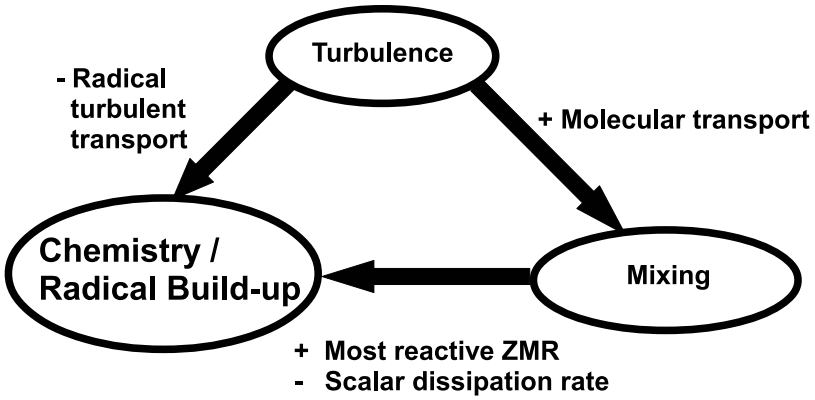

Figure 2.11: Schematics of the impact of turbulence on autoignition.

2.5 Autoignition in turbulent flows

The various interactions described in section 2.3 for laminar flows are further complicated in turbulent flows. It is a well known fact that the mixing between the fuel and oxidizer is an important factor that changes autoignition length. Turbulence is known to enhance mixing. This enhanced mixing between fuel and oxidizer should promote autoignition, as it creates the most reactive mixture fraction surfaces at a faster rate. On the other hand, increased turbulence also increase the transport of the radicals away from the most reactive mixture fraction zone, which is quantified by the scalar dissipation rate. This should prohibit ignition. Therefore, there are complex interactions between turbulence, mixing and pre-ignition chemistry. In the combustion community, it is disputed whether turbulence promotes or inhibits autoignition.

Various DNS studies [30, 45, 51, 52, 73, 101, 102] and experimental measurements [9, 10, 71] were performed recently to study the impact of turbulence on autoignition. All of them agree that auto-ignition takes place at a preferred mixture fraction called the "most reactive mixture fraction" and at locations of low scalar dissipation rate. The scalar dissipation rate describes the diffusive transport of heat and radicals away from the most reactive mixture fraction, delaying autoignition. This diffusive transport is caused by mixture fraction

gradients in non-premixed configurations, which do exhibit ignition delays longer than the ones observed in homogeneous reactors [73].

To the present point, there still remain controversies regarding the dependence of auto-ignition on the turbulence level. The early 2D laminar and turbulent mixing layer DNS study of Mastorakos et al. [73] showed that stronger turbulence results in faster mixing between fuel and air, which favors autoignition. Thus, it is expected that this trend should continue with a further increase in the turbulence level. Im et al. [45] performed 2D DNS of hydrogen mixing layer in homogeneous turbulence and pointed out that, depending on the characteristic time scale of ignition τ_{ign} and turbulence τ_t, ignition can be facilitated by weak to moderate turbulence, and retarded by stronger turbulence, with time scales substantially smaller than the ignition delay.

Sreedhara et al. [101, 102] studied autoignition in 2D and 3D isotropic, homogeneous decaying turbulence. They concluded that for turbulent time scales ($\tau_t = l_t/u^{'}$) larger than the ignition delay ($\tau_{ign} \ll \tau_t$), turbulence intensity did not have a strong effect on auto-ignition. On the other hand, for smaller turbulent time scales ($\tau_{ign} \gg \tau_t$), auto-ignition times were found to increase in 2D and decrease in 3D with increasing turbulence intensity. They attributed the discrepancy between the 3D and the 2D results to the effect of vortex stretching, which was absent in the 2D simulations. Echekki et al. [30] performed DNS with detailed hydrogen chemistry and indicated that the balance between radical production and dissipation determines the ignition process. The presence of high scalar dissipation rates can delay the radical build-up, which confirms the observation made by Mastorakos et al. [73], and in extreme cases can prohibit autoignition altogether.

Experimental measurements [9, 10, 71] performed at turbulent time scales smaller than ignition delay times ($\tau_t \ll \tau_{tign}$), i.e. mixing controlled regime, show that with increase in the turbulence intensity the autoignition length increases. Recently concluded 3D DNS by Kerkemeier et. al. [51,52] with detailed chemistry performed at different turbulent intensities in the regime are in line with the experimental observation. This is contradictory to the results of the 2D DNS of Mastorakos et al. [73] and 3D DNS of Sreedhara et al. [102] and is discussed at length by Mastorakos [72].

The reason for the discrepancies in the mixing-controlled regime ($\tau_t \ll \tau_{tign}$) between the DNS studies using reduced chemistry [73, 102] and detailed chemistry [30, 51] is debatable and not the point of discussion in the present work. As it is expensive to perform DNS studies, LES will be performed in this work to extensively study the impact of turbulence in a wide range of turbulent time scales.

The chapter 6 is dedicated to study the impact of turbulence on mixing and autoignition.

3 Review on turbulent autoignition modeling

Turbulent combustion is a multi-scale problem with a wide range of chemical and flow time scales. The interaction of the chemical and turbulent flow time scales is particularly complex in turbulent autoignition flows. The Damköhler number (Da), which is one of the quantities used to distinguish between various regimes of combustion, is defined as the ratio of flow to chemical time scale $Da = \frac{t_{flow}}{t_{chem}}$. The chemical time scales are larger than the flow scales before autoignition, and smaller after autoignition. Thus, a broad range of Da numbers is observed in autoignition stabilized flames.

Turbulent flows exhibit length scales from the geometrical range to the smallest Kolmogorov scales, which range from milli- to micrometers. Solving all these scales is a challenge from a computational cost point of view. Three numerical simulation approaches exist that differ according to the range of resolved scales : DNS (Direct Numerical Simulation) solves for all scales, LES (Large Eddy Simulation) solves for larger scales and assumes the smaller to be universal and models them, and RANS (Reynolds Averaged Navier Stokes) models all the scales. DNS and RANS can be considered as two extremes from the point of view of the modeling effort and computational cost. RANS has been the most favorable approach for industrial applications, due to its low computational cost. DNS, on the other hand, is too expensive to be suitable for industrial configurations at the current state of the computational capability. LES models small scales for which DNS spends most of the computational time. LES is capable of capturing transient phenomena like autoignition, extinction and reignition, due to their inherent unsteady formulation. LES, although costly in terms of computational time compared to RANS, has proven to be more reliable due to the reduced amount of modeling. With ever improving computational power, LES of industrial applications is becoming

more and more feasible.

Combustion takes place at micromixing scales, where fuel and oxidizer come in contact at the molecular level. These scales are unresolved in LES. Therefore, combustion needs to be modeled in LES. Most of the combustion models that are developed in the RANS context are taken over for LES [85]. Mixing, which has a paramount importance for non- or partially- premixed combustion models, is predicted better in LES. Therefore, all the combustion models developed in RANS context are expected to perform better in LES. In this chapter, a review on the combustion models available in the literature and suitable for autoignition are described in this chapter after a brief introduction to LES.

3.1 Conservation equations

To describe the motion of fluid, conservation equations equations for mass and momentum are solved. The conservation laws state that particular measurable properties of an isolated physical system do not change as the system evolves. Three quantities are conserved in a flow simulation: mass, momentum and energy.

The mass conservation equation is also known as the continuity equation. The continuity equation reads:

$$\frac{\partial \rho}{\partial t} + \frac{\partial (\rho u_j)}{\partial x_j} = 0 \tag{3.1}$$

where ρ is the density, and j corresponds to the Cartesian coordinates. The momentum is based on the Newton's law of motion. According to the law, the rate of change of momentum equals the sum of forces.

The momentum equation is described by

$$\frac{\partial \rho u_i}{\partial t} + \frac{\partial (\rho u_i u_j)}{\partial x_j} = -\frac{\partial p}{\partial x_i} + \frac{\partial \tau_{ij}}{\partial x_j} + f_i \tag{3.2}$$

where p is the static pressure and f_i are the external forces, e.g. the gravitational force. τ_{ij} is the stress tensor, which is modeled using molecular viscosity and velocity gradients. The stress tensor is then given by:

$$\tau_{ij} = \mu \left(\frac{\partial u_i}{\partial x_j} + \frac{\partial u_j}{\partial x_i} - \frac{2}{3} \delta_{ij} \frac{\partial u_l}{\partial x_l} \right) \tag{3.3}$$

where $\delta_{ij} = 0$ for $i \neq j$ and $\delta_{ij} = 1$ for $i = j$.

The conservation of enthalpy (h) reads:

$$\frac{\partial \rho h}{\partial t} + \frac{\partial \rho u_j h}{\partial x_j} = \frac{\partial p}{\partial t} + u_j \frac{\partial p}{\partial x_j} + \frac{\partial q_j}{\partial x_j} + \tau_{kj} \frac{\partial u_k}{\partial x_j} + \omega_E \tag{3.4}$$

In Eq. $\dot{\omega}_E$ is the combination of all the source terms for the equation due to chemical reactions, radiation or wall heat losses.The coupling between the energy equation and the momentum equation takes place through pressure and density given by the thermodynamic equation of state:

$$\rho = \frac{p}{R_u T \sum_{c=1}^{N_s} Y_c / M_c} \tag{3.5}$$

In addition to the above equations, species transport equations need to be solved. A general species transport equation is given by:

$$\frac{\partial \rho Y_c}{\partial t} + \frac{\partial \rho u_j Y_c}{\partial x_j} = \frac{\partial}{\partial x_j} \left(\rho D \frac{\partial Y_c}{\partial x_j} \right) + \dot{\omega}_c \tag{3.6}$$

The species transport equation has a chemical source term $\dot{\omega}_c$ that arises due to the chemical reactions.

3.2 Large Eddy Simulation

Large Eddy Simulation (LES), as the name suggests, is an approach of turbulent flow simulation that solves the large eddies (scales) of the turbulent flow and models the smaller (subgrid) scales. The eddies resolved in LES are of the order of the integral length scales, which contain the largest amount of the turbulent kinetic energy. A filter is used to filter out the small scales. The turbulent quantities are split into the resolved and unresolved components using a filter function. Any quantity ϕ is filtered using a filter G as shown by equation (3.7).

$$\bar{\phi}(x,t) = \int \phi(x^{'},t) G(x-x^{'}) dx^{'} \tag{3.7}$$

Various filters are available in the literature, e.g., top-hat, Gaussian, etc. The top-hat or box filter is the most popular, which is used throughout this work.

$$G(x) = \frac{1}{\delta^3} if |x_i| \leq \frac{\delta}{2} = 0 if |x_i| \geq \frac{\delta}{2} \tag{3.8}$$

$$\bar{\rho}\tilde{\phi}(x,t) = \int \rho\phi(x^{'},t) G(x-x^{'}) dx^{'} \tag{3.9}$$

In flows with combustion, a change in density is observed due to heat release. It is convenient to use density weighted average, called Favre average. Using Favre average, any quantity, e.g. $\phi(x,t)$, is split into $\phi(x,t) = \widetilde{\phi}(x,t) + \phi^{''}(x,t)$.

Using filtering of the velocity field and Favre averaging, one can derive the filtered LES equation (equation 3.10 and 3.11) from the Navier-Stokes equations.

$$\frac{\partial \bar{\rho}}{\partial t} + \frac{\partial \bar{\rho}\widetilde{u_j}}{\partial x_j} = 0 \tag{3.10}$$

$$\frac{\partial \bar{\rho}\widetilde{u_j}}{\partial t} + \frac{\partial \bar{\rho}\widetilde{u_j}\widetilde{u_i}}{\partial x_j} + \frac{\partial \bar{p}}{\partial x_j} = \frac{\partial \bar{\tau}_{ij}}{\partial x_j} - \frac{\partial}{\partial x_j}\left\{\bar{\rho}\widetilde{u_i u_j} - \bar{\rho}\widetilde{u}_i\widetilde{u_j}\right\} \tag{3.11}$$

The last term in the equation is the unresolved Reynolds stress, which is found in unclosed form. This term needs modeling. Out of the numerous models for this term, the Smagorinsky dynamic model has been used in this work. The dynamic Smagorinsky model devised by Germano [36] models the stress term by the eddy viscosity given by:

$$(\bar{\rho}\widetilde{u_i u_j} - \bar{\rho}\widetilde{u}_i\widetilde{u_j}) = \mu_{sgs}\left[\frac{\partial \widetilde{u}_i}{\partial x_j} + \frac{\partial \widetilde{u}_j}{\partial x_i}\right] = \bar{\rho}(C_s\delta)^2\left[\frac{\partial \widetilde{u}_i}{\partial x_j} + \frac{\partial \widetilde{u_j}}{\partial x_i}\right] \tag{3.12}$$

C_s is a dynamic constant determined using Smagorinsky dynamic model. This model has been used throughout this work. A detailed description on LES and the models is given in [93].

3.3 Combustion Models

Chemical reactions take place at the molecular level (scale), where reactants come into contact. LES does not resolve these scales, and therefore combustion models are required to consider the turbulence-chemistry interaction at subgrid levels [85]. An important characteristic of turbulent flows is fluctuation of all the physical and thermo-physical quantities. In turbulent flows, gradient of any physical (velocity, pressure, etc.) or thermo-chemical quantity (mass fraction of species, etc.), leads to its fluctuations. As the thermo-physical and -chemical quantities that are necessary for combustion modeling are not resolved in LES, statistical quantities (moments) are used to describe the state of a cell. The first two moments (mean and variance) are generally used for the description. A probability density function (PDF) based on the moments describes the distribution of the scalars at the subgrid level.

The method of obtaining the moments differentiates the approaches for the turbulence-chemistry interaction. Two approaches: presumed PDF and transported PDF methods are widely used. The presumed PDF solves deterministic transport equations for the moments in LES, whereas in the transported PDF methods, one solves for possible subgrid realizations. The ensemble of the possible realizations gives the two moments.

The transported PDF have a major advantage that the chemical source term is closed. The closure problem shifts to the micromixing model, which simulates mixing at unresolved scales. The presumed PDF has an advantage in terms of computational cost over the transported PDF method, but need models for the presumed PDF shape and the higher order moments. This is a major disadvantage for cases with multi-stream mixing. Although the computational cost is comparatively higher, the transported PDF method has the advantage that they are readily applicable to multi-stream mixing cases without additional assumptions or modeling complexities. A review on both these methods is given in the next sections.

3.3.1 Combustion models based on presumed PDF approach

The presumed PDF approach, as the name suggests, uses a presumed distribution of the subgrid thermo -physical and -chemical quantities as a function of the first two moments. Deterministic transport equations are solved in LES for the two moments. The model for the presumed shape of the probability density needs validation. Filtered transport equations [28] for the first (mean Y_C) and the second moment (variance $Y_C''^2$) of a general reactive scalar are shown below:

$$\frac{\partial \overline{\rho}\widetilde{Y_c}}{\partial t} + \frac{\partial \overline{\rho}\widetilde{u_j}\widetilde{Y_c}}{\partial x_j} = -\frac{\partial}{\partial x_j}\left[\frac{\partial \overline{\rho}(D+D_t)\widetilde{Y}_c}{\partial x_j}\right] + \widetilde{\dot{\omega}_c} \tag{3.13}$$

$$\frac{\partial \overline{\rho}\widetilde{Y_C''^2}}{\partial t} + \frac{\partial \overline{\rho}\widetilde{u_j}\widetilde{Y_C''^2}}{\partial x_j} = -\frac{\partial}{\partial x_j}\left[\frac{\partial \overline{\rho}(D+D_t)\widetilde{Y}_C''^2}{\partial x_j}\right] - 2\overline{\rho\chi_{Y_c}} + 2\overline{Y_c\dot{\omega}_c} \tag{3.14}$$

The moment transport equations need modeling. The first order moment needs model for the turbulent transport (second term in Eq. 3.13 and 3.14) term, which is normally done by the scalar gradient assumption. The second moment equation needs modeling for the scalar dissipation rate and the production of variance due to the chemical source term (second last and last terms in Eq. 3.14, respectively). The filtered chemical source term needs a

careful treatment, which is the main problem of combustion modeling. The chemical source term closure based on joint presumed PDF method has been attempted by [2]. The closure requires a PDF shape for the subgrid PDF distribution based on the two moments. If the PDF shape is known, the source term may be closed as given by Eq. (3.15).

$$\widetilde{\dot{\omega}_{Y_c}} = \int\int ... \int \dot{\omega}_{Y_c}(Y_1, Y_2, ..., Y_n) P(Y_1, Y_2, ...Y_n) dY_1 dY_2 ... dY_n \tag{3.15}$$

The problem with the joint presumed PDF method is that the joint (multi-dimensional) PDF shape $P(Y_1, Y_2, ...Y_n)$ for the intermediate species is not known. Independence can be presumed between the species [3] to get the simplified closure of the term given by:

$$\widetilde{\dot{\omega}_{Y_c}} = \int\int ... \int \dot{\omega}_{Y_c}(Y_1, Y_2, ..., Y_n) P(Y_1) P(Y_2) ... P(Y_n) dY_1 dY_2 ... dY_n \tag{3.16}$$

Apart from the errors one makes with the assumptions, the major problem with these methods is the high computational cost that increases with the number of species that are transported. Due to these disadvantages, the method is not popular in the combustion modeling field. Instead, models that consider the fluctuations of a key parameter called the mixture fraction (defined in equation (2.1)) are acknowledged and well established.

In the following sections, models based on mixture fraction are described. The advantage of using mixture fraction is that, being a conserved scalar, no chemical source term exists for in its transport equation. The fluctuation of the reactive scalars are related to the fluctuation of the mixture fraction. Various approaches exist to simplify the turbulence-chemistry interaction, which are described in the following subsection.

The transport equations for the mixture fraction mean and its variance are shown below:

$$\frac{\partial \overline{\rho} \widetilde{Z}}{\partial t} + \frac{\partial \overline{\rho} \widetilde{u_j} \widetilde{Z}}{\partial x_j} = -\frac{\partial}{\partial x_j} \left[\frac{\partial \overline{\rho} (D + D_t) \widetilde{Z}}{\partial x_j} \right] \tag{3.17}$$

$$\frac{\partial \overline{\rho}\widetilde{Z^2}}{\partial t} + \frac{\partial \overline{\rho}\widetilde{u_j}\widetilde{Z^2}}{\partial x_j} = -\frac{\partial}{\partial x_j}\left[\frac{\partial \overline{\rho}(D+D_t)\widetilde{Z^2}}{\partial x_j}\right] - 2\overline{\rho\chi_Z} \tag{3.18}$$

Any thermo-physical quantity can be closed using its joint PDF with the mixture fraction.

$$\widetilde{\dot{\omega}_{Y_c}} = \int \dot{\omega}_{Z,Y_c} P(Z,Y_c) dZ dY_c \tag{3.19}$$

If an independence may be assumed between the conserved and reactive scalars, the closure can be simplified.

$$\widetilde{\dot{\omega}_{Y_c}} = \int \dot{\omega}_{Y_c|Z} P(Y_c|Z) P(Z) dZ dY_c \tag{3.20}$$

Where $\dot{\omega}_{Y_c|Z}$ is the source term conditioned on the mixture fraction. The term $P(Yc|Z)$ describes the fluctuation of the reactive scalar conditioned on the mixture fraction. In case of negligible conditioned fluctuations of the reactive scalar, the closure can be simplified by presuming a Dirac function for the conditioned fluctuations:

$$\widetilde{\dot{\omega}_{Y_c}} = \int \dot{\omega}_{Y_c|Z} P(Z) dZ \tag{3.21}$$

The chemical source terms for the reactive scalars are closed practically using a PDF shape for the mixture fraction and considering a Dirac function for the conditional fluctuations. The β PDF is a validated model for the mixture fraction [6]. This closure is called the first order closure. The methods considering the conditioned fluctuations of reactive scalars is called the second order closure. The problem with the presumed PDF approach for reactive scalars is that the intermediate species that peak at the sub-grid level can not be treated properly. Modeling the PDF shape and variance are not trivial. To overcome these problems, various approaches based on the use of a conserved variable, the mixture fraction, have been popular in the combustion community. In the following, combustion models based on the mixture fraction are described.

3.3.1.1 Flamelet based models

The flamelet model for non-premixed combustion was derived by Peters [81]. The underlying concept in the flamelet model, as the name suggests, is that the flame reaction zones are thin, and their structure is essentially the same as in laminar flames subjected to the same scalar dissipation. These flamelets are largely undisturbed by the turbulent eddies. The flame responds immediately to changes in the flow field. The laminar flamelet model assumes fast chemistry. Following is the flamelet equation for reactive scalars as a function of mixture fraction and scalar dissipation rate:

$$\frac{\partial Y_\alpha}{\partial t} + \frac{\rho}{Le}\frac{\chi}{2}\frac{\partial^2 Y_\alpha}{\partial Z^2} + \dot{\omega}_\alpha = 0 \tag{3.22}$$

The steady laminar flamelet model (SLFM), also known as the flamelet model, assumes the chemical time scales to be shorter than turbulent ones and neglects the transient (first) in Eq (3.22). The following set of ordinary differential equations (ODEs) is solved to get the solution of the flame (species and temperature) distribution over the mixture fraction.

$$\frac{\rho}{Le}\frac{\chi}{2}\frac{\partial^2 Y_\alpha}{\partial Z^2} + \dot{\omega}_\alpha = 0 \tag{3.23}$$

The ODEs are solved for all species and temperature using a detailed kinetic mechanism for different values of scalar dissipation rate and is stored in a library. In CFD, transport equations are solved for the mixture fraction and its variance. The scalar dissipation rate is available as a function of the mixture fraction gradient. The thermo-chemical state of a cell is read from the flamelet library and convoluted over the presumed PDF shape of the mixture fraction. The overall setup of the flamelet model is shown in Fig. 3.1.

Within its range of validity, the flamelet model is an attractively easy way to include effects of complex chemistry in turbulent flame calculations. An early success was the improvement in matching experimental CO concentrations, in comparison with calculations assuming chemical equilibrium. However, strong arguments have also been put forward against flamelet models.

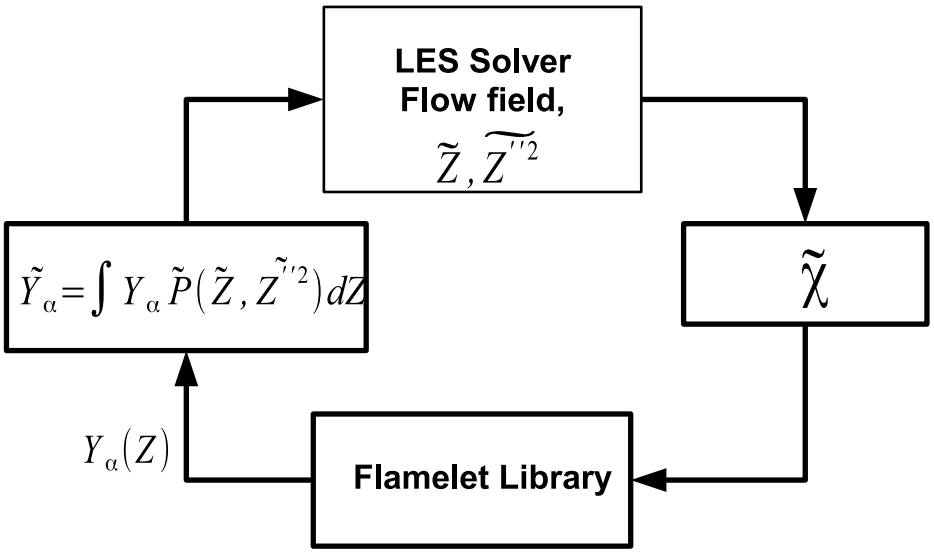

Figure 3.1: Steady Laminar Flamelet model setup.

These include the effects of variations in scalar dissipation through flamelets, and the influence of neglected advection and transient terms in the transport equations. It is clear that the SLFM paradigm cannot remain valid in the presence of local extinction and re-ignition, when unsteady and flame edge effects become important. In consequence, the question of the range of validity of flamelet models remains controversial. It cannot be denied that the laminar flamelet paradigm can provide an accurate description for combustion at high Da numbers.

The SLFM has been modified to include effects of transients. Pitsch et al. [86], considered the fluctuations of the scalar dissipation rate at the subgrid level. These changes can be helpful, particularly for extinction and re-ignition processes, and for kinetically slow species such as nitric oxide, carbon monoxide or soot. Large eddy simulations incorporating such a viewpoint have been successful. The unsteady flamelet model is an extension to the steady laminar flamelet model (SLFM) to capture the instationary effects. The transient flamelet equation considers the instationary term shown in Eq. (3.22). Various

methods of solution of the equation have been introduced. The methods differ in the way the equations are solved and tabulated. The time or space is not a convenient parameter to base the tabulation on. One of the most successful methods was introduced by Pitsch et al. [87],in which a progress variable is used to tabulate the flamelet solutions, in addition to the scalar dissipation rate. The progress variable could be a normalized temperature or products mass fraction. New interpretations of the flamelet paradigm continue to appear. Another factor that affects the flamelet paradigm is the competition between the broadening of flamelets and their extinction, both of which are governed by the local Karlovitz number and the level of mixture fraction fluctuations. Ihme et al. [43] studied a methane lifted flame using steady laminar flamelet model and concluded that the SLFM model is not capable of predicting proper lift-off height. Their formulation of transient flamelet model includes a progress variable, which describes the degree of reaction progress. This progress variable along with the scalar dissipation rate determines the thermo-physical quantities. Ihme et al. [43] also showed that the fluctuations of the progress variable also need to be considered. The model was applied to MILD combustion flame with success by Ihme et al [44].

The computational cost and modeling complexities are low for the transient laminar flamelet model. But, they are disadvantageous in multi-stream cases. The flamelet equation in case of multi-stream mixing will include additional terms with cross-scalar-dissipation rates. The dimension of the table increases nonlinearly with the number of dimensions. For a ternary (3-stream) mixing case, i.e. with two mixture fractions, the table will have five dimensions in addition to the progress variable dimension. The dimensions will be: (Z_1, Z_2, χ_1, χ_2, χ_{12}), where χ_{12} is the cross-scalar-dissipation-rate. For quaternary (4-stream) mixing case, the total dimensions will be 9, and so on. Apart from the dimensionality problem, the complexities and computational cost of convoluting over those dimensions and the multi-variate PDF make the model unattractive for multi-stream problems.

3.3.1.2 Conditional Moment Closure

Conditional moment closure (CMC) is a modeling viewpoint that has been inspired by the laser-diagnostic measurements in jet diffusion flames and reactive mixing layers experiments. It was evident that flamelet methods would not be appropriate for low Da number processes like the reaction between nitric oxide and ozone, which is slow and occurs throughout the mixed fluid. The CMC model was proposed independently by Bilger [7] and Klimenko [57]. Bilger derived the model from a flamelet type of method, while Klimenko derived it from the TPDF (Transported PDF) approach. The modeling equations are the same, although the approaches are different. The basic concept is that the fluctuations in temperature and composition that occur in turbulent combustion can be closely cross-linked to the fluctuations of the mixture fraction. Equations are derived and solved for the conditional means of the reactive scalars. The source term for the reactive scalars is closed using the mixture fraction PDF. The first order CMC neglects the variance of the scalars about the conditional value. In the second order CMC model, these fluctuations are considered. The unconditioned mean and variance are given by:

$$Y_\alpha = \langle Y_\alpha \rangle + Y'_\alpha \tag{3.24}$$

The conditioned mean with respect to the mixture fraction is defined as:

$$Q_\alpha = \left\langle Y_\alpha | \eta \right\rangle \tag{3.25}$$

$$Y_\alpha(x,t) = Q_\alpha(\eta; x, t) + y''_\alpha(x,t) \tag{3.26}$$

The assumption behind using the first order moment closure for the chemical source is:

$$y''_\alpha(x,t) \ll Y' \tag{3.27}$$

This means that the variations about the conditional means are neglected. This is not a severe assumption in absence of extinction and reignition. The known conservation equations for species and enthalpy can be reformulated

in terms of such conditional averages. They involve important terms for the conditional average reaction rates. Following is the transport equation for the conditional mean of species α:

$$\rho_z \frac{\partial Q_\alpha}{\partial t} + \rho_z \langle u_i | \eta \rangle \frac{\partial Q_\alpha}{\partial x_i} = -\rho_z \langle \chi | \eta \rangle \frac{\partial^2 Q_\alpha}{\partial Z^2} + \rho_z \langle \dot{\omega}_\alpha | \eta \rangle + e_Q + e_Y \tag{3.28}$$

All the terms in the CMC equation need modeling. The term e_Q, which represents molecular diffusion in physical space, is neglected for high Re number. The term e_Y, which represents turbulent diffusion in physical space, needs modeling. Models are necessary for the conditioned velocity and scalar dissipation rate. For closing the conditional chemical source term, fluctuations about the conditional averages are neglected. The conditional average reaction rates are well approximated using the conditional average temperature and species mass fractions. This CMC Eq. (3.28) is quite similar to the unsteady flamelet Eq. (3.22) except for two extra terms, which describe the transport in physical space viz. the conditioned velocity and e_Y. The overall model interaction with CFD is shown in Fig. 3.2.

The major advantage of CMC is that the CMC equations are not solved on the CFD grid, but on a so called CMC grid, which is much coarser. This is because the conditional mean along the iso-mixture fraction surface does not change as rapidly as the unconditioned. Peters [82] argues that the CMC model is not much different to the SLFM model. As it can be seen from the CMC Eq. (3.28) and the SLFM Eq. (3.22), the transport of species in physical space is present in the CMC equation, but absent in SLFM. This means that in case of intermediately slow chemistry, the chemistry could be much slower than the advective transport and the ignition can be delayed. In case of intermediately fast chemistry, where no ignition takes place, the SLFM model will fail. The so called "first-order CMC" achieves conditional reaction rate closure by neglecting the contributions of conditional variances and covariance. Many non-premixed problems, including flows with recirculation [21] and autoignition of sprays [53], have been successfully modeled using first order CMC. In flames with significant local extinction and re-ignition, it has been found that such first-order closure is not sufficiently accurate [55]. Second order closure [58] incorporates the effects of conditional variances and covariances in

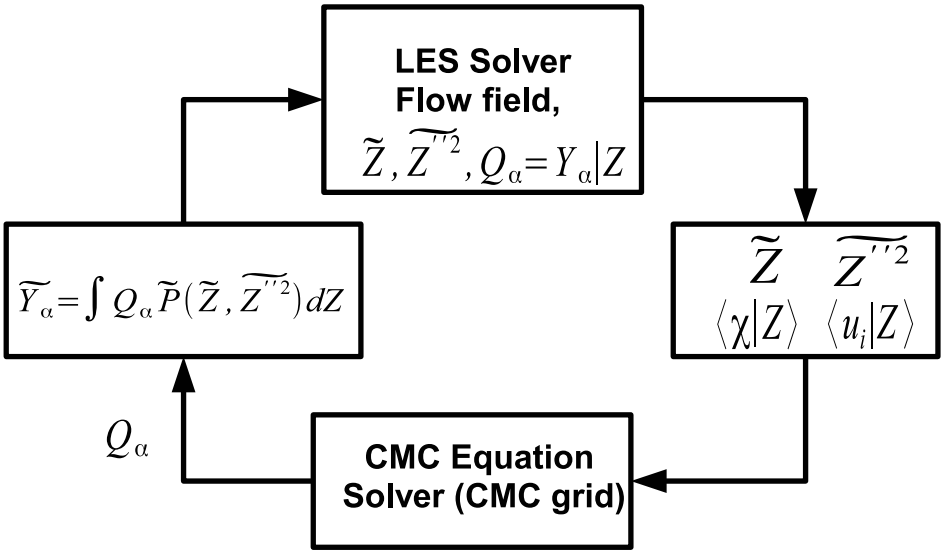

Figure 3.2: Conditional Moment Closure model setup.

the conditional reaction rates. Equations for these conditional variances and covariances can be formulated from the conservation equations. To keep the number of equations small, a reduced chemical mechanism can be used for second-order corrections to the reaction rates. This was done for hydrogen combustion by Kronenburg et al. [59] for improving prediction of the temperature sensitive species NO. For hydrocarbons, this approach has not been successful so far. Kim and Huh [53] have, instead, applied second-order corrections to the forward rates of only a few key reactions and achieved excellent results for piloted-jet diffusion flames. An alternative to second-order closure is to use double conditioning. Kronenburg [60, 61] uses conditional averaging on both mixture fraction and sensible enthalpy. Closure for conditional reaction rates is found to be in excellent agreement with DNS with multi-step chemistry under conditions with strong local extinction and reignition. Full closure will require models for other unclosed terms such as the double conditioned dissipation terms. Provided these challenges can be surmounted, double-conditioning CMC has considerable potential for applica-

tion to flames and practical combustors.

However, CMC model becomes complicated in case of multi-stream mixing. But, the CMC equation in multi-stream mixing will include terms with cross-scalar dissipation rates and velocity conditioned on multiple mixture fractions. Both these terms will need additional modeling and validation effort. Apart from these complex terms, the chemical source term would need a closure using multi-variate PDF, which increases the computational cost. With these complexities, the CMC model is the most complex among the models described in this chapter. But, above all there is an inherent problem for the CMC method for complex geometries: the CMC grid. The model solves the CMC equations on a coarse "CMC" grid, which needs to be carefully defined. For complex geometries this is not always trivial. Thus, with the complexities, and the computational cost, the CMC model is highly unattractive to multi-stream mixing cases.

3.3.1.3 Progress Variable approach

Methods based on progress variable for non-premixed combustion use two key variables to describe the flame: mixture fraction and progress variable. These methods consider the slow chemistry effects (low Da numbers) at a lower computational cost. Instead of using the scalar dissipation rate as a parameter in the flamelet library, the reaction progress variable is used for the parameterization, in addition to the mixture fraction. The source term for the progress variable is tabulated as a function of mixture fraction and progress variable using detailed chemistry. Pierce and Moin [83] [84] first applied the model for LES of a dump combustor stabilized by autoignition. In LES, an additional transport equation is solved for the filtered reaction progress variable, which can, for example, be defined as the sum of the mass fractions of products and intermediate species.

$$\frac{\partial \overline{\rho}\widetilde{Y_c}}{\partial t} + \frac{\partial \overline{\rho}\widetilde{u_j}\widetilde{Y_c}}{\partial x_j} = -\frac{\partial}{\partial x_j}\left[\frac{\partial \overline{\rho}(D+D_t)\widetilde{Y}_c}{\partial x_j}\right] + \widetilde{\dot{\omega}_c} \tag{3.29}$$

The filtered chemical source term in this transport equation is closed using

the flamelet library and a presumed joint FPDF of mixture fraction and reaction progress variable. The advantage of this different way of parameterizing the flamelet library is that it potentially gives a better description of autoignition, local extinction and reignition phenomena. For higher scalar dissipation rates, the reaction progress variable value reduces as a result of faster diffusion of the progress variable out of the reaction zone. This shows that the progress variable approach implicitly considers the effect of scalar dissipation rate. One challenge of using the reaction progress variable is that, in order to close the model, the joint FPDF of mixture fraction and reaction progress variable needs to be provided. In the application of the model to a non-premixed dump combustor geometry by Pierce and Moin [83] [84], a delta-function was used for the FPDF of the reaction progress variable. Comparison with experimental data demonstrated substantial improvement of the predictions compared to SLFM. The progress variable model can be interpreted as a two-variable intrinsically low dimensional manifold (ILDM) model [65], where the ILDM tabulation is generated with a flamelet model. In a priori tests using data from DNS of non-premixed combustion in isotropic turbulence, Sripakagorn et al.[38], Ihme et al. [40] investigated potential areas for improvement of the progress variable model. The model for the presumed FPDF for the reaction progress variable was identified as important. It was also found that the steady-state assumption of the flamelet solutions, especially during reignition at low scalar dissipation rate, is inaccurate. The beta function was proposed as a possible improvement for the reaction progress variable FPDF, and a closure model for the reactive scalar variance equation was provided. New developments include the evaluation and application of the statistically most likely distribution [91] as a new model for the reactive scalar FPDF [41, 42] . The progress variable model can include the non-adiabatic effects with enthalpy as an extra dimension to the table. Various tabulation techniques can be used in the progress variable approach. The choice of the tabulation method depends on the type of flame. To simulate a premixed flame, tabulation based on premixed flame setup is necessary. For autoignition cases, 0D plug flow reactors should be used. In the following, some of the traditional tabulation techniques are briefly described

1. Intrinsic Low Dimensional Manifold ILDM

Maas and Pope's original work [65] proposed an automatic method to apply the steady-state and partial-equilibrium approximations over all possible thermo-chemical states of the system (state space). A thermo-chemical system can be characterized by fast and slow reactions. It is assumed that the fastest reactions can be decoupled from the slow ones. Then, the decoupled fast reactions (those that are faster than the flow time scales) can be ignored while those with slow time scales (rate limiting) are tracked using progress variables. For example, for a particular mechanism, three variables (enthalpy, pressure, and mass fraction of N2) could be selected as the progress variables. By this means, a limited number of progress variables can be used to characterize the entire thermo-chemical system. Once these variables are calculated, all state-space variables, including mass fractions of chemical species, temperature, entropy, and reaction rates, are known. Since the progress variables completely describe the system, only these variables must be transported in CFD. This leads to a dramatic reduction of CPU time for solving the chemistry in a reacting flow calculation.

The ILDM method has been implemented successfully for laminar premixed CO-H2-O2-N2 flames [66]. The CO-H2-O2-N2 ILDM tracks all species, including radicals, within 3% error. In addition, there is a speedup in the calculation of the chemistry by a factor of 10. Xiao et al. [111] simulated a turbulent non-premixed CH4-H2-air flame. A piloted CO-H2-N2-air diffusion flame simulation shows that extinction can be predicted within 5% of the experimental value [78]. A CH4-air combustion system simulation by Yang et al. [112] show that the ILDM method is 1,500 times faster in computing chemistry than a skeletal mechanism GRI 2.11.

The ILDM method is especially suited for non-premixed reacting flow calculations where mixing controls much of the chemical reaction. In partially-premixed reacting flow calculations, ILDM method can lead to higher dimensional manifolds that are more difficult to implement in realistic combustion simulations. Although the ILDM method has been very successful and is widely applied for model reduction in complex hydrocarbon combustion mechanisms, it has some major drawbacks. Calculation of an ILDM is attempted over the whole state space even though some domains of the state

space are never accessed in practical applications. Fixed parameterization does not guarantee the uniqueness or existence of solutions and can yield ill-conditioned equation systems for the manifold. Higher-dimensional manifolds may be required in some regions of the state space (low temperature regions). This means that too few progress variables are tracked and could lead to errors typical of an invalid steady-state approximation. Some ideas have been proposed how to extend the method, but until today no wide-ranging implementation came into application. From the application point of view, a further problem is the fact that the computation of ILDMs for a full concentration range of reaction progress variables is computationally expensive because of the extensive eigenspace decomposition procedures required for each iteration of the algorithm.

2. Flame Prolongated ILDM (FPI) and Flamelet Generated Manifold (FGM)

The ILDM tabulation method described above has a strong mathematical basis, but has a major disadvantage that it does not capture the slow preignition chemistry. The ILDM method is based on time scale separation assumptions, assuming that most chemical processes have a much smaller time scale than the flow time scale. These assumptions, however, give poor approximations in the 'pre-ignition' or 'colder' regions of a flame, where chemical reactions are negligible. There is an important region in flames where reaction and diffusion are in balance. A better approximation of the mixture composition in these regions can be found if we take the most important transport processes also into account.

For turbulent premixed flames, Bradley and co-workers [12] suggested a "laminar flamelet model", where the probability density function ("PDF") of a reaction progress variable based on temperature rise is approximated by a beta function. Mean values of reaction progress and chemical species are obtained by integration over a detailed chemical kinetic laminar flame structure, weighted with the presumed PDF of the reaction progress variable. The influence of turbulent strain on mean reaction progress was taken into account by considering strained laminar flames and/or extinction at a critical strain rate [13]. In the mid-90's, this approach was used at ABB to model (partially) premixed combustion in gas turbines, including the case of non-homogeneous

mixture fraction [4, 90]. A similar approach for modeling autoignition under high pressure Diesel engine conditions was proposed by Chang et al. [20]. A flamelet library for the source term of the progress variable with 5 dimensions (progress variable, mixture fraction mean, mixture fraction variance, scalar dissipation rate and pressure) was built in the pre-processing step. The source term for the progress variable was weighted with the presumed beta-PDF shape of the reaction progress variable (CO_2).

The flamelet model with lookup-table was generalized to more than one progress variable by de Goey and co-workers [25], who coined the popular term FGM "flamelet generated manifolds". The FGM method can be considered as a combination of two approaches to simplify flame calculations, i.e. a flamelet and a manifold approach. The Flamelet-Generated Manifold (FGM) [107] method, shares the idea with flamelet approaches that a multi-dimensional flame may be considered as an ensemble of one-dimensional flames. The implementation, however, is typical for manifold methods: a low-dimensional manifold in composition space is constructed, and the thermo-chemical variables are stored in a database which can be used in subsequent flame simulations. In the FGM method a manifold is constructed using one-dimensional flamelets. Like in other manifold methods, the dimension of the manifold can be increased to satisfy a desired accuracy. The manifolds are built from a set of flamelets, each corresponding to a different mixture fraction. A flamelet is the solution of a low-Mach-number formulation of the one-dimensional Navier-Stokes equations supplemented with detailed chemistry.

Two types of flamelet generated manifolds are possible, viz. premixed and non-premixed [109]. In both manifolds, the chemistry is parameterized as a function of mixture fraction and a progress variable. The chemical source term is divided in a production and a consumption part, consisting of the positive and negative contributions, respectively. In a non-premixed flamelet, fuel enters at one side, and oxidizer enters at the other side. The parameter that determines a single non-premixed flamelet is the strain rate applied on the oxidizer side. To construct a non-premixed manifold, flamelets are computed for a range of strain rates. The function $Z(x)$ is monotonic for each non-premixed flamelet. In a premixed flamelet, fuel and oxidizer enter on the same side,

which is expressed by Dirichlet boundary conditions at the inlet and Neumann boundary condition at the outlet. The flamelet corresponding to the maximum value of strain rate of computed non-premixed flamelets is close to the region of extinction, where steady non-premixed flamelets do not exist. A linear interpolation scheme is used to fill the manifold between the (Z, Y_c) curve represented by the flamelet corresponding to the maximum value of strain rate and the horizontal Y=0 axis. The steady non-premixed flamelet equations do not cover that region. Bilinear interpolation is used when manifold is accessed to return the mass fraction values as a function of mixture fraction and progress variable. FGM was implemented recently by Vreman et. al. [109] for Sandia D and E flames in LES context with respect to mean temperature, mixture fraction and number of species like CO2. However the non-premixed manifold outperforms the premixed manifold for CO and H2. There has been no attempt to simulate an autoignition flame with FGM. Domingo et al. [28] used the FPI with 0D homogeneous reactor tabulation (next section) method for autoignition stabilized flame.

The major advantage of the progress variable methods is the low computational cost for the physical effects that can be captured. This approach is computationally more efficient than the CMC model, and is comparable to the transient laminar flamelet model. But, the model suffers with the disadvantages of the presumed PDF methods, viz. modeling of higher order moments, multi-variate PDF and computational cost of convolution to close the chemical source term. The computational effort of convolution can be reduced by tabulating the convoluted chemical source terms is a function of the first and second order moments. But, the dimension of the table increases non-linearly with the number of mixture fractions. As discussed earlier for the CMC model, the table dimension for ternary will be 5, for quaternary will be 9, and so on. This makes the approach unsuitable for multi-stream mixing. If the problems related to the convolution using multi-variate PDF could be solved, the progress variable approach will be promising for multi-stream mixing problems at relatively low computational cost.

3.3.2 Combustion Models based on Transported PDF approach

The presumed PDF methods described above are advantageous due to their low computational cost. This makes the presumed PDF approaches attractive for industrial applications. However, the disadvantage of the above mentioned presumed PDF approach is that the filtered chemical source term is closed using a model for the PDF shape. The fluctuations of the reactive species are not properly considered. Statistical independence between the mixture fraction and the reactive scalars is usually presumed. Although these assumptions might not be so severe in the partially premixed cases, the major disadvantage of the presumed PDF methods appears for multi-stream mixing configurations. These presumed PDF methods in multi-stream mixing cases need modeling for the higher moments (variances and covariances) as well as the presumed shape of the multi-variate PDF. The transported PDF methods, on the other hand, have an advantage in those respects as the chemical source term is found in a closed form. The extension of this approach to multi-stream cases can be done without additional modeling complexities or assumptions. The only modeling needed in this method is the micromixing term. This term is also crucial in the presumed PDF methods, which is the destruction of the scalar variance in equations (3.18) and (3.13), called as the scalar dissipation rate.

The transported PDF method was introduced by Pope [92]. A transport equation for density weighted one point PDF $\widetilde{f}_\phi$ in time and space for scalar variables $\phi(x,t)(=\phi_1,\phi_2,...\phi_{N_{sp}})$ was derived, which is shown below:

$$\overline{\rho}\frac{\partial\widetilde{f_\phi(\psi)}}{\partial t}+\widetilde{\rho u_j}\frac{\partial\left(\widetilde{f}_\phi(\psi)\right)}{\partial x_j}-\sum_{\alpha=1}^{N_{sp}}\frac{\partial}{\partial\psi_\alpha}\left[\overline{\rho}\dot{\omega}_\alpha(\psi)\widetilde{f_\phi(\psi))}\right]$$
$$=\frac{\partial}{\partial x_j}\left[\left(\overline{\rho}\widetilde{u_j}-\rho u_j|_{\alpha=\psi}\right)\widetilde{f_\phi(\psi)}\right]-\sum_{\alpha=1}^{N_{sp}}\sum_{\beta=1}^{N_{sp}}\frac{\partial^2}{\partial\psi\partial\psi}\left\{\left(D\frac{\partial\phi_\alpha}{\partial x_j}\frac{\partial\phi_\beta}{\partial x_j}\right)|_{\phi=\psi}\widetilde{f_\phi(\psi)}\right\} \tag{3.30}$$

$\psi(x,t)=(\psi_1,\psi_2,...\psi_{N_{sp}})$ is the phase space (sample space variable) for ϕ, u is the mean velocity and $u_i|_{\alpha=\psi}$ the expected value of the fluctuating velocity

conditional on the set of scalars taking the value ψ.

The dependent variable $f_\phi(x,t)d\psi$ is the probability of obtaining the scalar concentration of species ϕ at time t and position x between ψ and $\psi + d\psi$. Each term of the equation is described below:

Left hand side:

1. Temporal variation of the PDF
2. Convection of PDF due to mean velocity u of the flow
3. Chemical reaction (closed).

Right hand side:

1. Conditional turbulent transport term (needs modeling)
2. Micro-mixing term: This term dissipates the scalar fluctuation, i.e. the variance is diminishes and the PDF evolves towards Dirac delta (needs modeling).

The conditional turbulent transport term (first term on the right hand side) is normally modeled by a gradient flux assumption, as done for a general transport equation. The fifth term, viz. the micromixing term that describes the dissipation of the scalar variance, is the only difficult term of the method that needs modeling. The reason for the difficulty is that the one point PDF has no information about the length scales and the scalar gradients. This term is modeled by so called mixing models. The three main issues with the mixing models in PDF methods are that firstly, there is no explicit coupling between mixing and reaction. Secondly, most of the models are non local, i.e. the realizations that have extreme values interact, although this is not possible in reality at the molecular level. None of the models includes a physically realistic representation of fluctuations in scalar dissipation rate. The micromixing term is the weakness of the model, and its modeling is an area of active research.

The numerical solution of the above equation is prohibitively high with conventional finite-difference methods, which was done by Dopazo and OBrien [29] in 1974. Monte Carlo methods are used to solve them as the cost of computation increases only linearly with the number of dimensions.

There are various approaches to solve these equations. The approach introduced by Pope [92] uses Lagrangian particles that represent possible subgrid realizations. The particles carry all the species from the chemical mechanism, and are free to move in the computational domain. In another approach, called the Eulerian particle method, the particles are stationary and jump across the cells according to certain laws. Another approach introduced by Valino [106] and Sabelnikov [100] used an Eulerian approach to model the PDF transport equation. The Lagrangian particle and the Eulerian Stochastic Fields method will be described in the next sections.

3.3.2.1 Lagrangian Particle Monte Carlo Method

Pope [92] developed a method to solve the transported PDF method, which has now become standard. It is based on a Monte Carlo procedure. In this method, the fluid is thought to be comprised of virtual particles.The particles are free to move in space and simultaneously evolve in the composition space. The transport of the particles is governed by following equation:

$$\frac{dx_i^{(j)}}{dt} = v_i^{(j)}(x) \tag{3.31}$$

The velocity vector $v^{(j)}(x)$ consists of convective, drift and stochastic parts. The drift term is the relaxation to the local mean flow velocity. The stochastic term is modeled by Wiener process, which simulates the random walk. For more details on each term, please see [92].

The particles carry species from the chemical mechanism. The composition of a particle evolves according to the following equation:

$$\frac{d\alpha^{(j)}}{dt} = -\frac{\alpha^j - \bar{\alpha}}{T_{turb}} + \omega^j \tag{3.32}$$

The first term is the micromixing term, and the second term is the chemical source term. The chemical source term is a function of the thermo-chemical state of the particle. The chemical source term is thus closed, as no further information is needed. The mixing term shown in Eq. (3.32) is the IEM (Interaction by Exchange with the Mean) model. Many refined micromixing models are available in the literature. The importance of the micromixing term can be demonstrated with an example of a non-premixed flame, where black colored fuel particles are injected in white colored oxidizer particles, and the micromixing term is tuned off. In such a case, the particles maintain their composition and no chemical reactions are possible, as only grey particles (close to stoichiometric) are able to react. At a location, the ensemble of the particle gives the mean mixture fraction and its variance, which describes the macromixing of the particles. The variance would never be zero for mixture fractions other than pure air and fuel stream. Only the micromixing term can bring fuel and oxidizer in contact, and initiate the chemical reactions. The other extreme of the micromixing model is the infinitely fast mixing case, which would lead to no subgrid segregation. Therefore, modeling the mixing term is the most critical issue in the transported PDF methods.

Each particle is assigned a mass. The actual PDF is recovered by sampling the particles falling into all of the finite volume cells and by determining a mean density for each cell. However, such a mean density is not guaranteed to be the same as the one obtained from the finite volume method as the particles move with the mean velocity and some random motions. Similarly, when the joint scalar-velocity PDF is solved, the mean value of fluctuating velocity is likely to deviate from zero (the expected correct value). Correction algorithms are needed to maintain a correct spatial distribution of particles so that the consistency between the finite volume solutions and the stochastic solutions can be maintained at the numerical level. Several studies have been devoted to this difficult numerical issue (e.g., Muradoglu et al, [76] and Chen [8]). So far, these correction algorithms are at best 2nd-order accurate

in space, and they are far from perfect. More critically, these correction algorithms only ensure consistency for statistical averages, but not at any instant, a requirement that is not only highly desirable but perhaps mandatory for LES applications. Hence, Lagrangian hybrid method do not naturally display stochastic convergence in the sense defined above. Tracking and sorting particles consume the majority of computational time. In addition, the CPU time used for such corrections can be significant. Experiences with the RANS applications revealed that the Eulerian Monte Carlo approach, described in the next section, is computationally faster (by roughly a factor of 10) and easier to implement than the corresponding Lagrangian method [75]. Furthermore, for practical geometries, extending the Lagrangian approach to unstructured grids is a challenging task [104], but this extension is straightforward using the Eulerian approach. Finally, creating adaptive Lagrangian schemes appears as a daunting task, given the impossibility of controlling the location of the stochastic particles in the flow field. As a consequence of all of the observations above, the solutions obtained from Lagrangian hybrid algorithms do not display the property of stochastic coherence and are also rich in implementation difficulties. Although the application of transported PDF method substantially increases the computational time, the feasibility of this method for LES was demonstrated in simulation of Sandia D and E flames by Pitsch [97].

3.3.2.2 Eulerian / Stochastic Fields Monte Carlo Method (SF)

The stochastic field method formulated by Valino [106] in 1998 is based on deriving a system of stochastic partial differential equations (SPDE) equivalent to the closed form of the PDF evolution equation. The idea is to represent P_{SGS} by an ensemble of N stochastic fields ξ_α^n twice differentiable in space:

$$\widetilde{f}_\phi(\psi, x, t) = \frac{1}{N}\sum_{n=1}^{N}\prod_{\alpha=1}^{N_{sp}}\delta\left[\psi_\alpha - \xi_\alpha^n(x,t)\right] \tag{3.33}$$

where δ represents the Dirac delta function and N_{sp} is the total number of species α. The N stochastic fields are not a realization of the real field, but constitute a stochastic system equivalent to it. ξ_α^n are differentiable functions

in space at the grid-size level, which is not the case for the real field. In reality, the fields are smooth only at the Kolmogorov length scale. These fields represent possible subgrid scalar values for the thermo-chemical quantities. The above equation is equivalent to the classical representation of the scalar PDF. But ξ_α^n in the present context is not a real field realization, but an Eulerian smooth, grid-size level differentiable field. This is the reason for naming the present method pure Eulerian.

These stochastic fields evolve according to:

$$\begin{aligned}\overline{\rho} d\xi_\alpha^n = &-\overline{\rho}\tilde{u}_i \frac{\partial \xi_\alpha^n}{\partial x_i} + \frac{\partial}{\partial x_i}\left[D\frac{\partial \xi_\alpha^n}{\partial x_i}\right] dt + (2D)^{1/2} D \frac{\partial \xi_\alpha^n}{\partial x_i} dW_i^n \\ &- \frac{\rho}{2\tau_{SGS}}\left(\xi_\alpha^n - \tilde{\phi}_\alpha\right) dt + \rho^n \dot{\omega}_\alpha^n(\xi_\alpha^n) dt\end{aligned} \tag{3.34}$$

This method has been applied to some practical flames in LES context. Mastorakos [35] implemented the method for a reacting plume application with 4 species and 100 fields. Mustata et al. [77] applied the method to Sandia D flame successfully with 16 and 8 stochastic fields with 9 species and found that 8 fields were enough to get satisfactory results. The method was also applied by Jones et. al. [47, 48] to Markides' experiment [70] and the Cabra flame [17] with good prediction of auto-ignition and flame propagation with 9 species and 8 fields. It was recently applied by Jones [50] to the Sandia D, E and F flame with 19 species and 10 stochastic fields.

Finally, it is important to consider the computational cost of the stochastic models in LES. These models need a large number of realizations, i.e. particles or fields, in order to reduce the statistical errors. The number of realizations needed in LES are reduced due to the reason that for a good LES grid, the variance (intensity of unresolved fluctuation) is less than RANS. But, the inherent transientness of LES increases the computational cost. For every time step the stochastic equations should be solved for each realization for all the species. The number of equations to be solved every time step are: $N_{species} * N_{fields/particles}$. This makes the approach too expensive to use them for industrial applications with a full set of chemical species.

4 Model formulation

4.1 Combustion model assessment

The principal objective of the present work is to conceptualize and implement a turbulent combustion model suitable for autoignition in LES for industrial applications. Industrial applications involve various complexities like complex geometries, broad range of turbulent scales and multi-stream mixing. Apart from these aspects, the computational cost and model implementation effort should be kept as small as possible.

The combustion models described in the previous chapter are argued to be suitable for autoignition. Intensive work has been carried out on the validation of the models as discussed in the previous chapters. But, most of the validation work has been carried out on laboratory size experimental measurements with two stream mixing. Table 4.1 compares the models qualitatively for various criteria. Only those models that have been validated in the literature have been included.

Table 4.1: Qualitative model comparison

Criteria	Transported PDF (detailed chemistry)	CMC (detailed chemistry)	Progress Variable Methods (Tabulated Chemistry)	
			Transient Flamelet	Autoignition tabulation
Autoignition	++	++	+	++
Flame Propagation	+	+	+	+
Multi-stream mixing	++	--*	--*	--*
Computational cost	--	-	++	++
Implementation effort	--	--	-	+

* maximum 3 streams (ternary mixing)

The first two criteria, i.e. autoignition and flame propagation, must be fulfilled by the model. Multi-stream mixing is one of the major aspects that is behind the motivation of the present work. The other two criteria, viz. the computational cost and implementation effort, are generally applicable for all industrial applications. The implementation efforts involve the complexity of the model, the validation effort and errors that comes with it. The models are rated with "+" and "-" symbols. A double rating is given in order to include a relative comparison between the models.

The transported PDF methods using detailed chemistry, both Lagrangian and Eulerian, capture autoignition and flame propagation. No scale separation (fast or slow chemistry) is made in the formulation of the model. They are not only applicable for autoignition cases, but also for premixed (propagating) and diffusion flames. The models also allow for multiple number of streams, but have have a major drawback of computational cost, especially in LES. The contributors to the computational cost are the number of realizations and in addition the number of species in the chemical mechanism. Although the Eulerian transported PDF model (stochastic fields) using detailed chemistry has been applied to academic test cases [47–50], its computational cost with complex chemical mechanisms is too high to be used for industrial applications. For e.g., using the stochastic fields method with 8 fields and GRI chemical mechanism for hydrocarbon combustion [31] with 53 species, the number of transport equations to be solved is $53 \times 8 = 424$. The computational cost of solving these equations will depend on the efficiency of the solver. But, in relation to the equations solved in LES for the conservation of mass, momentum, energy as well as the species transport (53), the number of additional model equations is at least 8 times. Even with the ever increasing computational processing speed, the use of the transported PDF model with detailed chemistry is impractical, at least in the near future. In addition to the computational cost, the memory demand is also intractable. For detailed mechanisms with hundreds of species and thousands of reactions, the model becomes unattractive from the industrial applications point of view. The final criterion, the implementation effort, is highest for the transported PDF method among the models mentioned in table 4.1. Major implementation efforts are needed in the memory management. The computational cost is too high to validate the

model in LES.

The remaining models in table 4.1, viz. CMC and progress variable, are based on presumed PDF method for the turbulence-chemistry interaction. The table shows a negative rating for all these models when it comes to multi-stream mixing cases. There are three major problems related to approaches based on presumed PDF methods for multi-stream mixing configurations:

1. Modeling second order moments, i.e variances and co-variances. The transport equations for the co-variances involve complex cross-scalar dissipation rates, which are difficult to model.
2. Modeling the multi-variate presumed PDF shape: The PDF shape should not only consider the variances, but also co-variances of the various streams. The modeling complexity and computational effort for a multi-variate PDF increases rapidly with the number of streams.
3. Filtered source term calculation (convolution time): The time for convolution over the various dimensions of the conserved scalars increases exponentially with the number of streams. The convolution time can be reduced by tabulating the chemical source term as a function of the first and second order moments in a pre-processing step. This is possible for a small number of streams (up to ternary mixing). But, with large number of streams, the increased number of dimensions make it unrealistic to tabulate the source term. For example, in a 4-stream mixing case, 9 dimensions are necessary (3 means, 3 variances and 3 covariances).

For multiple number of streams, the modeling complexity, computational cost and errors make the presumed PDF methods disadvantageous. Apart from these general problems with presumed PDF approach, there are some specific problems related to individual models. The CMC model is computationally expensive due to the numerous transport equations for conditioned reactive scalars that need to be solved. The number of CMC equations depend on the number of species and number of points in the mixture fraction space, on which the species are conditioned. The computational cost can not be compared with directly with the transported PDF method, as the CMC

equations are solved on a coarse ”CMC grid”. Almost all the terms in the CMC equation 3.28 need to be modeled. Implementing the model needs a lot of effort in validating those terms. The conditioned scalar transport equations involve terms with scalar dissipation rate conditioned on mixture fraction, which needs to be modeled. In case of multiple mixture fractions, the terms with multiple conditioned cross-scalar dissipation rates arise. Modeling these terms is on one hand difficult, and on the other hand is complex and introduces errors. Another problem with the CMC model is that it needs a proper distribution of the ”CMC grid-points” in the computational domain. The quality of CMC results depend on the distribution of these points, on which the CMC equations are solved. For complex industrial geometries, the distribution must be carefully controlled and needs a check each time the geometry changes.

The progress variable methods with transient flamelet and autoignition (reactor based) tabulation have low computational cost. The transient flamelet model has been validated for autoignition stabilized flames [40–44], but not for various regimes of auto-ignition described in section 2.2. Therefore it has only one ”+” sign in table 4.1 for autoignition. The implementation effort is lower compared to the transported PDF or CMC, but more in comparison to progress variable.

The only models that satisfy most of the criteria are the transported PDF approaches and the progress variable methods with tabulated chemistry and presumed PDF. The former has computational cost disadvantage, whereas the later has unavoidable modeling complexities or inaccuracies. With these disadvantages of the available combustion models, the need of a combustion model in LES to capture complex multi-stream mixing and autoignition at low computational cost becomes evident.

4.2 Model conceptualization

The model assessment in previous section shows that there is no computationally efficient combustion model available in the literature for industrial

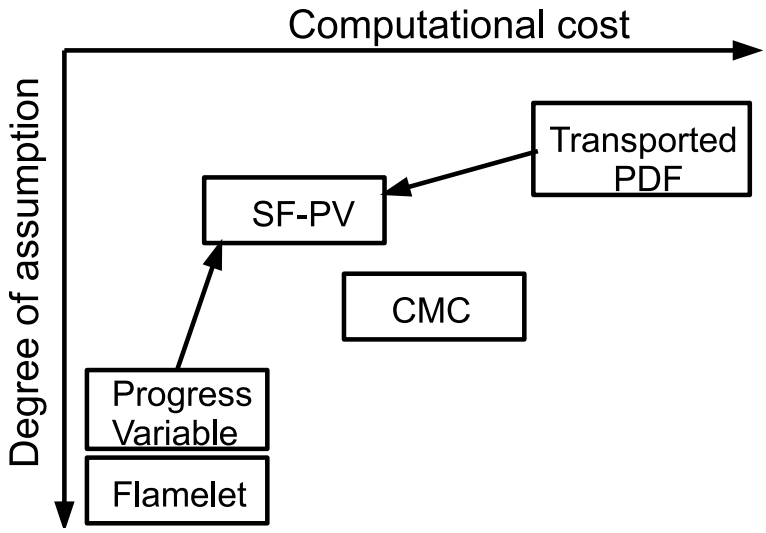

Figure 4.1: Overview of models for autoignition modeling.

applications with multi-stream mixing in LES context. This section describes a novel model that combines the advantages of some of the available models described in section 4.1and fulfills all the criteria mentioned in table 4.1.

The combustion models described in the previous chapter are qualitatively compared in Fig. 4.2. On the X-axis is the relative computational cost and Y-axis is the relative degree of assumptions made in the formulation of the model. The suitable model should be as close to the origin as possible with low computational cost and low degree of assumptions that capture the physics of the problem.

The transported PDF model fulfills all the criteria, but is located towards far extreme on the computational cost axis. The progress variable approach is computationally efficient but suffers for multi-stream mixing configurations due to the presumed PDF approach, which need numerous assumptions and introduce errors and modeling complexities. The novel approach proposed in this work combines the two models located on far extremes and results in a model that is computationally less expensive, captures all the necessary physical phenomena and exclude modeling complexities and errors. Out of

the two transported PDF methods described before, viz. Lagrangian particle method and Eulerian fields method, the later has been chosen. The tabulated chemistry method used in the progress variable approach is used for chemistry reduction. Thus, the proposed model treats the conserved scalars (mixture fractions) and the progress variable stochastically rather than an entire set of chemical species in a mechanism, as done in classical transported PDF methods. The modeling difficulties of presumed PDF shape and second order moments are avoided by the transported PDF model, whereas the computational cost is reduced by the use of tabulated chemistry. The computational cost is reduced as only very few conserved and reactive scalars, i.e. mixture fractions and progress variable, are transported in the model.

One of the inherent advantages of the model is that regardless of the type of fuel and the size of chemical mechanism, the computational cost in LES is unchanged. The tabulation time depends on the size of the chemical mechanism, but is generally negligible compared to the cost of LES. The model also provides freedom to choose the method of tabulation depending on the type of the flame. As the present work concentrates on auto-ignition modeling, tabulation based on 0D homogeneous (plug flow) reactors is used. But, other methods like FGM, FPI, or their combination can also be used. This also implies that the model can be used as a framework for various types of flames.

The following section 4.3 describes the stochastic fields turbulence chemistry interaction model using tabulated chemistry, followed by an example of the extension of the model to multi-stream mixing.

4.3 Model description

The model proposed in the present work for turbulent autoignition in LES is based on tabulated chemistry and stochastic fields turbulence chemistry interaction model. Both the elements of the model are described in the following two subsection. The combined model is subsequently described for binary (2-stream) and ternary (3-stream) mixing cases.

4.3.1 Tabulation method

Various methods of chemistry tabulation are described in section 3.3.1.3. The ILDM method has a drawback at low temperatures, which makes it unsuitable for auto-ignition applications. The FGM and FPI tabulation methods are based on the reaction-diffusion balance, and only burning solutions are available. However, the radical build-up during the induction period, which is comparatively slow and not associated with significant heat release, does not lead to the formation of thin reactive-diffusive structures, as shown by the DNS of Mastorakos et al. and Sreedhara et al. [73, 102]. An adaptation to auto-ignition in a turbulent jet-in-cross-flow configuration, as it is found in reheat combustors, was proposed by Brandt et al. [14, 15, 46], with a progress variable based on intermediate species formed during the induction period. Their work was based on tracking CH2O radical, which is an excellent indicator of autoignition for hydrocarbons. This is evident from the Fig. 2.8. The lookup-table was built from 0D reactors with detailed chemistry, rather than reactive-diffusive structures. For large eddy simulation of partially premixed or non-premixed flames, formulations based on progress variable and mixture fraction were proposed by Pierce and Moin [83, 84] and Vervisch and coworkers [27,28,108]. These approaches extended the definition of the progress variable to include product species in addition to the intermediate. Combustion products ('CO2' for hydrocarbons and 'H2O' for hydrogen) are used. This definition of the progress variable extends to equilibrium, which includes the "autoignition location" and "heat release" phases of combustion during the build-up of the progress variable.

The proposed definition of the composite progress variable (intermediate and product) for hydrocarbons proposed in the present work is defined as: $CH_2O + CO + CO_2$. For hydrogen combustion, H_2O is a natural choice for the product species. The HO_2 radical is an excellent representative of the radical pool build-up. Thus, for hydrogen combustion the composite progress variable is defines as: $HO_2 + H_2O$.

The tabulation method used in the present work is based on the following system of ODEs (Ordinary Differential Equations) that is solved by the chemical

kinetics code (Cantera [38] in the present work):

$$\rho \frac{\partial Y_\alpha}{\partial t} = \dot{\omega}_\alpha \tag{4.1}$$

where $Y_\alpha = (Y_i, h)$. Initial conditions of the reactors are imposed as a function of the mixture fraction given by:

$$Y_\alpha^{t=0} = Y_{\alpha,oxidizer} + Z(Y_{\alpha,fuel} - Y_{\alpha,oxidizer}) \tag{4.2}$$

The initial conditions of the reactors are calculated by equation (4.2) using the fuel and oxidizer boundary conditions. The reactors are run independently from the mixing state to the equilibrium. During the marching of the reactor, the rate of change of progress variable (chemical source term) is tabulated along the progress variable build-up. Figure 4.2 shows typical results obtained with the mechanism for hydrogen oxidation of Li et al. [64]. On the right hand side of Fig. 4.2, the initial source term is shown as a function of mixture fraction. It is interesting to note that the source term is not zero at PV=0.0. This is the reason why at low temperature conditions, where steady state or partial equilibrium assumptions may not be invoked, the concept of chemistry tabulation based on mixture fraction and progress variable was shown to perform better than the ILDM method [37]. The source term is maximum for leaner mixtures $Z < Z_{st}$ ($Z_{st} = 0.17$), due to the mixing between cold fuel and hot oxidizer. Figure 4.2 on the left shows a non-linear increase in the source term as the reactions progress (increase in PV).

There is no interaction between the reactors during the evolution. This is a strong assumption. To testify this assumption Brandt et al. [14] performed 0D reactor mixing studies. The overall error remained below 10%. Both the build-up of radical species during the induction period and the rapid conversion of fuel and oxidizer to final products after ignition control the distribution of heat release in autoignition combustion [30]. When defining a progress variable, one must ensure that for given mixture fraction, the progress variable Y_c increases monotonously from initial conditions up to equilibrium [84]. Recently, the method was tested for hydrogen autoignition by Galpin et al. [32]

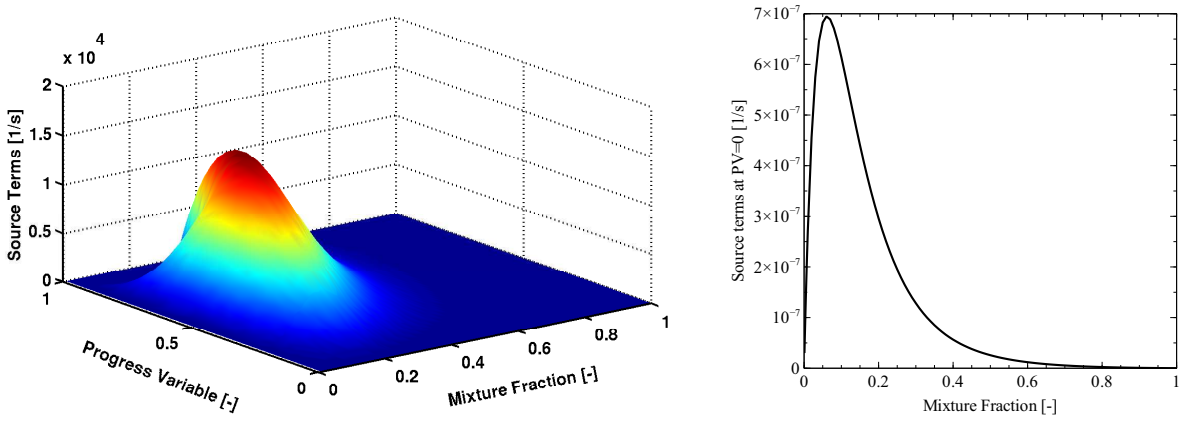

Figure 4.2: Left: Progress variable source term $\dot{\omega}_{Y_c}$ vs. mixture fraction Z and normalized progress variable PV for Case 0 computed with Li [64] mechanism. Right: Initial PV source term ($PV = 0.0$). Boundary conditions: Case 0 described in table 5.1.

using a presumed PDF approach. Kulkarni et al. [62] validated the method for the same case and demonstrated the capability of the model to capture various regimes of autoignition described in Fig. 2.4. They used combined HO_2 and H_2O as the definition of the progress variable. The chemistry was tabulated by running 0D premixed plug-flow reactors for various mixture fractions. The combined homogeneous reactors and FPI tabulation was shown to be applicable for methane lifted flames by Domingo et al. [28].

The model is suitable for the simulation of partially premixed case, but its extension for multi-stream cases is not trivial. One has to model the second order moments (variance, co-variance) and needs a presumed shape of the PDF in multi-dimensions. This increases the complexity and errors. Moreover, the time for convolution over the multi-dimension increases with the number of streams.

4.3.2 Turbulence-chemistry interaction

The stochastic fields model for a general reactive scalar was derived by Sabelnikov [100] and Valino [106] using Stratonovich and Ito calculus, respectively.

Ito and Stratonovich calculus extend classical calculus to stochastic processes. They allow one to integrate one stochastic process with respect to another stochastic process. The major difference between Ito and Stratonovich is that Ito integral considers ”left hand sum”, i.e. information available from the previous time-step, whereas the Stratonovich considers ”mid-point sum” by estimating a value for the next time-step. The Ito formulation does not ”look into the future”. In financial mathematics, the Ito interpretation is usually used as one only has information about the past events, and hence the Ito interpretation is more natural. For the Ito formulation, the restriction from the point of view of modeling is that for solvers using implicit time schemes (internal iterations), the stochastic term should be evaluated only once per time step, i.e. in the first iteration, and should be kept constant throughout the time-step. The Stratonovich calculus does not put these restrictions, and classical calculus rules can be used. The stochastic PDEs derived by Sabelonikov using Stratonovich calculus is a convection-reaction type with diffusion modeled by additional convective-drift terms. These type of equations are numerically inefficient from computational cost and convergence point of view. The formulation based on Ito calculus by Valino is convective-diffusive-reactive type, which does not suffer from these numerical drawbacks.

The Stratonovich integral can readily be expressed in terms of the Ito integral. Whichever formulation one takes, the results should be similar provided that they are implemented properly [33]. The Ito formulation is used in this work due to its numerical advantage for Eulerian solvers. A detailed derivation is provided by Valino [106]. The one point transported PDF Eq. 3.30 by Pope [92] is the starting point in the derivation.

The one point transported PDF has no length information and therefore needs modeling for the term containing the scalar gradient. The terms are the conditioned velocity and the micro-mixing. The conditioned velocity term is modeled using the scalar gradient assumption. Various models are available for the micro-mixing term. The one used by Valino, called the IEM (Interaction by Exchange with the Mean), is used in this work. According to [106], only those mixing models that are continuous can be used in the Eulerian formulation of the stochastic fields. The convected PDF Eq. (3.30) using the two models is

given by:

$$\overline{\rho}\frac{\partial\widetilde{f_\phi(\psi)}}{\partial t}+\widetilde{\rho u_j}\frac{\partial\left(\widetilde{f}_\phi(\psi)\right)}{\partial x_j}-\frac{\partial}{\partial\psi_\alpha}\left[\rho(\psi)\dot{\omega}_\alpha\widetilde{f_\phi(\psi)}\right] \tag{4.3}$$

$$=\frac{\partial}{\partial x_j}\left(D_{eff}\frac{\partial\left(\widetilde{f}_\phi(\psi)\right)}{\partial x_j}\right)-\frac{\partial}{\partial\psi_\alpha}\left[\frac{\psi_\alpha-\bar{\alpha}}{T_{eddy}}\right]$$

The stochastic fields method uses a number of Eulerian 'stochastic fields' defined by ξ_α^n, with $n=1...N_f$, where N_f is the number of fields. Number of fields is variable and is an important model parameter. Each of the fields is extended over the whole spatial domain of the flow. Each field contains a value for all the transported scalars of interest α at a node. The ensemble of the values of the scalar over all the fields at a certain node is statistically equivalent to a one point joint PDF at that point.

$$\xi_\alpha^n(x,t)=\frac{1}{N}\sum_{n=1}^{N}\sum_{\alpha=1}^{N_s}\delta\left[\psi_\alpha-\xi_\alpha^n(x,t)\right] \tag{4.4}$$

Equation 4.3 can be converted to an equivalent Fokker Planck equation using the chain rule. For the Fokker Planck equation, there is an equivalent stochastic PDE given by:

$$\begin{aligned}\overline{\rho}d\xi_\alpha^n&=-\overline{\rho}\tilde{u}_j\frac{\partial\xi_\alpha^n}{\partial x_j}dt+\frac{\partial}{\partial x_j}\left[D_l+D_{sgs}\frac{\partial\xi_\alpha^n}{\partial x_j}\right]dt\\&+\overline{\rho}(2D_l+D_{sgs})^{1/2}\frac{\partial\xi_\alpha^n}{\partial x_j}dW_i^n-\frac{\rho}{2\tau_{SGS}}\left(\xi_\alpha^n-\tilde{\phi}_\alpha\right)dt\\&+\rho^n\dot{\omega}_\alpha^n(\xi_\alpha^n)dt\end{aligned} \tag{4.5}$$

The equation has a model for the two terms, i.e. the conditioned convection and the micro-mixing, but the chemical source term is closed. This closed chemical source term is the major advantage of this method. The above

stochastic partial differential equation is generally solved for all the species in the chemical mechanism. The source term for a species on a field are function of all the thermo-chemical properties of the mechanism. As the stochastic fields are continuous in space (twice differentiable), an existing Eulerian solver can be used to solve the above equations. Care should be taken for solving the stochastic term. The Wiener process in the stochastic term is independent of the time step. Therefore, the term should either be solved explicitly (by splitting the time step) or kept constant throughout the time step while using iterative solvers.

The first and the second term on the right hand side of the equations are the convective and diffusive terms, respectively. The third term on the right hand side is the stochastic term. The stochastic term depends on the effective diffusivity, gradient of the scalar and the Wiener term. The Wiener term is approximated by time-step increments $dt^{1/2}\eta_i$, where η_i is a dichotomous random number. The dichotomous random number η_i [-1,+1] is not the same in different directions, but is same for a particular field for all the scalars. The random number is different for different fields. One of the restrictions on the random numbers is that the sum of all the random numbers in a direction should sum up to 0. The fourth term is the micro-mixing model. The one used in this work is the IEM (Interaction by Exchange with the Mean) model. The sub-grid time scale is $\tau_{sgs} = \left(\frac{\mu+\mu_{sgs}}{\bar{\rho}\Delta^2}\right)^{-1}$.

The above stochastic partial differential equation has been used with detailed chemistry for modeling autoignition [47,48], diffusion flames [50,77] and premixed flames [94]. The computational cost of the model is high due to the number of SPDEs to be solved ($N_{species} * N_{fields}$). For industrial applications with complex fuels, using the above equation for all the species is impractical. In the present work, the above model is combined with the tabulation methods described in section 3.3.1.3. Instead of using detailed chemistry, only key parameters (i.e. the dimensions of the tabulated chemistry) are transported. Following section describes the model for a binary autoignition case.

4.3.3 Model Concept for Autoignition in Binary Cases

The stochastic fields turbulence-chemistry interaction described above has a modeling advantage over the presumed PDF approaches, but comes at a higher computational cost. To reduce it, attempts have been made to reduce the chemical mechanism [50]. The performance of the overall approach using reduced chemistry and the stochastic fields model depends on the accuracy of the reduced chemical mechanism.

The tabulation methods described in section 3.3.1.3 use key parameters like the mixture fraction and progress variable to describe the thermo-chemical states attained during combustion. The tabulation methods have been validated and provided excellent results with the presumed PDF approaches at low computational cost [28, 32, 62]. The present work proposes a combination of the tabulated chemistry and the stochastic fields method for combustion. The method of tabulation may differ depending on the type of flame one wants to simulate. The present subsection considers a binary (two-stream) mixing case. In the next section, the extension of the model to ternary case will be described.

Equation (4.5) is valid for both conserved and non-conserved scalar. The SPDEs for a conserved scalar will have no chemical source term. The fields would describe the mixing state, i.e. the mean and the variance. In the tabulated chemistry approach based on mixture fraction, the table consists of two dimensions: conserved (mixture fraction Z) and reactive (progress variable Y_c). In the combined stochastic fields - tabulated chemistry approach, SPDEs are solved for the two dimensions. The SPDEs solved in the model are equivalent to the SPDE 4.5. Eq. 4.6 and 4.7 describe the SPDEs for the mixture fraction Z and the progress variable Y_c, respectively:

$$\begin{aligned}\bar{\rho}\frac{dZ^n}{dt} &= -\bar{\rho}\widetilde{u}_j\frac{dZ^n}{dx_j} + \bar{\rho}\frac{d}{dx_j}\left[(D_l + D_{sgs}))\frac{dZ^n}{dx_j}\right] \\ &+ \bar{\rho}(2(D_l + D_{sgs}))^{1/2}\frac{dZ^n}{dx_j}\frac{dW_i^n}{dt} - \frac{\bar{\rho}}{2\tau_{sgs}}\left(Z^n - \widetilde{Z}\right)\end{aligned} \tag{4.6}$$

$$\begin{aligned}\bar{\rho}\frac{dY_c^n}{dt} &= -\bar{\rho}\widetilde{u}_j\frac{dY_c^n}{dx_j} + \bar{\rho}\frac{d}{dx_j}\left[(D_l + D_{sgs}))\frac{dY_c^n}{dx_j}\right] \\ &+ \bar{\rho}(2(D_l + D_{sgs}))^{1/2}\frac{dY_c^n}{dx_j}\frac{dW_i^n}{dt} - \frac{\bar{\rho}}{2\tau_{sgs}}\left(Y_c^n - \widetilde{Y_c}\right)dt \\ &+ \bar{\rho}\dot{\omega}_c^n(Z^n, Y_c^n)\end{aligned} \tag{4.7}$$

The stochastic fields $Z^n(x,t)$ correspond to an equivalent stochastic system of one-point PDFs. The last term in Eq. (4.7) is the chemical source term of the progress variable. This term is absent in the mixture fraction PDE as the mixture fraction is a conserved scalar. The source term of the progress variable is a function of the mixture fraction and the progress variable of that particular field.

The fields can be used to represent the density-weighted sub-grid PDF of the scalar by

$$P_{sgs}(Z;x,t) = \frac{1}{N}\sum_{n=1}^{N}\delta\left[Z - Z^n(x,t))\right] \tag{4.8}$$

The first two moments (mean and variance) can be evaluated by

$$\widetilde{Z} = \frac{1}{N}\sum_{n=1}^{N} Z^n \tag{4.9}$$

$$\widetilde{Z^{"2}} = \frac{1}{N}\sum_{n=1}^{N}\left(Z^n - \widetilde{Z}\right)^2 \tag{4.10}$$

The source terms for the species and the energy equation solved in LES can be calculated from

$$\widetilde{\dot{\omega}_\alpha} = \bar{\rho}\frac{1}{N}\sum_{n=1}^{N}\dot{\omega}_\alpha^n(Z^n, Y_c^n) \tag{4.11}$$

The performance of the proposed approach will depend on the assumptions made in the individual models. These assumptions are listed in the following:

1. The reaction progress is described by a progress variable Y_c. The mixture fraction and the progress variable describe the thermo-chemical state attained during combustion. For auto-ignition, a composite progress variable including an intermediate species is appropriate, as described in section 4.3.1.

2. No thin reaction-diffusion structures, as used for the description of the diffusion flames, are formed during the induction period [73, 102] in an autoignition case. The tabulation method used in the present work is consequently based on homogeneous reactor data, and not on flamelet type of tabulation like FGM, FPI or SLFM described in section 3.3.1.3. Although no reaction-diffusion structures are found before ignition, the SDR affects the chemical reactions through micro-mixing of radicals. The effect of SDR of species/radicals is considered by the micro-mixing term in the SPDEs 4.6,4.7. Other tabulation methods described in section 3.3.1.3 can also be used, depending on the physics of the flame that one wants to capture. For example, in case of diffusion flames, tabulation based on flamelet based methods can be used. Similarly, for premixed flames, tabulation based on FPI can be used.

3. The mixing at the molecular level (micro-mixing) is modeled using the IEM (Interaction by Exchange with the Mean) model. The choice of the model in the present work is made due to its simplicity and widespread use.

Following are the major advantages of the model:

1. As the chemical source term is a function of the mixture fraction and the progress variable for a particular field, the chemical source term is found in closed form. No higher order moment and presumed PDF shape modeling is necessary. This is the inherent advantage of the transported PDF methods to simplify its extension to multi-stream mixing from the modeling point of view. The extension to multi-stream mixing cases is described in the next section.

2. Although higher than the presumed PDF approaches, the computational

cost of the approach is considerably lower than the transported PDF methods with detailed chemistry.

3. The model is applicable for any kind of fuel, provided a suitable progress variable is chosen.The computational cost of the combustion model in LES does not change with the type of fuel or the size of the detailed chemical mechanism. The size of the chemical mechanism increases the tabulation time, but is usually negligible compared to LES.

4. The model described in this chapter considered adiabatic cases, but can be extended to include non-adiabatic effects. In adiabatic cases, the total enthalpy is conserved. In non-adiabatic cases, the heat (total enthalpy) loss information should be included as an extra dimension in the look-up table. One can either transport the total enthalpy on the stochastic fields or make a simplifying assumption of low total enthalpy subgrid segregation and use its filtered value for all the fields. This extension does not include any modeling complications, and can be included with a reasonable additional computational cost.

4.3.4 Model Extension to Multi-stream Mixing Cases

For modeling multi-stream mixing, the tabulation methods based on progress variable approaches should include multiple mixture fractions. For a general system with N_s number of streams, the look-up table has $Z_1, Z_2, ...Z_{N_s-1}$ dimensions in addition to the progress variable. The general equations for multi-stream mixing are described in this section.

For the description of the stochastic fields for the mixture fraction Z_1^n, subscript corresponds to the mixture fraction and the subscript corresponds to the field on possible subgrid realization. N is the number of stochastic fields. A single field n consists of the following set of transported scalars: $Z_1^n, Z_2^n, ...Z_{N_s}^n, Y_c^n$. Following SPDEs describe the mixing between the streams:

$$
\begin{aligned}
&\bar{\rho}\frac{dZ_1^n}{dt} = -\bar{\rho}\widetilde{u}_j\frac{dZ_1^n}{dx_j} + \bar{\rho}\frac{d}{dx_j}\left[(D_l + D_{sgs}))\frac{dZ_1^n}{dx_j}\right] \\
&+ \bar{\rho}(2(D_l + D_{sgs}))^{1/2}\frac{dZ_1^n}{dx_j}\frac{dW_i^n}{dt} - \frac{\bar{\rho}}{2\tau_{sgs}}\left(Z_1^n - \widetilde{Z_1}\right) \\
&\qquad\qquad\qquad\qquad . \\
&\qquad\qquad\qquad\qquad . \\
&\qquad\qquad\qquad\qquad . \\
&\bar{\rho}\frac{dZ_{N_s}^n}{dt} = -\bar{\rho}\widetilde{u}_j\frac{dZ_{N_s}^n}{dx_j} + \bar{\rho}\frac{d}{dx_j}\left[(D_l + D_{sgs}))\frac{dZ_{N_s}^n}{dx_j}\right] \\
&+ \bar{\rho}(2(D_l + D_{sgs}))^{1/2}\frac{dZ_{N_s}^n}{dx_j}\frac{dW_i^n}{dt} - \frac{\bar{\rho}}{2\tau_{sgs}}\left(Z_{N_s}^n - \widetilde{Z_{N_s}}\right)
\end{aligned}
\tag{4.12}
$$

The mixture fractions develop independently. The progress variable equation for the multi-stream mixing problem is given by:

$$
\begin{aligned}
&\bar{\rho}\frac{dY_c^n}{dt} = -\bar{\rho}\widetilde{u}_j\frac{dY_c^n}{dx_j} + \bar{\rho}\frac{d}{dx_j}\left[(D_l + D_{sgs}))\frac{dY_c^n}{dx_j}\right] \\
&+ \bar{\rho}(2(D_l + D_{sgs}))^{1/2}\frac{dY_c^n}{dx_j}\frac{dW_i^n}{dt} - \frac{\bar{\rho}}{2\tau_{sgs}}\left(Y_c^n - \widetilde{Y_c}\right)dt \\
&+ \bar{\rho}\dot{\omega}_c^n(Z_1^n, ..., Z_{N_s}^n, Y_c^n)
\end{aligned}
\tag{4.13}
$$

All the terms in the above equations are similar except the chemical source term, which is a function of the mixture fractions and the progress variable. It is important to observe at this point that the co-variance of the mixture fractions is considered implicitly by the model, which is generally neglected in the presumed PDF approaches. Also, the fluctuations of the progress variable are considered by the stochastic fields method. The presumed PDF methods neglect the mixture fraction conditioned fluctuations of the progress variable, which might be important in extinction and reignition cases. This makes the model suitable for cases with a wide range of Da numbers. In the following subsection, an example of the model extension to ternary mixing case is presented.

4.3.5 Model description for ternary mixing

A ternary mixing case can be described by two mixture fractions Z_1 and Z_2. Tabulation of the reaction source term needs to be carried out for combinations of the two mixture fractions. The constraint for the tabulation is that the summation of the two mixture fraction is less than one, leading to a triangular zone for the tabulated region shown in Fig. 4.3.

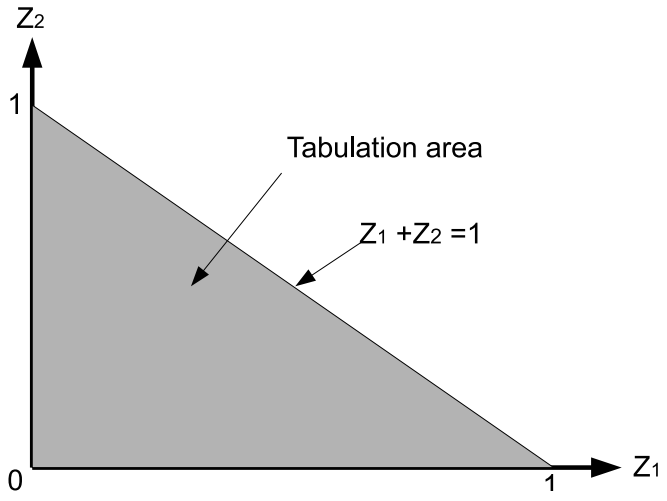

Figure 4.3: Tabulation triangle for ternary mixing.

The initial conditions (reactant mass fractions and enthalpy) for the homogeneous reactors are calculated using:

$$\alpha_i^{t=0} = Z_1 * \alpha_{i,Z_1} + Z_2 * \alpha_{i,Z_2} + (1 - Z_1 - Z_2) * \alpha_{i,Z_3} \tag{4.14}$$

0D homogeneous reactors with species and enthalpy as a linear combination of the mixture fractions are run from the initial state to equilibrium. The look-up table has three dimensions: two mixture fractions and the progress variable. Equation 1 is valid for both mixture fractions.

$$\begin{aligned}\bar{\rho}\frac{dZ_1^n}{dt} &= -\bar{\rho}\widetilde{u}_j\frac{dZ_1^n}{dx_j} + \bar{\rho}\frac{d}{dx_j}\left[(D_l + D_{sgs}))\frac{dZ_1^n}{dx_j}\right] \\ &+ \bar{\rho}(2(D_l + D_{sgs}))^{1/2}\frac{dZ_1^n}{dx_j}\frac{dW_i^n}{dt} - \frac{\bar{\rho}}{2\tau_{sgs}}\left(Z_1^n - \widetilde{Z_1}\right)\end{aligned} \tag{4.15}$$

$$\begin{aligned}\bar{\rho}\frac{dZ_2^n}{dt} &= -\bar{\rho}\widetilde{u}_j\frac{dZ_2^n}{dx_j} + \bar{\rho}\frac{d}{dx_j}\left[(D_l + D_{sgs}))\frac{dZ_2^n}{dx_j}\right] \\ &+ \bar{\rho}(2(D_l + D_{sgs}))^{1/2}\frac{dZ_2^n}{dx_j}\frac{dW_i^n}{dt} - \frac{\bar{\rho}}{2\tau_{sgs}}\left(Z_2^n - \widetilde{Z_2}\right)\end{aligned} \tag{4.16}$$

Eight fields are used in the present work. Each field carries a reactive scalar, i.e. the progress variable, in addition to the conserved mixture fractions. The source term for the progress variable in Eq. (4.7) is then a function of the mixture fractions and the progress variable for a particular field $\bar{\rho}\dot{\omega}_c^n(Z_1^n, Z_2^n, Y_c^n)$. The equation would be:

$$\begin{aligned}\bar{\rho}\frac{dY_c^n}{dt} &= -\bar{\rho}\widetilde{u}_j\frac{dY_c^n}{dx_j} + \bar{\rho}\frac{d}{dx_j}\left[(D_l + D_{sgs}))\frac{dY_c^n}{dx_j}\right] \\ &+ \bar{\rho}(2(D_l + D_{sgs}))^{1/2}\frac{dY_c^n}{dx_j}\frac{dW_i^n}{dt} - \frac{\bar{\rho}}{2\tau_{sgs}}\left(Y_c^n - \widetilde{Y_c}\right)dt \\ &+ \bar{\rho}\dot{\omega}_c^n(Z_1^n, Z_2^n, Y_c^n)\end{aligned} \tag{4.17}$$

The filtered source terms for the species and heat release will also be a function of the mixture fractions and the progress variable given by Eq. (4.17).

$$\widetilde{\dot{\omega}_\alpha} = \bar{\rho}\frac{1}{N}\sum_{n=1}^{N}\dot{\omega}_\alpha^n(Z_1^n, Z_2^n, Y_c^n) \tag{4.18}$$

The chemical source term for the progress variable is thus closed avoiding the problem of modeling the higher order moments of the mixture fraction

and the multi-dimensional PDF, which is necessary in the presumed PDF approach. Also, the fluctuations of the progress variable are considered.

The model can be extended in a similar manner to include a larger number of streams. For every stream an additional mixture fraction scalar is transported. The transport of this mixture fraction is independent of the other mixture fractions. The source term for the progress variable includes the additional mixture fraction. This shows the capability of the model to simulate multi-stream mixing cases without additional modeling complexity and errors.

The SF-PV (Stochastic Fields - Progress Variable) model was implemented in commercial CFD code Fluent (v12) [1] to consider up to five streams. The implantation is briefly described in appendix A.1. The model is validated against four turbulent autoignition cases: three experiments and a DNS (Direct Numerical Simulation). The validation results are presented in next chapter, followed by a parameter study on the impact of turbulence on autoignition location. The model was also validated for reheat combustor in Alstom GT 24/26 engine with four-stream mixing, but no results are presented in this dissertation due to confidentiality reasons.

5 Model validation

The model proposed in this work, based on tabulated chemistry and stochastic fields turbulence chemistry interaction, is validated in this chapter. The model is validated against four auto-ignition cases [63, 95, 96]. The first validation case is the hydrogen autoignition experiment performed at Cambridge university [68, 70]. The second case is a hydrogen autoignition 3D DNS with detailed chemistry performed at ETH Zürich by Kerkemeier et al. [52]. The DNS setup is similar to the Cambridge experiment, but delivers detailed data like the scalar dissipation rate and mixture fraction distribution for validation of the model. The third case is vaporized n-heptane autoignition that was performed on the same experimental setup of the Cambridge experiment [69]. The last validation case is the Delft flame also known as DJHC (Delft Jet in Hot Coflow) flame. This flame emulates flameless or MILD mode of combustion. The flame was experimentally observed to be stabilized by autoignition. Simulation of this mode is a challenge for most combustion models. The Delft flame is a multi-stream mixing problem, which makes it an excellent case for the model validation.

5.1 Hydrogen autoignition experiment

Markides et al. [68, 71] studied the ignition of a hydrogen jet in a hot co-flow. The purpose of the measurements was to study the effect of co-flow temperature on auto-ignition length and different regimes of autoignition. This section validates the approach of the LES combustion model proposed in this work. The LES combustion model is validated against the experimental auto-ignition lengths and flame behavior in various autoignition regimes.

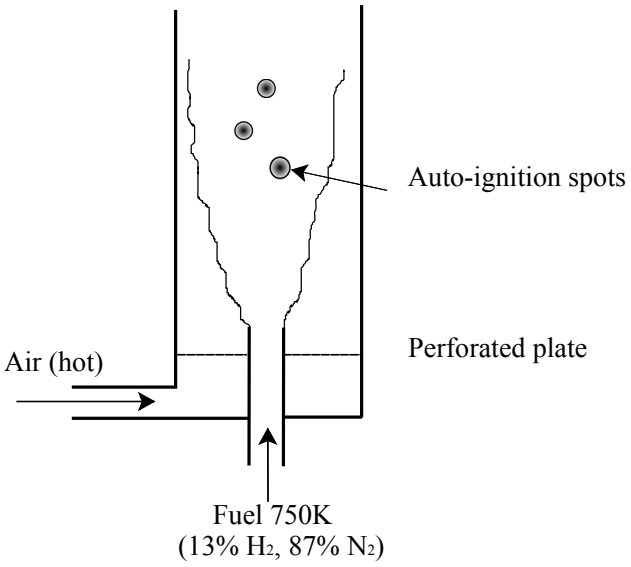

Figure 5.1: Schematic of the experimental setup [68].

Table 5.1: Simulated Cases

Case	Air Temperature [K]	Fuel Temperature [K]	Bulk velocity [m/s]	Observation
0	950	750	26	Random Spots
1	955	750	26	Random Spots
2	960	750	26	Random Spots
3	980	750	26	Flashback

5.1.1 Experimental setup

The experiment consists of a jet of diluted hydrogen (13 % hydrogen and 87 % nitrogen by mass) injected into a coflow of hot air, which flows through a quartz tube. Both, the jet and the coflow, have same bulk mean velocity. Fig. 5.1 shows the schematics of the experiment.

The air stream is heated electrically and enters into the quartz tube through a perforated plate (3 mm holes and 44 % blockage) to promote turbulence.

The integral length scales and the turbulence intensities were measured in the co-flow at the injector plane. The bulk velocity of air is controlled at 26 m/s. Diluted hydrogen is passed through a 2.25 mm injector at 26 m/s. The temperature of air and the velocity of the fuel were varied to obtain different autoignition regimes. OH chemiluminescence was used in the experiments to determine the autoignition lengths. Four different regimes were observed depending on the co-flow temperature, which are shown in Fig. 2.3.

The “no-ignition” regime was observed at very low temperatures, followed by “random spots regime” (case 0,1, and 2), where ignitions kernels occur sporadically and are transported out of the tube. The third regime is “flashback”, in which autoignition occurs downstream of injection, and then the flame propagates upstream towards the injector, resulting in an anchored or lifted flame (case 3).

5.1.2 0D Reactor Calculations

For combustion modeling, and perhaps in particular for the prediction of auto-ignition, the chemical kinetic mechanism is crucially important. When validating or comparing turbulence-chemistry interaction models, the same chemical mechanism should be used, if possible, or the impact of the chemical mechanism on modeling results should be appraised.

The mechanism of Yetter et al. [113], which is validated for CO and H_2 fuels over a wide range of temperature, was used previously by Navarro-Martinez et al. [48] for LES of the case considered in this study. Stanković et al. [103] compared different chemical mechanisms with respect to autoignition delays and used the Li mechanism [64] for LES. In the DNS study [52], the Li mechanism was used. Hence, in order to validate the model based on the previous LES studies, the Li mechanism was used throughout the present work for hydrogen combustion. Zero-dimensional plug flow reactor calculations (only time dimension) were performed in order to compare the ignition delay times for the cases described in Table 5.3. In Fig. 5.2 the ignition delays predicted by the Li mechanism are plotted over the mixture fraction. The stoichiometric mixture fraction line is also shown as a reference.

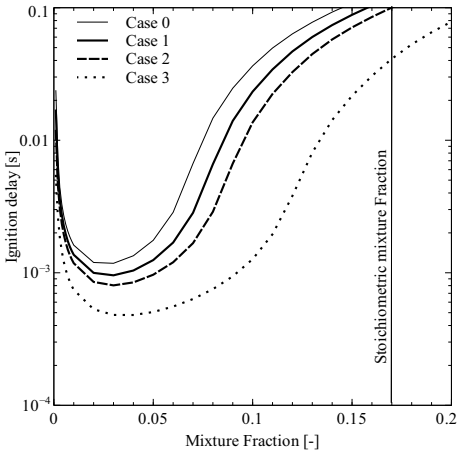

Figure 5.2: Autoignition delays for the cases described in table 5.3 using Li et al. mechanism [64].

The figure shows that the minimum ignition delays are found for mixture fractions much leaner than the stoichiometric ($Z_{st} = 0.17$). This is due to the higher temperature of the oxidizer (leaner mixture fractions). The higher the temperature, the leaner is the most reactive mixture fraction.

The tabulation of chemistry was carried out using the open source code Cantera [38]. The boundary conditions from table 5.3 were used to solve the plug flow reactor ODEs (4.2) for 101 points in the mixture fraction dimension and about 80 in progress variable. The mixture fraction points were clustered about the most reactive mixture fraction. The initial condition of the reactors was calculated using Eq. (4.1).

The progress variable used is defined as a combination of an intermediate species (OH) and product H_2O.

$$Y_c = Y_{HO_2} + Y_{H_2O}. \tag{5.1}$$

Figure 4.2 shows the progress variable source term as a function of the mixture fraction and the progress variable for case 0 (see Table 5.3). The time for tabulation was less than 10 minutes with a DualCore laptop. The size of the table was about 0.5 MB.

5.1.3 Numerical details

The commercial CFD solver Fluent v12 [1] was used for the simulations. All the simulations considered in this work are performed with the incompressible solver. The dynamic Smagorinsky-Lilly model was used as a sub-grid model. The tabulation was done using the open source code Cantera.

For the experimental test case described in section 5.1.1, two meshes with 150x70x48 and 200x90x52 nodes in axial, radial and azimuthal directions were used for the mesh quality study. The nodes were distributed uniformly in the axial direction and an O-grid was used in the azimuthal direction. The points were distributed non-uniformly in the radial direction with more points clustered towards the center. The mesh quality study is included in the appendix B. As the coarse mesh satisfied the quality criteria and performed as good as the fine mesh, the coarse mesh was used for the LES.

The 'vortex generator' boundary condition was used for the simulation of the turbulent co-flow inlet boundary. In the vortex generator method, to generate a time-dependent inlet condition, random vortices are added on a specified mean velocity profile via a fluctuating vorticity field. The vortex method is based on the Lagrangian form of the evolution equation of the vorticity and the Biot-Savart law. A particle discretization is used to solve this equation. These particles, or vortex points are convected randomly and carry information about the vorticity field. Refer to [1,74] for more details about the method. A constant pressure boundary condition was used at the outlet of the domain. For the walls no-slip boundary conditions were used as was done in the DNS studies. As the reactive regions are close to the tube axis, the wall boundaries would not play a major role.

Second order upwind schemes were used for all the scalars and energy except for the momentum, for which a bounded central scheme was applied. A time stepping of 1e-6 s was used for all the simulations, which corresponds to a Courant number below unity. The experimental test case LES was run for 15 ms, which corresponds to 4-5 residence times. Both the DNS and the LES (second test case) were run for 9 ms, which also corresponds to 4 residence times. The required CPU time for the simulation of the Cambridge experiment

is 520 CPU hours (QuadCore Computer: 150 hours). For comparison, the simulation time reported by [48] using the stochastic fields method with detailed chemistry was about 4000 CPU hours. The mesh size in that study was comparable to the one used in the present work.

5.1.4 Mixing

The time averaged resolved mixture fraction and scalar dissipation rate distribution along the axis of the flow are shown in Fig. 5.3. The time average was taken over 20 ms of the simulation run, which corresponds to about 6 residence times (L/U_{bulk}) of the flow. Although the mixture fraction distribution does depend to some extent on co-flow temperature and the heat release distribution, only one case (Case 0) is shown here for clarity.

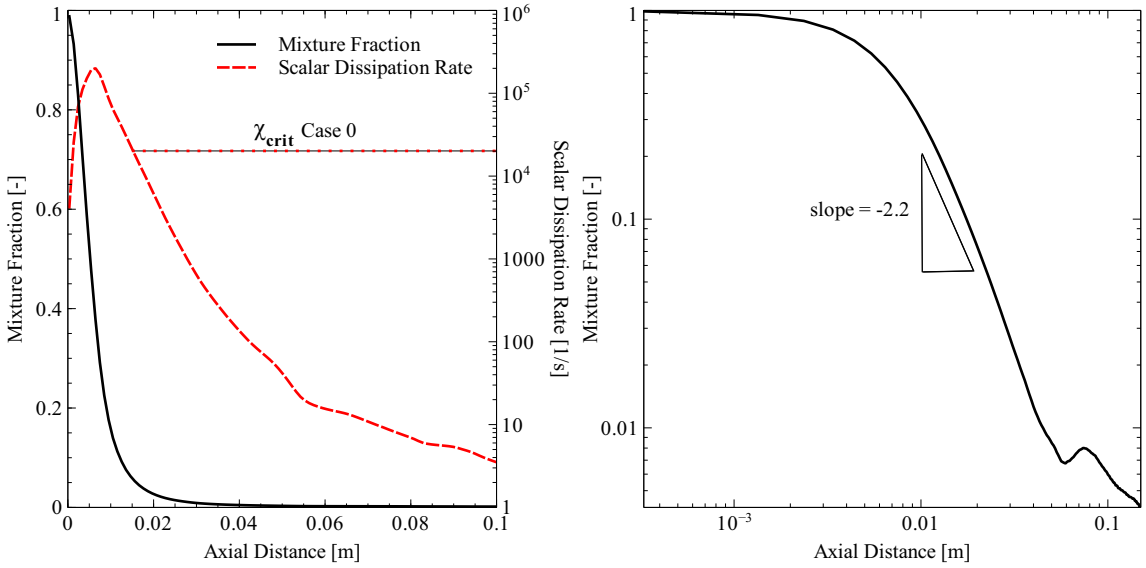

Figure 5.3: Time averaged resolved mixture fraction and scalar dissipation rate.

According to Taylor's diffusion theory [105], the mean mixture fraction profile obeys an x^{-2} power law at short distances from the nozzle and x^{-1} power law at larger distances. Fig. 5.3 (right) shows that the mixture fraction decay along the axial direction x at longer distances from the injector obeys an $x^{-2.2}$ power

law. Taylor's law is generally applicable to low turbulence intensities, while the test case has a high turbulence intensity of 14 %, which explains the observed discrepancy.

In Fig. 5.3 (left) the critical scalar dissipation rate line is shown for Case 0. The critical dissipation rate is determined by solving the steady laminar flamelet equation with the scalar dissipation rate as a parameter. The minimum scalar dissipation rate that extinguishes the flame is the critical one. The critical scalar dissipation rate in this work was calculated using the flamelet model implemented in Fluent [1]. According to the flamelet theory [12], autoignition should take place at locations where the scalar dissipation rate is lower than critical value. For the case considered here (Case 0), the autoignition location should be less than 20 mm downstream from the injector. It will be seen later in the next subsection that the minimum auto-ignition location for this case is more than 40 mm. This shows the importance of considering the fluctuations of the scalar dissipation rate for the prediction of autoignition, as shown by Ihme et al. [43] for the Cabra flame. From a Lagrangian point of view, the fluctuations in the scalar dissipation rate experienced by a particle, change its history of the radical pool build up. A particle that is exposed to large fluctuations of the scalar dissipation rate, progresses slower towards the autoignition point due to rapid loss of heat and radicals. In extreme cases, the particle would never reach the autoignition point, although the local scalar dissipation rate might be much smaller than the critical. To consider this effect, Ihme et al. [43] used an unsteady formulation of the flamelet model by introducing an additional progress variable dimension. The models based on progress variable approach consider the "history" effect through the build up of the progress variable.

5.1.5 Autoignition Length

It is found experimentally that the autoignition length and the flame behavior depend strongly on the co-flow temperature. With higher temperatures, the chemical reaction rates increase, leading to faster chemical reactions, or shorter chemical time scales relative to the flow. This results in reduced au-

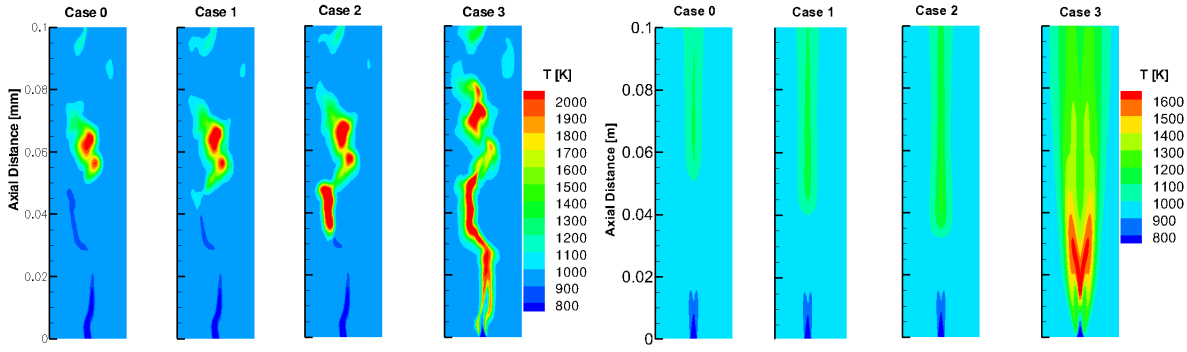

Figure 5.4: Left: Resolved temperature snapshots. Right: Time averaged resolved temperature.

toignition length. At very low temperatures, the flow time scales are smaller than the chemical ones. If the temperatures are lower than the ignition point, autoignition can be totally avoided ('no ignition regime'). With an increase in the temperature, the probability of ignition increases. After ignition, the ignition kernels are too weak to overcome the convective transport acting downstream and are eventually convected out. This regime is called the 'random ignition spots'. With further increase in the temperature, the expanding ignition kernel can balance the convective force, leading to a lifted flame. At very high temperatures, the kernel flashes back and an attached flame is observed. This regime is called 'flash-back'. Fig. 5.4 shows snapshots of the resolved temperature contour on the left. It is observed that ignition spots appear in cases 0, 1 and 2. The location of the appearance moves downstream with decreasing co-flow temperature. Figure 5.4 on the right shows the corresponding time averaged resolved temperature.

The flame behavior of the two extreme conditions, Case 0 and 3, are depicted in Fig. 5.5. In case 0, random ignition spots are visible. In case 3, after appearance, the ignition kernel flashes back and an attached flame is observed. The rate of flash-back would change with a change in the co-flow temperature. For cases 1 and 2 (not shown), a random spots ignition regime was observed as in case 0, but with different autoignition lengths (refer Fig. 5.4). The time averaged plots provide the evidence that no flashback was observed in those

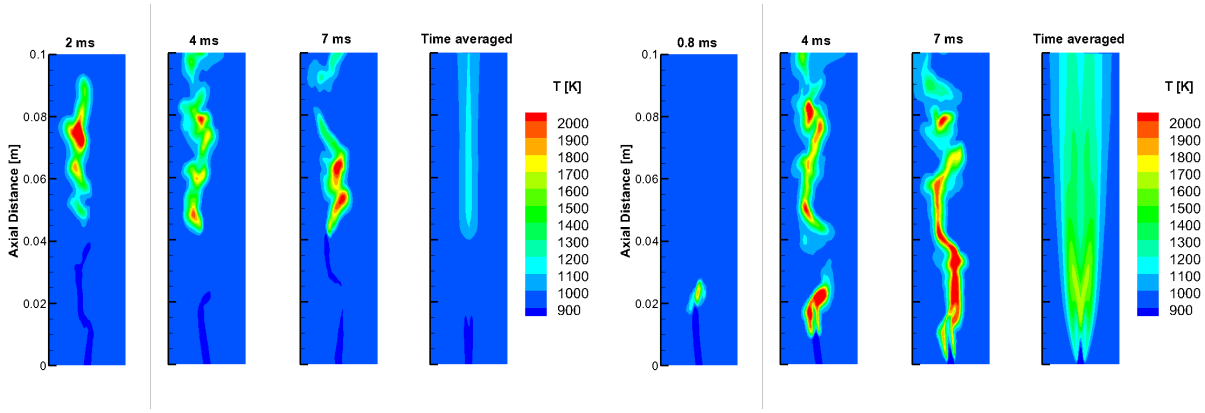

Figure 5.5: Left: Case 0 flame behavior. Right: Case 4 flame behavior.

cases. This shows the capability of the model to capture various autoignition regimes observed experimentally.

The scatter plots in Fig. 5.6 show the development of OH mass fraction at various times in the entire computational domain. To reduce the size of the plots and make them more readable, every tenth point is shown (10% of all the points) in the figure. The first plot shows the mass fraction of OH just before the appearance of the first autoignition kernel. It is seen that the OH mass fraction develops close to the most reactive mixture fraction (Z=0.035), which was observed from the ignition delay curve from Fig. 5.2. The subsequent plots show that the OH mass fraction develops towards the stoichiometric (Z=0.17) and leaner mixture fractions. This represents the growth of the kernel. The peak OH mass fraction is found at Z=0.07, which is smaller than the stoichiometric mixture fraction ($Z = 0.17$). The time averaged OH distribution shows that the OH mass fraction reaches its peak close to the most reactive mixture fraction with most of the distribution concentrated in the leaner areas. The reason for this distribution is the growth of the ignition kernels downstream of the mean ignition location, where lean mixture fractions are present. As the ignition kernels do not flash back, the OH mass fraction close to or stoichiometric ($Z = 0.17$) or on the richer side is negligible.

Figure 5.7 shows the OH scatter plots for the case 3. Autoignition takes place at lean mixture fractions close to the most reactive mixture fraction. The au-

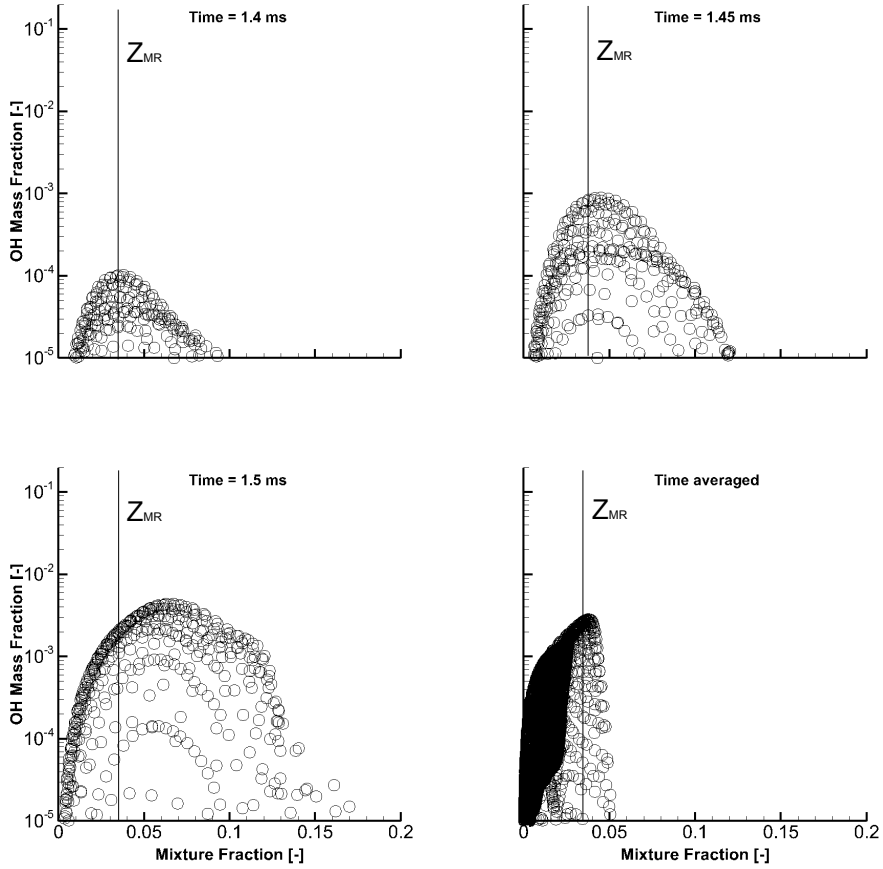

Figure 5.6: Case 0 OH mass fraction scatter plot for first autoignition spot.

toignition delay curve in figure 5.2 suggests that a broad range of mixture fractions (Z=0.01 to 0.1) has ignition delay under 1 ms. The points in the figure 5.7 show that the OH mass fraction reach the ignition criteria for all the mixture fractions up to 0.3. The ignition delays for mixture fraction richer than 0.15 are larger than the residence time (10 ms). The scatter plots for Case 0 show no OH build up close to the stoichiometric mixture fraction. This shows the upstream propagation of the flame for the case 3. The time averaged distribution of OH over mixture fraction shows values for very rich mixture fractions close to Z=1. This is only possible in case of the transport of OH radicals from the lean reactive zone to the rich zone. The richer mixture fractions are not expected to ignite as the autoignition reactions are negligible.

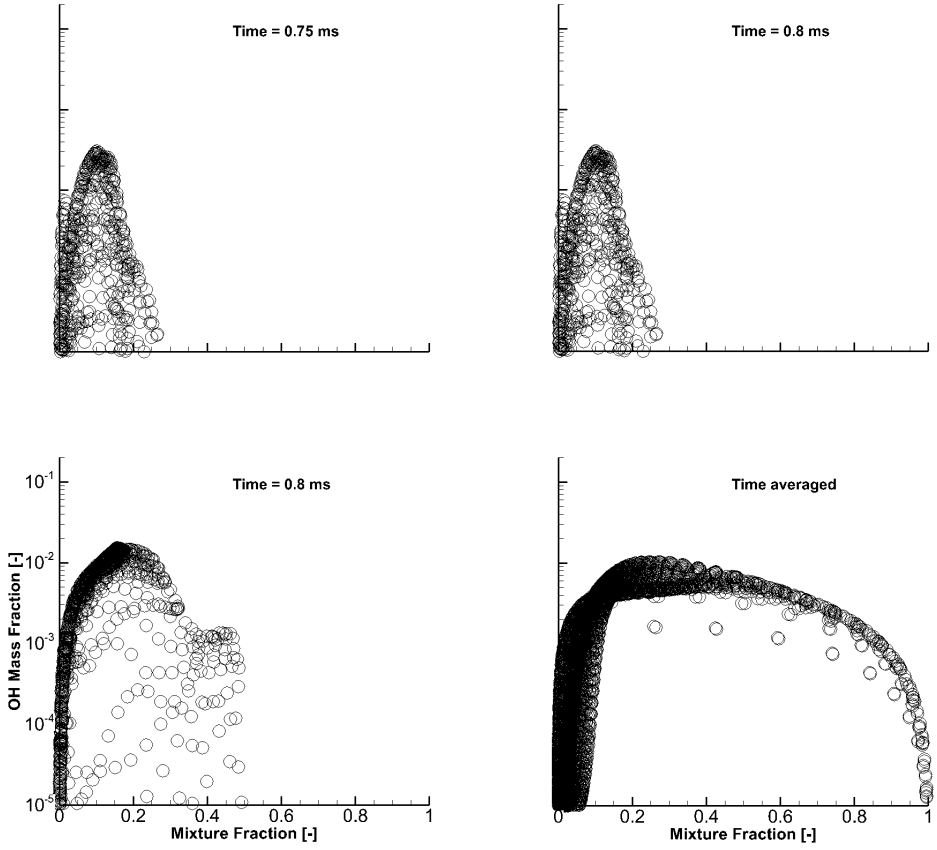

Figure 5.7: Case 3 OH mass fraction scatter plot for first autoignition spot.

In the experiment, average OH chemiluminescence images were used to determine the mean and minimum auto-ignition length. A time averaged OH signal value of 3% was considered to be the minimum auto-ignition location and the peak of the averaged OH distribution was considered to be the mean autoignition location. Figure 5.8 shows the mean (time average) distribution of the resolved OH mass fraction. Also the 3% of maximum OH mass fraction iso-line is shown. The line indicates the minimum autoignition delay. The peak of the OH contour corresponds to the mean autoignition location. The corresponding locations are compared with the experimental measurements on the right hand side of Fig. 5.8.

It is interesting to observe in figures 5.6 and 5.7 the reduced level as well as a low axial distribution of the time averaged OH mass fraction from case 0

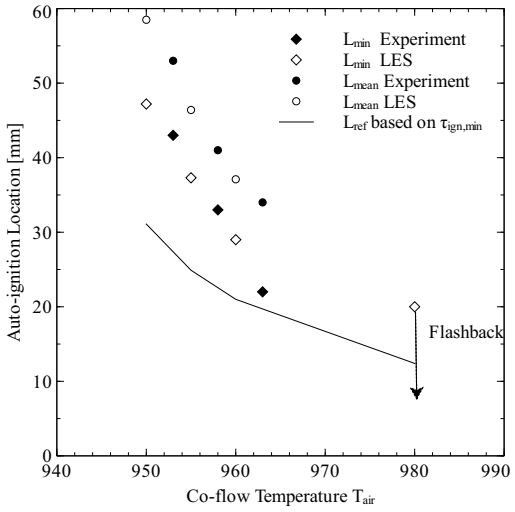

Figure 5.8: Minimum and mean autoignition locations.

to 3. For case 3, a minimum autoignition location is the location where the first ignition kernel appears. This is followed by flashback. An attached flame is observed for this case. It is interesting to observe that although the diffusion transport (along and across the mixture fraction) is not considered in the tabulation method, the model is capable of predicting a flashback. The increased rate of progress variable production and diffusion overcome the convective force, which is acting downstream. This imbalance between the transport leads to upstream propagation of the flame. The flame stabilizes at a location where diffusion-reaction terms balance the convection term in the progress variable transport equation.

This shows the capability of the combustion model to consider the non-linearity of the combustion depending on the temperature. The random ignition spots and flashback effects are also captured. The next section validates the model against the DNS data in more detail.

5.2 Hydrogen Autoignition 3D DNS

In the previous section, the combustion model was validated for autoignition lengths and flame behavior observed in experiments. DNS provides more de-

tailed data for the validation of the overall LES combustion model. The 3D DNS was performed at the ETH Zürich by Kerkemeier et al. [51, 52] and was inspired by the Cambridge experiment, described in the previous subsection.

5.2.1 DNS setup

Few changes are made to the boundary conditions from the experiments to reduce the computational domain size (figure 5.9). The domain size was 55 mm in length and 16 mm in diameter. The nozzle diameter was 2.25 mm. The test case consists of a jet of diluted hydrogen (14% by mass) at 850K injected into a co-flow of hot air (955K). The bulk mean velocities of the jet and the co-flow are 26 m/s. A parabolic velocity profile is used for the fuel jet. For the DNS, the co-flow turbulence was generated using a digital-filters method [56]. A low Mach number DNS code based on spectral element method was used. The domain was descretized into 963,264 elements approximated with 4^{th} order Lagrangian polynomial. The total time of simulation was 9 ms preceeded by 4.3 ms cold-flow without fuel injection. The Schmidt number was assumed to have a constant value of 0.71 in the LES and DNS simulations. More details can be found in [51, 52].

5.2.2 Numerical details

The computational domain and the boundary conditions shown in Fig. 5.9. The commercial code Fluent v12 [1] with Smagorinsky dynamic model was used for the LES.

The mesh structure and the node density for the ETH DNS test case were equivalent to the experimental test case. Therefore, the mesh quality study is not repeated here. The mesh used for the ETH DNS consisted of 65×50×48 nodes in the axial, radial and azimuthal directions, respectively.

A time stepping of 1e-6 s was used for the LES. Both the DNS and the LES (second test case) were run for 9 ms, which corresponds to 4 residence times. The computational cost for one single LES combustion simulation using the

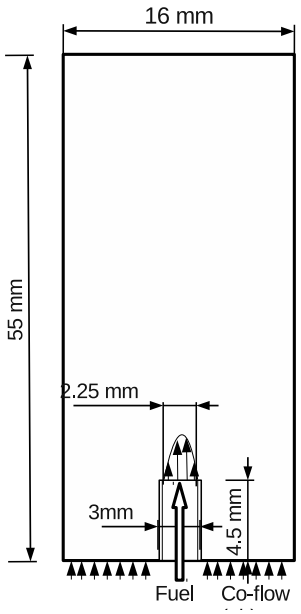

Bulk jet velocity U_j	26 m/s (parabolic profile)
Co-flow velocity $U_{co\text{-}flow}$	26 m/s
Fuel temperature Tf	855K
Co-flow temperature $T_{co\text{-}flow}$	955 K
H_2 mass fraction in fuel	0.14
Co-flow turbulence intensity	15%
Co-flow integral length scale	3 mm
Reference length $r_{ref}=r_j$	1.125 mm
Reference time $t_{ref} = r_j / U_j$	43e-6 s
Total simulation time	9 ms

Figure 5.9: Schematics of the ETH test [51, 52] case geometry and the boundary conditions.

model is 800 CPU hours. For comparison, the computational cost of the DNS for one run was 12 million CPU hours [51].

5.2.3 Mixing

The performance of the combustion model depends largely on a proper flow and scalar field description. LES has an advantage over RANS in this respect. To validate the mixing field, the time averaged resolved mixture fraction mean, its variance and the scalar dissipation rate from the LES are compared against the time averaged DNS results in figure 5.10. Mixture fraction describes the mixing between fuel and oxidizer. LES predicts a faster rate of mixture fraction decay close to the jet core ($z < 5$). At a later stage, the mixture fraction curve for LES lies above DNS. The figure on the right shows the distribution on a logarithmic scale. The overall distribution of LES is satisfactory compared to DNS.

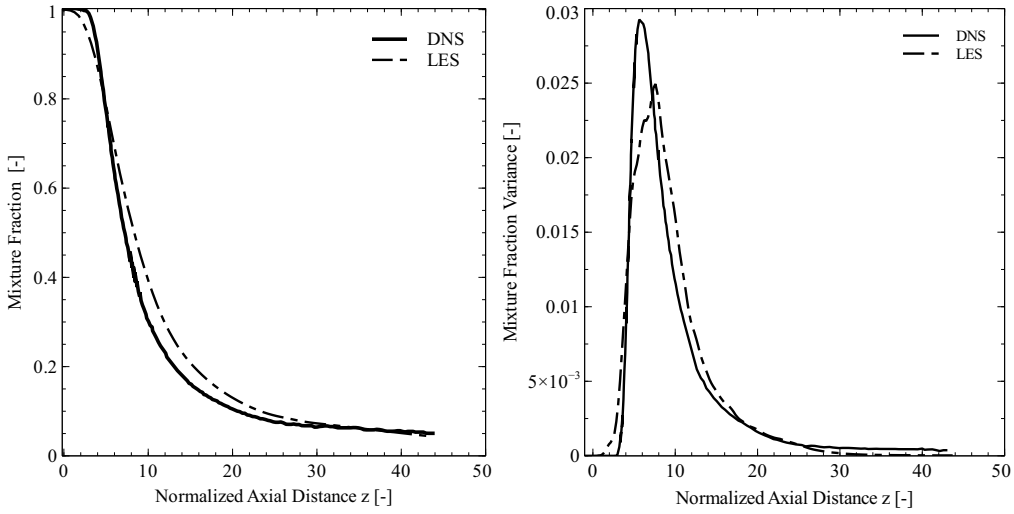

Figure 5.10: Streamwise distribution of mixture fraction mean (left) and variance (right).

The scalar dissipation rate describes the rate of mixing. It is the rate of destruction of the scalar inhomogeneity and describes the time scale of mixing. Equation 5.2 defines the resolved scalar dissipation rate:

$$\widetilde{\chi} = (D + D_t)\left(\frac{\partial \widetilde{Z}}{\partial x}\right)^2 \tag{5.2}$$

The scalar dissipation rate depends on the gradient of the scalar in space. The larger the gradient, the larger is the scalar dissipation rate. Figure 5.11 compares the time averaged scalar dissipation rate (SDR) along the centerline on the left and the SDR conditioned on the most reactive mixture fraction on the right. The magnitude of the scalar dissipation rate in LES starts increasing earlier than in DNS. This is because of the faster decay of the mixture fraction close to the nozzle in LES visible in Fig. 5.10. The discrepancy between the SDRs can be attributed partly to the grid resolution and partly to the fact that the curve for LES does not consider the subgrid SDR.

The peaks of the scalar dissipation rate in LES and DNS are at a normalized axial distance of 5.8 from the nozzle. The magnitude of the peak scalar dissipation rate in LES is much lower than that of DNS. The decay of scalar dissipation rate is faster in DNS compared to LES. This is as expected from the

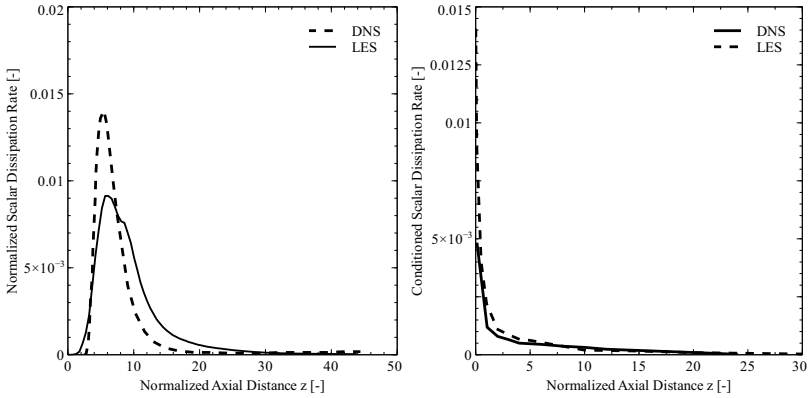

Figure 5.11: Left: Stream-wise scalar dissipation rate distribution. Right: Stream-wise conditioned scalar distribution on the most reactive mixture fraction.

mixture fraction curve 5.2. The scalar dissipation rate conditioned on most reactive mixture fraction is more important than the scalar dissipation rate along the axis. The chemical reaction at the most reactive mixture fraction are fastest on the most reactive mixture fraction iso-surface. The scalar dissipation rate, which describes the diffusion transport of the radicals, on this iso-surface is important for predicting the autoignition location. Larger scalar dissipation rate means faster transport of the radicals from the iso-surface, leading to reduced chemical reaction rates. Figure 5.11 on the right shows an excellent match between the scalar dissipation rate on the most reactive mixture fraction.

5.2.4 Autoignition Length

Figure 5.12 shows the ignition delay times computed with homogeneous reactors for varying mixture fractions. The OH mass fraction of 1e-4 was considered as a criteria for autoignition. The most reactive mixture fraction is found to be 0.04, which is very lean compared to the stoichiometric value of 0.17. A very small difference in the ignition delay times is observed for a wide range of most reactive mixture fractions (0.03-0.05).

Figure 5.13 shows snapshots of the temperature contour at various simula-

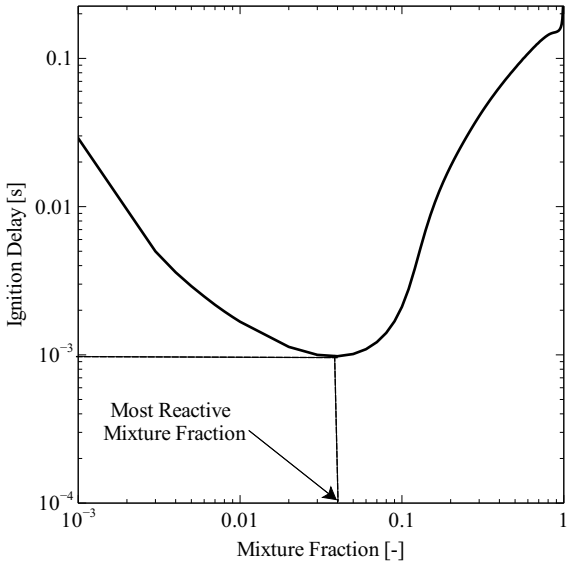

Figure 5.12: Ignition delays times for the ETH Zürich DNS test case from homogeneous reactors. [52]

tion times. The iso-line shows the most reactive (Z_{MR} = 0.04) and the stoichiometric (Z_{st} = 0.17) mixture fractions. The first contour plot shows the first autoignition spot, which appears at approximately 1.5 ms. The ignition in LES did not take place at a mixture fraction very close to the most reactive mixture fraction ($Z_{st} = 0.17 > Z_{MR} = 0.04$). After appearing, the ignition kernel evolves in all directions but is not able to propagate upstream against the flow. This is shown by various snapshots in Fig. 5.13. An interesting observation in the figure is that the iso-line of the most reactive mixture fraction is not closed in the domain and the stoichiometric line closes far upstream of the mean autoignition location, which is also observed in the DNS simulations.

The autoignition length determines the location of the flame. Different ignition criteria have been used in the literature. The OH mass fraction of 1e-4 criteria was used in the ETH DNS study [51]. A temperature rise of 1% over the coflow temperature [49] was also used. Both the temperature and OH mass fraction depend on the mixture fraction. In progress variable approach, the normalized progress variable is independent of the mixture fraction. A progress variable value of approximately 0.1 corresponds to the point of thermal runaway. In the present LES study, three different criteria have been compared.

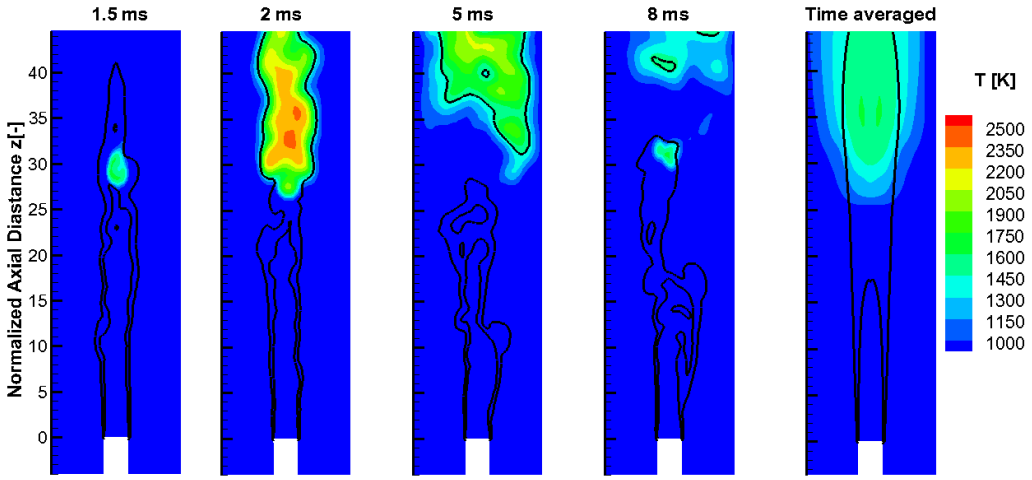

Figure 5.13: LES snapshots and time averaged temperature contour. Iso-line: Stoichiometric ($Z_{st} = 0.17$) and most-reactive ($Z_{st} = 0.17$) mixture fraction.

Following are the criteria used here:

1. OH mass fraction of 1e-4 [51].

2. 1% temperature rise over the co-flow temperature (965K) [48] and

3. A normalized progress variable value of 0.1.

Figure 5.13 shows the time averaged contours of the heat release rate and the variables of the three criteria mentioned above. The iso-lines show the corresponding ignition criterion.

In the 3D DNS test case, a mean autoignition length of 25.6 normalized axial distance was observed. The autoignition length determined by various criteria are:

1. OH criterion:25.1

2. T criterion:25.25

3. PV criterion:25.3

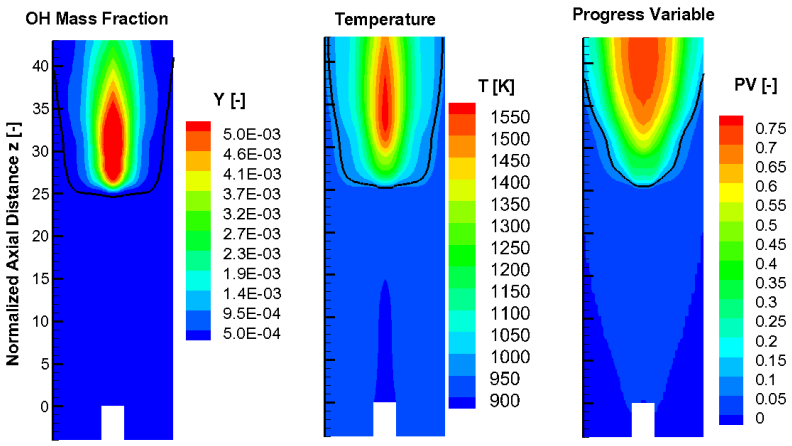

Figure 5.14: Time averaged distribution of the ignition criterion. Iso-lines: Ignition criterion.

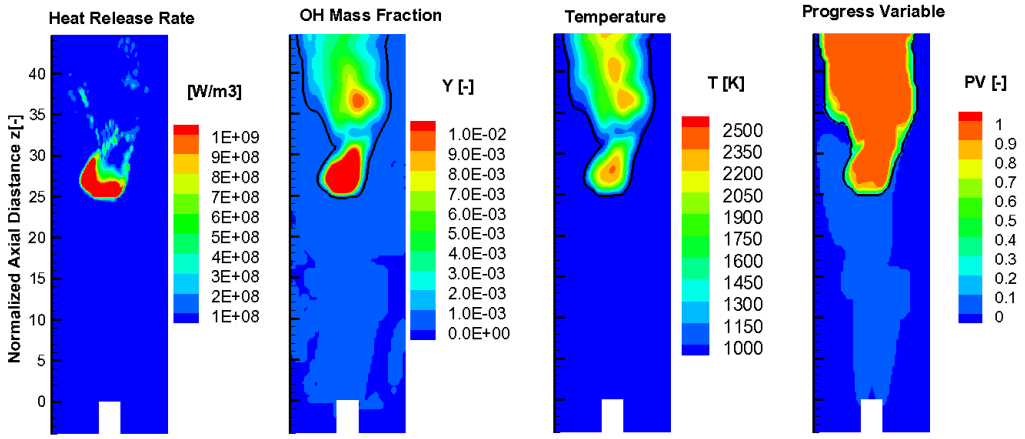

Figure 5.15: Snapshots of the ignition criteria. Iso-lines: Ignition criteria.

A small difference (less than 1%) is observed in the autoignition length using different criteria. Also, a 1.5% error is found between DNS and LES autoignition location using the OH criterion.

The snapshots show ignition kernels being convected downstream after appearance. Also no considerable difference is observed in the flame location using the three criteria. With the above results, it can be safely said that the LES approach using tabulated chemistry based on 0D premixed reactors and

stochastic fields turbulence chemistry interaction model are capable to reproduce the autoignition lengths and the random autoignition spots behavior satisfactorily within 2% error.

Figure 5.16 shows a scatter plot of OH mass fraction vs. mixture fraction for the first autoignition kernel appearance. The OH mass fraction at 1.4 ms approach the ignition criterion of 1e-4. The development of OH is seen predominantly close to the most reactive mixture fraction (Z=0.04). At the point of ignition, the OH peak is close to the most reactive mixture fraction, which is far away from the stoichiometric (Z=0.17) value.

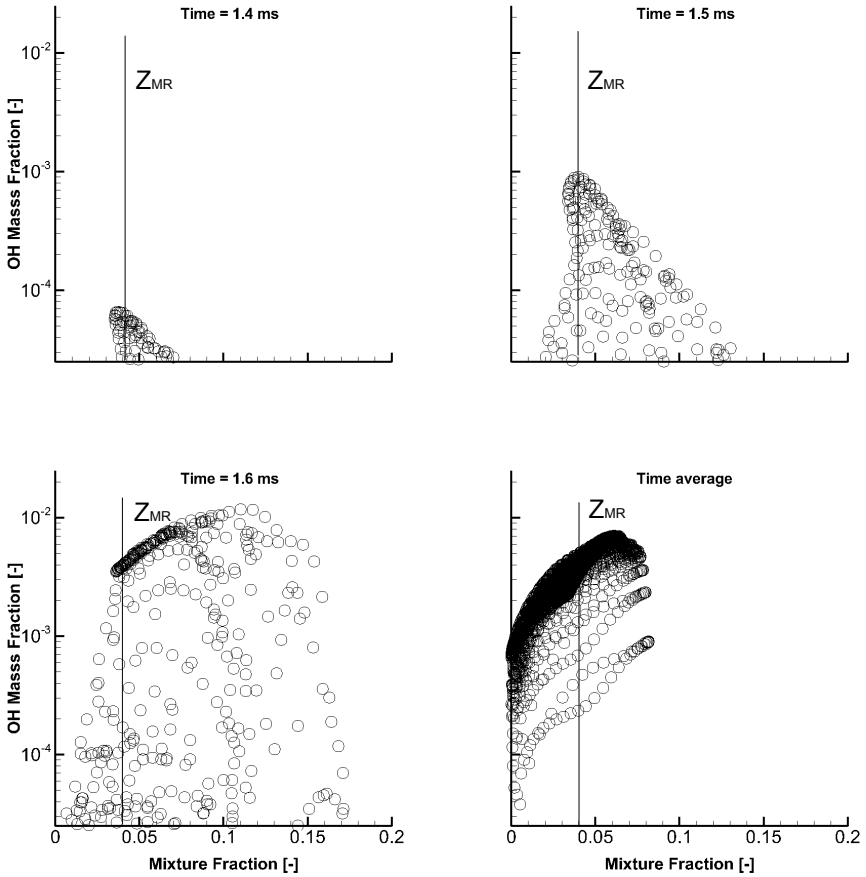

Figure 5.16: OHmass fraction scatter plot for first autoignition spot.

The time averaged OH plot shows that the OH is present only in the lean region, which was also observed for the cases 0,1 and 2 for the Cambridge

autoignition experiment. Thus, the distribution of OH mass fraction in the lean regions can be considered as an indicator of the "random ignition spots" regime for jet-in-hot-coflow configurations.

5.3 nHeptane auto-ignition experiment

The two previous sections validated the combustion model for hydrogen autoignition. The model proposed in this work should be applicable for all types of fuel, provided a suitable progress variable is chosen and a detailed reaction mechanism exists. For the simulation hydrogen autoignition, a composite progress variable (OH and H_2O) was considered. For hydrocarbon fuels, the definition of the progress variable needs to be changed. In this section, the model is validated against the Cambridge experiment using vaporized n-heptane fuel.

5.3.1 Test Case Description

The experimental setup is the same as described in section 5.1.1. Instead of hydrogen, a nitrogen-diluted pre-vaporized (gaseous) n-heptane (95 % by mass) is injected throgh the nozzle. The coflow air is electrically heated to higher temperatures (1110-1140K) than the hydrogen cases. The bulk mean velocities range between 10 and 20 m/s. A bulk mean velocity of 17.8 m/s is considered in this work. The measured tubulence intensity and integral length scale at the nozzle are 14% and 3-4 mm, respectively. For further details on the experimental setup, please refer to [69].Table 5.2 describes the boundary conditions for the simulated cases. For the n-heptane case, only random autoignition regime is considered.

Table 5.2: n-Heptane Autoignition Experiment Simulated Cases

Case	Air Temperature [K]	Fuel Temperature [K]	Observation
0	1113	1018	Random Spots
1	1125	1030	Random Spots
2	1133	1038	Random Spots
3	1138	1043	Random Spots

5.3.2 Numerical Setup

As described earlier, for combustion simulation, the choice of a suitable chemical mechanism is of utmost importance. Markides et al. [69] and De Paola et al. [26] successfully predicted the autoignition length with the Bikas chemical mechanism [5] using the first and second order CMC turbulence-chemistry interaction, respectively. Jones et al. [48] simulated the case using Liu et al. mechanism [34] in LES using the stochastic fields turbulence-chemistry interaction model. They had to reduce the co-flow temperature to match the LES results with the experiments. The autoignition delays for the four cases predicted by the Bikas [5] and Liu et al. mechanisms are shown in figure 5.17. In this work, the Bikas [5] mechanism is used, as it delivered satisfactory results with the CMC model [26, 69]. A composite progress variable consisting of (CH_2O+CO+CO_2) was used for tabulation.

5.3.3 Autoignition Length

Figure 5.18 shows the snapshots and the time averaged temperature distribution for the four cases (table 5.2). A random ignition spots regime was observed for all the cases. This is in accordance with the experiments [69].

The time averaged distribution of temperature shows the sensitivity of the autoignition length to the co-flow temperature. The autoignition length was determined in the experiments using 200 OH* chemiluminescence images [69]. Two autoignition lengths were defined, as was done in the hydrogen case:
1. L_{MIN}, the minimum auto-ignition length, was defined by a 3% rise in signal

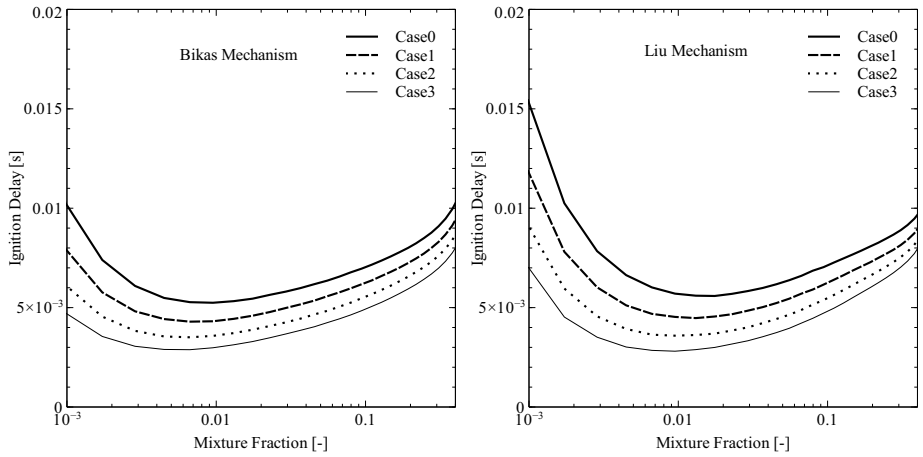

Figure 5.17: Autoignition delays Left: Bikas mechanism [5]. Right: Liu et al. mechanism [34].

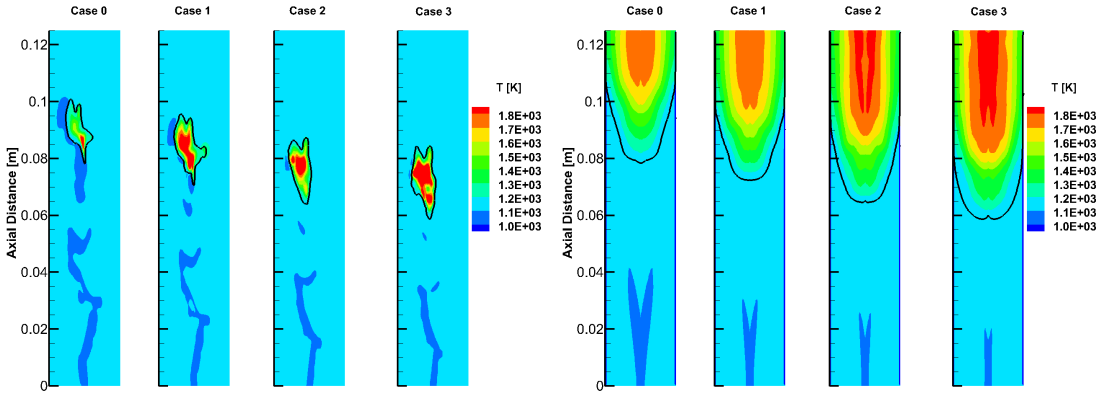

Figure 5.18: Temperature contours Left: Snapshot Right: Time averaged.

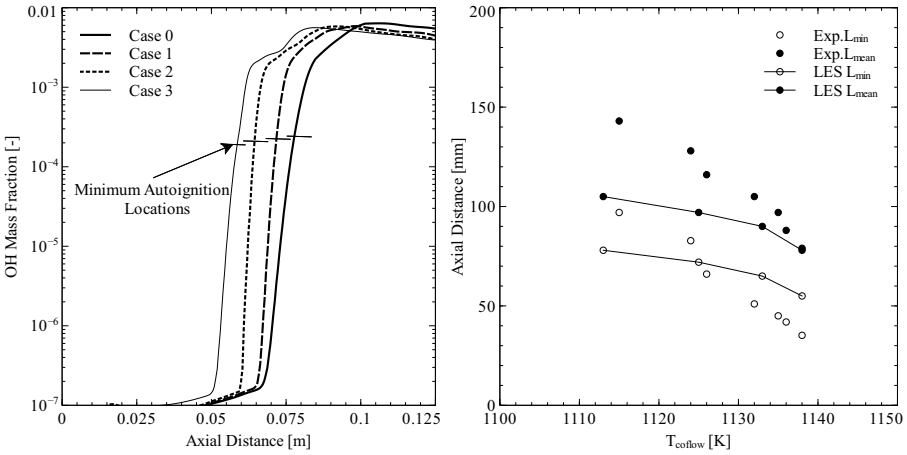

Figure 5.19: Left: Time averaged centerline distribution of OH. Right: Experimental and LES autoignition location.

from the background relative to the peak intensity.
2. L_{MODE}, the mode or most likely autoignition location, was the location of the peak intensity.

Accordingly, for LES the 3% of the maximum OH mass fraction was considered to be the L_{MIN} and its peak as the L_{MODE}. Figure 5.18 on the left shows the OH mass fraction distribution along the centerline. The minimum location of ignition are also marked. These correspond to the 3%of the peak OH mass fraction. The graph on the right in the figure 5.18 shows the experimental and LES autoignition lengths. The flame behavior as well as the effect of co-flow temperature are satisfactorily captured by the model.

The autoignition lengths, both minimum and mean, are under predicted by the LES combustion model. The minimum autoignition lengths from LES are comparable to the RANS-CMC model [26]. This shows that the discrepancy in the results should be due to the chemical mechanism. These results show the potential of the model for complex hydrocarbon fuels, but indicates the necessity of developing more accurate chemical mechanisms.

5.4 Delft Jet in Hot Co-flow (DJHC) lifted flame

Combustion systems operating at low peak temperatures have been identified as an attractive alternative to conventional combustion systems for improving thermal efficiency and reducing pollutants [110]. The low-temperature combustion phenomenon, referred to as MILD (Moderate and Intense Low Oxygen Diluted) oxidation is achieved by preheating the oxidizer and reducing its oxygen content. This can be achieved by recirculating the burnt gases or by using a sequential combustion system. The recirculation gas temperature is typically higher than the auto-ignition temperature. This reduced peak temperature reduces NOx emissions. Cavaliere [18] gives a detailed review on the history, fundamentals and applications of MILD combustion. Out of various industrial applications including furnaces in steel industry or HCCI engines, to name a few, one of the industrial examples related to power generation close to MILD combustion mode is the reheat combustor in ALSTOM's GT24/GT26 sequential gas turbine power plant [18]. For the development of these applications, understanding of the MILD combustion in turbulent flows is important.

Figure 5.20 shows the principle of flameless combustion. On the left, the schematics of the temperature distribution over mixture fraction is shown for normal and flameless combustion. The important requirement of flameless combustion is reduced oxygen content, which can be achieved by recirculation gases. The temperature of the oxidizer is increased by the recirculation gases (vitiated). This is shown by an increase in temperature in figure 5.20 on the left. The temperature of the oxidizer should be higher than the ignition temperature. The maximum temperature attained is lower than the normal flame, due to reduced oxygen content. Figure 5.20 on the right shows the reactor temperatures for different oxygen contents with 1300 K initial temperature and atmospheric pressure for stoichiometric mixture. An increase in the ignition delay time is observed, due to reduced chemical reaction rates. Lower peak temperatures are attained as the oxygen content is reduced. It is interesting to note the non-linear behavior of the peak temperature with the reduced oxygen content. With reduction of oxygen content from 23 to 10 %, the peak temperature reduced by about 120 K. With further reduction of the oxygen

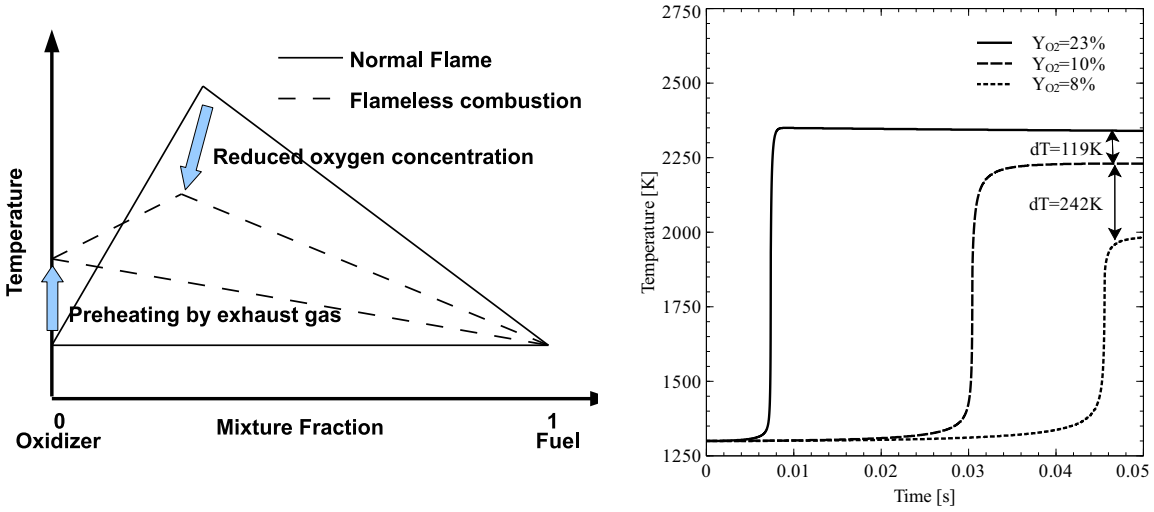

Figure 5.20: Flameless combustion principle: Left: Maximum temperatures attained in normal and flameless combustion. Right: Temperature evolution in reactors for varying oxygen content for methane.

content to 8%, the peak temperature diminished by 242 K. This shows that for the effectiveness of the flameless combustion mode, very low oxygen concentrations (high recirculation rates) are necessary. In addition to the oxygen content, the specific heat capacity of the mixture increases with temperature. This increase in the specific heat capacity plays a significant role in presence of combustion products.

NOx emissions depend nonlinearly on the temperature. As seen above in Fig. 5.20, the potential of flameless combustion can be utilized at extremely low oxygen contents. Oxygen contents as low as 3% were tested in laboratory experiments [23].

Laboratory scale flames with vitiated co-flow with reduced oxygen content include: Cabra [16], Adelaide [23] and Delft [79, 80] flame. The Cabra flame with 12% oxygen by mass in the coflow can be considered to be a border case for MILD combustion. The Adelaide flame and the Delft flame with 3-9% and 7-11% oxygen, respectively, can be considered to be definitely in the MILD combustion regime. The Delft flame, called DJHC (Delft Jet in Hot Coflow) from

here on, is considered in this work

The DJHC flame set up consists of a jet of natural gas injected at high velocity into a coflow of burnt gases produced by a secondary burner. Measurements were carried out for various jet velocities. A decrease in the lift-off height was observed experimentally with an increase in the jet velocity. This makes the case important to study the interdependence of turbulence, mixing and chemistry in the MILD combustion regime. Another interesting feature of the DJHC flame is the non-uniform boundary conditions in the coflow. The oxygen content and the temperature in the co-flow are not uniform. In addition to these complexities, simulation of MILD combustion is in general a challenge for turbulent combustion models. The MILD combustion flames cannot be categorized into non-premixed (diffusion) or premixed flames.

Coelho et al. [22] applied an Eulerian Particle Flamelet model (EPFM) in RANS to predict NO in the furnace studied by Plessing [88]. Kim et al [54] used CMC to simulate the Adelaide burner [23]. Ihme et al. [44] extended the Flamelet Progress variable (FPV) model for the Adelaide burner. To consider the non-uniform co-flow an extra conserved scalar (mixture fraction) was used. The chemistry was tabulated by solving the laminar steady flamelet equation. A presumed Probability Density Function (PDF) approach was used for the turbulence-chemistry interaction. Beta PDF model was used for the mixture fractions (conserved scalars) and a Dirac function for the progress variable. De et al. [24] simulated the Delft flame in 2D with the EDC model [67] in RANS context with reduced methane mechanisms. The EDC model captured the decreasing trend of lift-off height with jet Reynolds number, but quantitatively the lift-off heights predicted were too short and the temperatures were over predicted.

5.4.1 Test Case

The test case in this work is the Delft Jet in Hot Coflow (DJHC) performed by Oldenhof et al. [79, 80] at Delft University. The design of the burner is similar to the Adelaide burner [23]. A jet of fuel enters into a coflow of vitiated coflow (air mixed with combustion products) with low oxygen content. The high tem-

perature ensures ignition of the injected fuel. The experimental setup consists of a primary burner and a partially premixed secondary burner. Figure 5.21 shows the sketch of the setup. The diameter of the injector is 4.5 mm. The coflow is generated by an annular secondary burner of 82.8 mm diameter upstream of the primary burner. It consists of a ring of premixed flames with air injected on both sides of the ring. The fuel tube is cooled using air stream. Due to the cooling air and the air injected along the secondary burner, the coflow at the inlet of the primary burner consists of a strongly nonuniform profile of temperature and species. The temperature and mass fraction of oxygen in the coflow at the inlet of the primary burner are shown in fig 5.22. Measurements were carried out for various coflow temperature and minimum oxygen mass fractions at the inlet. In this work the case with minimum amount of oxygen is considered for various jet Reynolds numbers. Table 5.3 shows the boundary conditions for the fuel jet and the coflow.

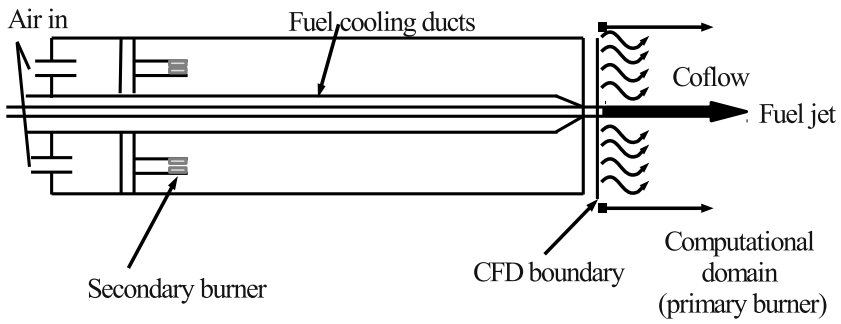

Figure 5.21: Test case sketch

Velocity and Temperatures were measured at 3, 15, 30, 60, 90, 120 and 150 mm downstream of the primary burner. Favre averaged velocities and Reynolds stresses were measured using Laser Doppler Anemometry (LDA). The temperature was measured using Coherent Anti-Stokes Raman Spectroscopy (CARS). The radial profile of oxygen concentration was measured using probe measurements.

The flame lift-off height was determined using chemiluminescence images obtained with intensified high speed camera. It was observed experimentally that the flame is stabilized by autoignition. Auto-ignition kernels appeared

randomly and were convected downstream. The size of the kernels increased, while moving downstream. Interestingly, but perhaps counter-intuitive, the lift-off height was found to drop down with an increase in the jet velocity. The lift-off height depended strongly on the co-flow temperatures.

5.4.2 Extension of the SF-PV model for ternary mixing

To consider the non-uniform boundary condition due to the burnt gases from the secondary burner mixed with air, an extra conserved scalar was used in addition to the one used for the fuel. The mixture fraction Z_1 was used for the fuel stream and Z_2 for the cold vitiated air (CVA). At any location the sum of the mixture fraction subtracted from unity gives the amount of hot vitiated air (HVA). Figure 5.22 on the left shows the method of determining the temperature and oxygen mass fraction at the inlet of the primary burner. The Z_2 (CVA) boundary condition is located at a jet radius of 2.25 mm.The maximum temperature and the minimum oxygen concentration in the co-flow were considered as boundary conditions for the hot vitiated air (HVA).

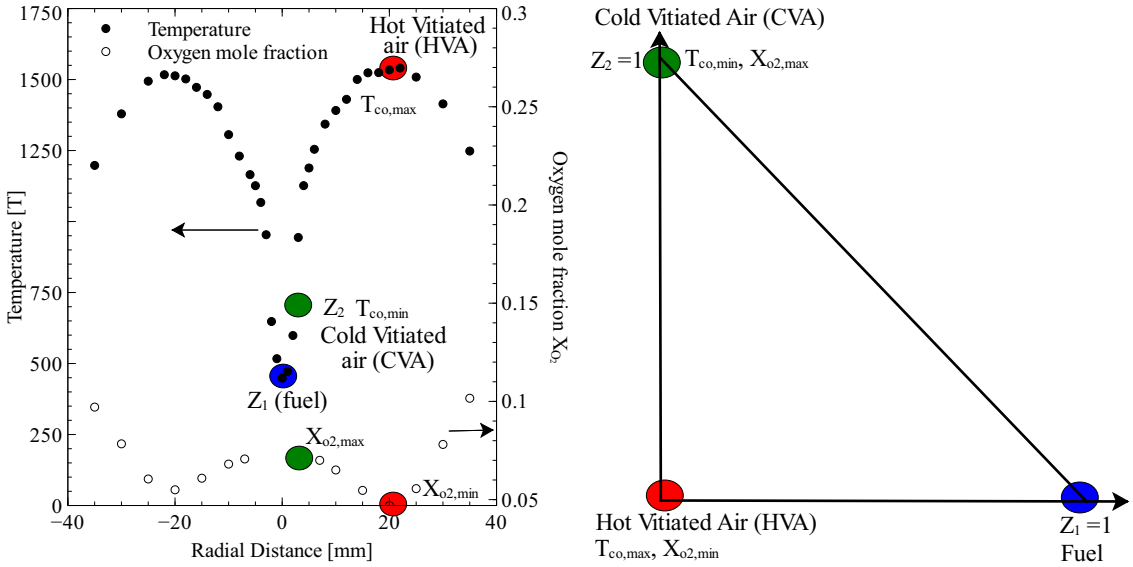

Figure 5.22: Left: Definition of the mixture fractions. Right: Tabulation triangle with boundary condition.

At the boundary conditions the additional mixture fraction Z_2 is calculated as

a function of the temperature. Equation 7 describes the method of calculating the second mixture fraction at the inlet:

$$Z_2 = \frac{T_{co,max} - T}{T_{co,max} - T_{air}} \tag{5.3}$$

The assumption behind this equation is that the oxygen concentration and temperature are correlated, which is true closer to the axis. But, this is not necessarily true for the outer part of the co-flow due to wall and radiation heat losses. These effects are neglected in this work. These effects can be included by introducing an extra dimension in the look-up table. Tabulation is done for various combinations of the two mixture fractions with the constraint that the summation of the two mixture fractions is less than unity, leading to a triangular zone for the tabulated region. On the right of Fig. 5.22, the mixture fraction triangle is shown.

In LES, stochastic fields for the mixture fractions Z_1 (fuel) and Z_2 (CVA) and the progress variable Y_c are solved. The transport equations solved by the combustion model are described in section 4.3.4. Eight stochastic fields are used in this study. Each field carries a reactive scalar, i.e. the progress variable, in addition to the two conserved scalars, the mixture fractions Z_1 and Z_2. The source term for the progress variable in equation (4.17) is then a function of the mixture fractions and the progress variable for a particular field $\bar{\rho}\dot{\omega}_c^n(Z^n, Y_c^n)dt$ (refer to equation (4.17)).

5.4.3 Numerical details

The look-up table was generated using the boundary conditions described below in table 5.3 using Cantera [38]. The GRI30 chemical mechanism [31] was used. The look-up table had about 41 points non-uniformly distributed in the two mixture fraction directions. About 80 points were used in the progress variable direction. The table size was 8 MB and the tabulation time was approximately 30 minutes with a 2.5 GHz QuadCore computer.

The LES simulations were performed using FLUENT. The Smagorinsky dy-

Table 5.3: Delft flame simulated Cases

Case	Re_j	$T_{co,max}$ [K]	$T_{co,min}$ [K]	$X_{co,min}$ [-]	$X_{co,av}$ [-]	T_f
DJHC-I	4100	1540	695	0.055	0.076	430
DJHC-I	8800	1540	695	0.055	0.076	460
DJHC-V	4600	1460	695	0.066	0.088	380

namic model was used for the subgrid eddy viscosity. Adiabatic no-slip boundary conditions are used at the walls. The Schmidt number was constant (0.9) for all the species and scalars (mixture fraction and progress variable).

The simulation time for a single run (120 ms) was 10 days on a 16 core computer. The simulations were carried out with a time stepping of 2e-6 s, which ensures a CFL < 0.7.

Table 5.3 shows the boundary conditions for the cases considered in this work. The temperature and oxygen content at the boundary conditions are shown in Fig. 5.23 on the left. The velocities for the Re=4100 and Re=8800 cases are shown on the right. The velocity boundary conditions for the DJHC-V case are the same as that of the DJHC-I with Re=4100.

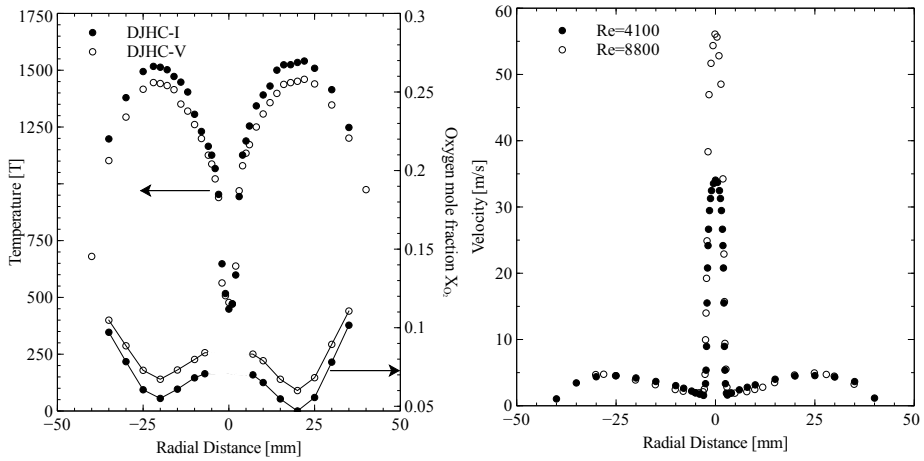

Figure 5.23: Left: Temperature and oxygen mole fractions at the boundary conditions for DJHC-I and DJHC-V. Right: Velocity boundary conditions for the DJHC-I (Re=4100 and 8800). DJHC-V velocity boundary conditions are same as DJHC-I with Re=4100

Figure 5.23 on the left shows that with an increase in temperature, the oxygen percentage is also reduced correspondingly. On one hand the increase in temperature will promote reactions, while the reduction in oxygen content will hinder them. Those two effects will counteract each other. Depending on which one of them is dominating, the lift-off length will change. The combustion model has to consider these effects along with the mixing between hot gases and air in the co-flow.

5.4.4 Velocity and Mixing Field

The combustion process in MILD combustion is kinetically controlled. The chemical reactions are a strong function of the mixing between fuel, air and hot gas. The success of any combustion model depends on the quality of prediction of flow and mixing field. In this sub-section the velocities from the LES simulations are compared with the experimental measurements. Fig. 5.24 shows the radial velocity distribution at various axial locations for DJHC-I at Reynolds numbers of 4100 and 8800, respectively. A satisfactory velocity distribution is obtained in the LES.

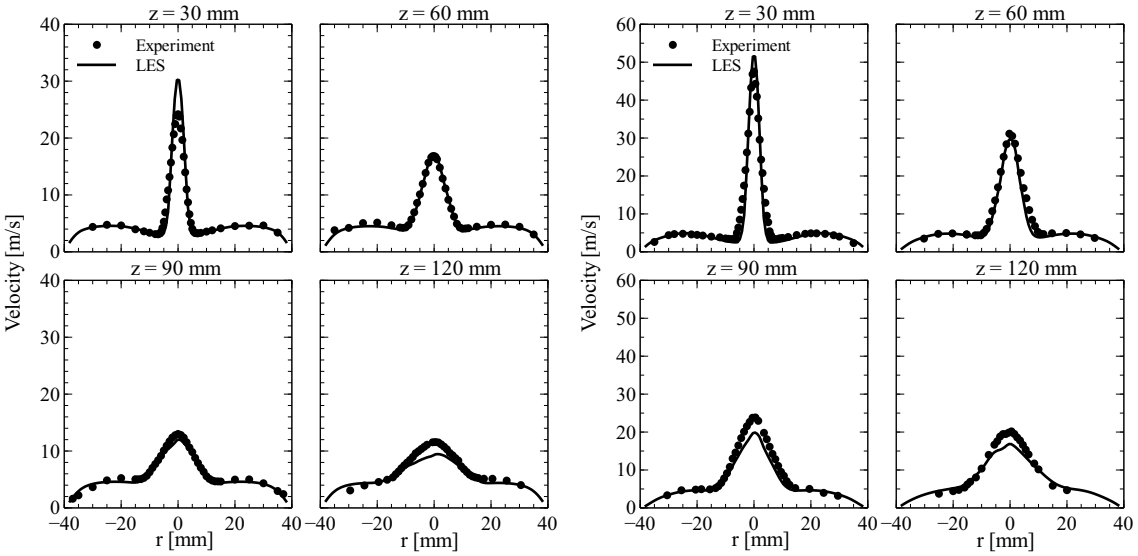

Figure 5.24: Radial velocity distribution for DJHC-I Re=4100 and Re=8800 at various downstream locations

Fig. 5.25 compares the mixture Z_2 (CVA) fraction for the cases studied in this work. A line showing the most reactive mixture fraction $Z_{1,st}$ = 0.02 (fuel) is also shown . The distribution of Z_2 (CVA) on the iso-line of most reactive fuel mixture fraction $Z_{1,st}$ is important, as the reactions are fastest at mixture fractions close to this value for a given cold vitiated air Z_2. A lower value of Z_2 (CVA) will mean a higher amount of hot gas at that location. The hot gas accelerates the chemistry due to the higher temperature. The distributions of Z_2 (CVA) for DJHC-I 4100 and DJHC-V 4500 are quite similar due to similar jet Reynolds numbers. For DJHC-I with Re=8800, a lower amount of Z_2 is observed in comparison to the other two cases. This is because of the faster entrainment of the hot gases into the jet. This was also observed in the RANS simulation of De et al. [24] This point is discussed at length in [80]. The enhanced entrainment should lead to faster chemistry and lower lift-off height. This is the point of discussion in section 5.4.6.

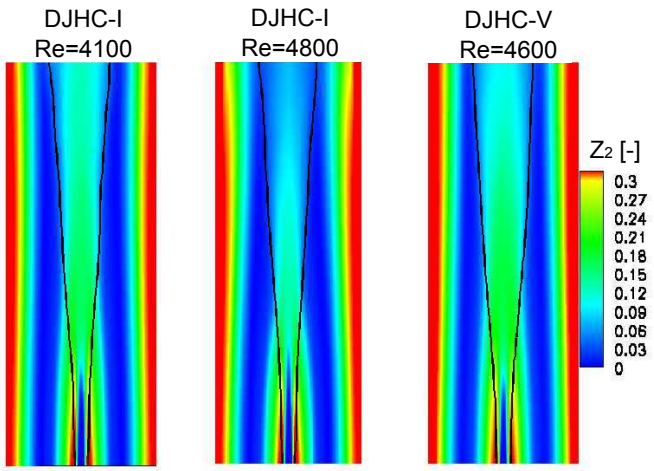

Figure 5.25: Time averaged air mixture fraction distribution at the central cross section. Line: Most reactive fuel mixture fraction.

5.4.5 Temperature Distribution

The temperature distribution for the DJHC-I cases with Re= 4100 and 8800 are shown in figure 5.26. In Fig. 5.26, an additional line for the mixing temperature (computed without heat release by combustion) is also plotted for reference.

At downstream locations greater than 30 mm, a larger discrepancy is observed between LES temperature (both with and without combustion) and the measured temperature close to the walls. This might be due to the radiation or wall heat losses, which are not considered in the simulation. The discrepancies might also be contributed to measurement error. Also in the work done by De et al. [24], a large discrepancy in temperature was observed between the measured and RANS results. This was contributed to a lower lift-off height predicted by the EDC model. The temperature curve for pure mixing in Fig. 5.26 suggests that the combustion model alone is not responsible for the discrepancy.

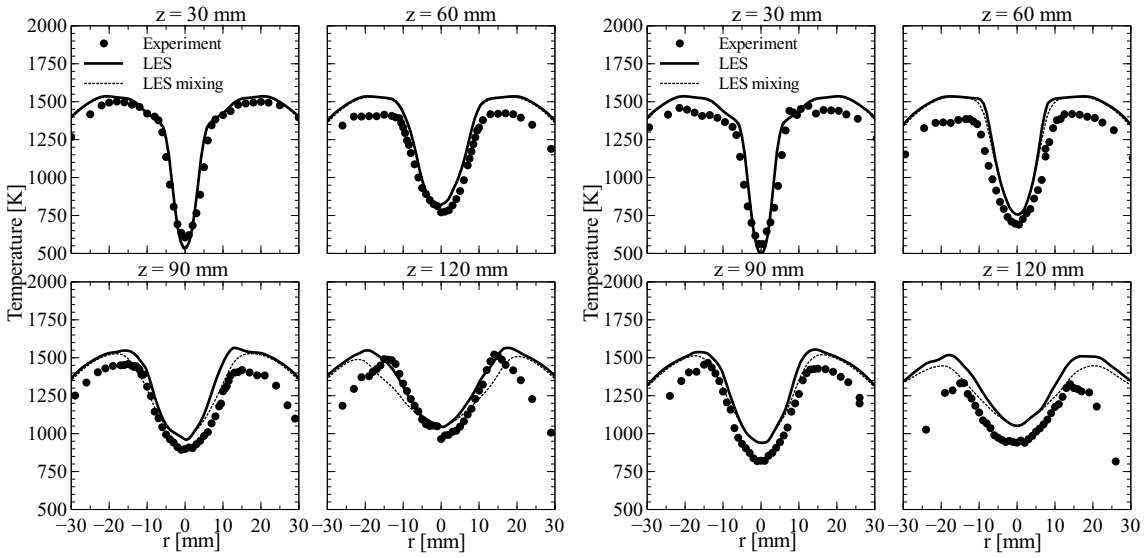

Figure 5.26: Radial temperature distribution for DJHC-I Re=4100 (top) and Re=8800 (bottom) at various downstream locations

The lines with and without combustion are indistinguishable for portions of 30 and 60 mm downstream of the nozzle. An increase in the temperature is observed from 90 mm onwards. This indicates that the flame is stabilized between 60 and 90 mm downstream of the nozzle. Determining the lift-off height is the topic of the next sub-section. The temperature measurements overall show a good agreement with the measured temperatures close to the axis. It is interesting to observe from the difference between the LES curves with and without combustion that a very low amount of heat is released compared compared to traditional combustion systems. No significant over prediction is

observed. This shows the capability of the model to quantitatively and semi-quantitatively capture the slow chemistry or kinetically controlled combustion processes in MILD regime.

5.4.6 Lift-off Height

For the prediction of lift-off height, various criteria are available in the literature. In many measurements, OH chemiluminescence has been considered as an indicator of heat release and thus the lift-off height. In various simulation works related to lifted flames, lift-off heights based on an increase in the temperature over mixing temperature [28], or OH mass fraction [52] have been used. In the experimental work by Oldenhof et al. [24] on the DJHC flame, the lift-off height was based on a different approach.

The lift-off height was related to the probability of the presence of flame pockets. A flame pocket is defined as a region where an OH mass fraction attained a value of 1e-3. Two different flame probabilities were defined., P_{b1} and P_{b2}. $P_{b1}(z)$ is the probability of finding a flame pocket anywhere on a radial line stretching outward from the burner axis as a function of the axial height. The second probability $P_{b2}(z)$ is that of finding a flame pocket at a certain axial height. The probability P_{b1} has been used in this work. In this method, a location with OH signal of 1e-3 was assigned a probability count of 1. For each location, the number of counts where a "burning" location was found was divided by the total number of images, producing a flame probability P_{b1}. As suggested by Oldenhof et al. [80], a $P_{b1} = 0.5$ is defined as the lift-off height. For the total 120 ms simulation run, about 60 ignition spots were observed. This corresponds to about an ignition spot every 2 ms. The ignition kernels appeared randomly and caused a lot of fluctuations in the ignition location. Fig. 5.27 shows the probability P_{b1} for the cases studied in this work vs. the axial length. For the probability curve shown in 5.27, 600 sample points were used. The time averaged axial distribution of OH mass fraction is shown in 5.27 on the right.

Figure 5.27 clearly shows an decrease in the lift-off height for an increase in the jet Reynolds number for DJHC-I case. This observation is due to the faster

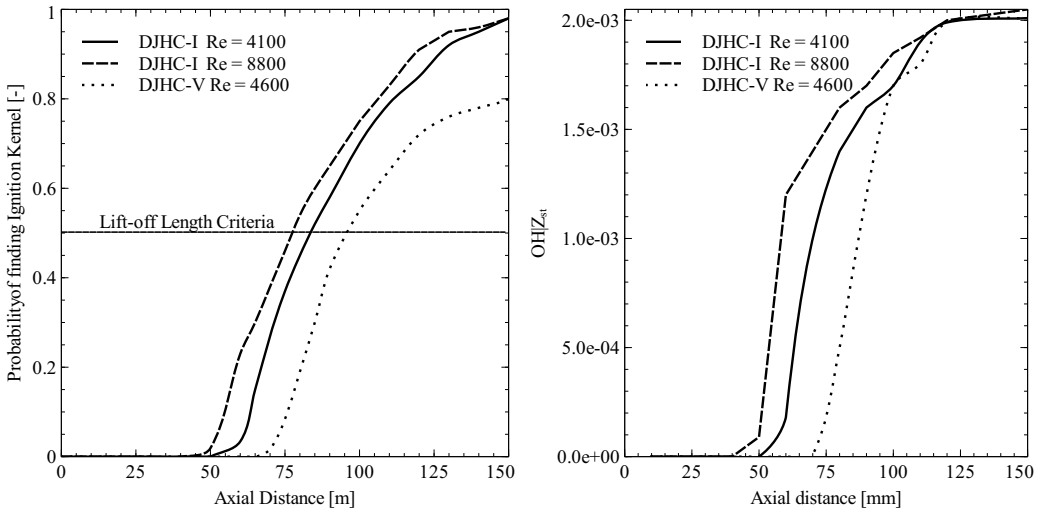

Figure 5.27: Left: Probability distribution of ignition kernels over the tube length. Right: Time averaged OH mass fraction conditioned on the most reactive mixture fraction.

Table 5.4: Mean Lift-off heights

Case	Experimental [mm] [80]	LES [mm]
DJHC-I $Re_j = 4100$	80	85
DJHC-I $Re_j = 8800$	78	78
DJHC-V $Re_j = 4600$	100	95

mixing between the hot gases and the jet, which promotes reactions and reduces the auto-ignition length. This observation is in agreement with the previous works of De et al. [24]. With reduced coflow temperature (DJHC-V) at similar Reynolds number, the autoignition length increases. This effect is expected due to the reduced reaction rates or increased ignition delays with reduced temperatures. Table 6.3 lists the experimentally observed lift-off heights and those from the LES simulations.

Figure 5.28 shows snapshots and the time averaged OH mass fraction distribution for the cases. The trend in the lift-off height is clearly visible in the snapshots and the time averaged OH mass fractions in Fig. 5.28. These results show

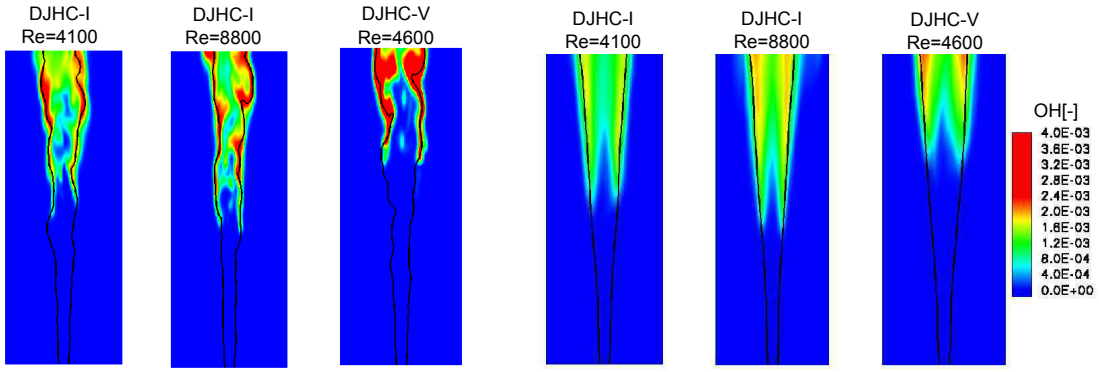

Figure 5.28: OH mass fraction distribution. Left: Snapshot Right: Time averaged. Isoline: Most reactive mixture fraction (Z_1=0.01)

the capability of the proposed model of tabulated chemistry and stochastic fields turbulence chemistry interaction to consider cases with multi-stream mixing. The extension of the model in this respect, without the need for any additional model complexities or assumptions, is the major advantage of the approach over the presumed PDF methods.

6 Impact of turbulent flow characteristics on autoignition

In industrial applications like reheat gas turbines or HCCI engines, turbulent autoignition plays a vital role in the flame stabilization. Such flows pose a challenging problem due to the direct (explicit) coupling between the turbulent mixing and slow pre-ignition reactions. Understanding the coupling between turbulence, mixing and chemical reactions is important for further development of these industrial devices. The impact of turbulence level and integral length scale on fuel-air mixing and autoignition delay is the topic of the chapter. In addition, the impact of bulk mean velocity on the location of autoignition will be studied. It is intuitive to expect the autoignition location to increase proportionally with the bulk mean velocity. The next subsection investigates if this is true, and whether a simple scaling law based on bulk mean velocity ratio can be used to predict autoignition location. The results presented in this chapter can be found in [96].

6.1 Impact of bulk mean velocity on autoignition location

With an increase in the bulk mean velocity at fixed turbulent intensity, the velocity fluctuations will increase, which will affect mixing and chemical reactions. There are two major effects of the changes that take place with an increase in the bulk mean velocity:

1. The convective transport is increased. Due to this, the auto-ignition length increases. This is the argument behind the scaling laws to predict autoignition based length based on bulk mean velocity ratios.
2. The scalar dissipation rate (strain rate) increases. This should on the one

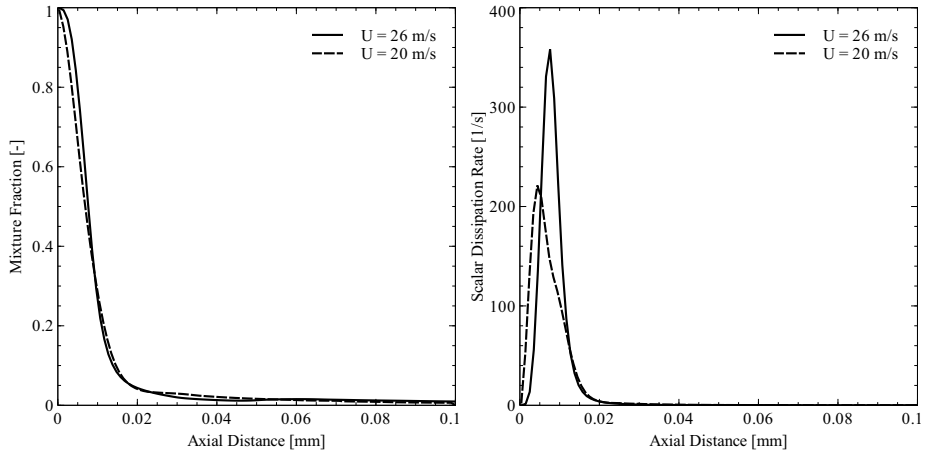

Figure 6.1: Mixture fraction and scalar dissipation rate along the centerline for different bulk mean velocities.

hand promote faster mixing between the fuel jet and the co-flow creating larger most reactive mixture fraction surfaces and on the other hand retard the radical pool growth, due to faster transport of the radicals and heat away from the most reactive mixture fraction surface. Therefore, the mixing rate (scalar dissipation rate) plays a complex role, which is the main topic of the following sub-sections.

Two test cases are considered here to illustrate the impact of a change in bulk mean velocity of the co-flow. The autoignition locations predicted by LES are validated against experimental results.

6.1.1 Hydrogen autoignition

The first case is the Cambridge hydrogen experiment [68, 70]. The case with 950K co-flow temperature (Case 0) is considered. The bulk mean velocity of the jet and the co-flow in the base case was 26 m/s. The simulation was repeated with a bulk mean velocity of 20 m/s. The mixture fraction distribution and the scalar dissipation rate for the two cases are shown in fig. 6.1. The figure shows that the mixture fraction distribution with lower velocity did not change significantly, whereas the scalar dissipation rate was decreased.

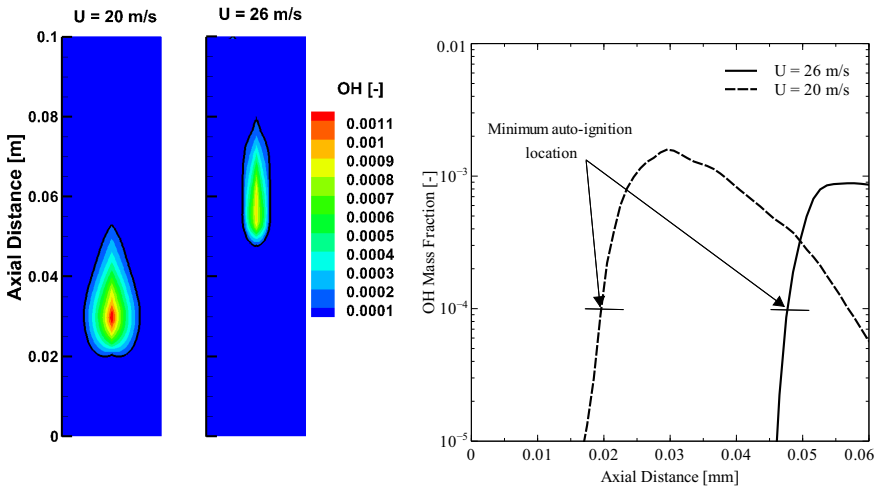

Figure 6.2: OH mass fraction distribution for different bulk mean velocities Left: Contour at the central section Right:Along the centerline.

Table 6.1: Impact of bulk mean velocity on hydrogen autoignition location.

	Lmean		Lmin	
	Experiment	LES	Experiment	LES
20 m/s	32	29	24	20
26 m/s	55	54	47	47

Figure 6.1 (left) shows the OH mass fraction contour at the central section. The centerline distribution of OH is shown along with the ignition criteria in the graph on the right. The corresponding minimum and mean autoignition lengths from experimental measurements and LES are shown in table 6.1.

The experimental measurements and the LES results show that with a 23% decrease in the bulk mean velocity, the mean autoignition length decreased respectively by 41.8% and 43.6%. Scaling the autoignition length with bulk mean velocities would result into an autoignition length of 41 mm, which is more than the one observed experimentally and predicted by the LES simulations. This shows that with a change in the bulk mean velocity at constant turbulent intensity, the auto-ignition length changed disproportionately. Although the mixture fraction distribution did not change significantly, the scalar dissipation rate decreased with reduced bulk mean velocity. This decrease in the

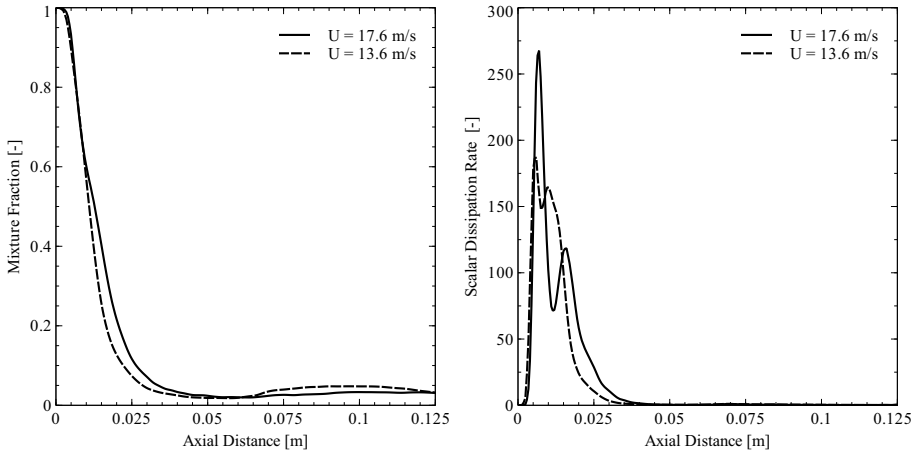

Figure 6.3: Mixture fraction and scalar dissipation rate along the centerline for different bulk mean velocities.

scalar dissipation rate should be expected due to proportional decrease in the velocity fluctuations. Reduced scalar dissipation rate will reduce the radical transport from the most reactive mixture fraction, and will result in further decrease in the autoignition length. Thus, the reduction in autoignition length can be attributed to decrease in the scalar dissipation rate along with the bulk mean velocity.

6.1.2 n-Heptane autoignition

The second case is the n-heptane auto-ignition experiment shown in Fig. 5.3.1. The case with 1113 K co-flow temperature is considered here. The base case has a bulk mean velocity of 17.6 m/s. The bulk mean velocity is changed to 13.8 m/s, keeping the other boundary conditions constant. The mixture fraction and scalar dissipation rates along the centerline are compared in Fig. 6.3. As was seen in the previous case, the mixture fraction distribution did not change and the scalar dissipation rate is reduced with a decrease in the bulk mean velocity.

Figure 6.4 shows the OH mass fraction distribution at the central cross-section for both the cases. The centerline distribution of OH is shown along with the ignition criteria in the graph on the right. The corresponding minimum

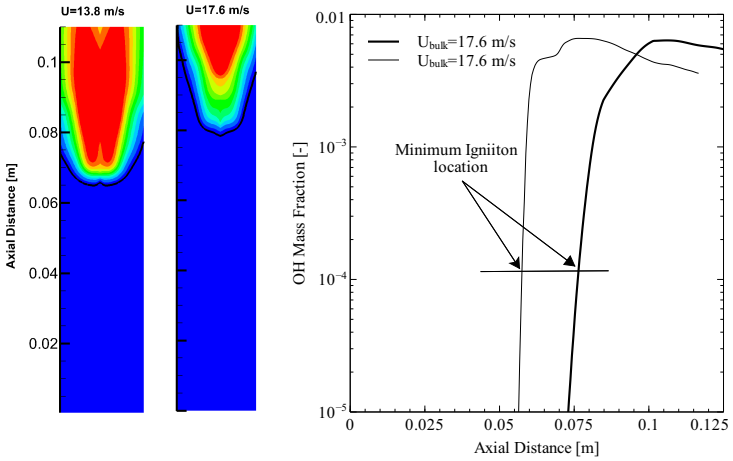

Figure 6.4: OH mass fraction distribution for different bulk mean velocities Left: Contour at the central section Right:Along the centerline.

Table 6.2: Impact of bulk mean velocity on n-Heptane autoignition location.

	Lmean		Lmin	
	Experiment	**LES**	Experiment	**LES**
13.8 m/s	100	**76**	50	**57**
17.6 m/s	140	**105**	90	**77**

and mean autoignition lengths from experimental measurements and LES are shown in table 6.2.

The experimental measurements and the LES results show that the mean autoignition length reduces by 40 % with a 27% decrease in the bulk mean velocity. This case also shows a disproportionate increase in the autoignition length with the bulk mean velocity. With an increase in the bulk mean velocity for the same turbulent intensity, the effective velocity fluctuations increased. The above cases predict a delaying effect of turbulence on auto-ignition.

To separate the effect of convective transport, parameter studies need to be performed with the same bulk mean velocity. The ETH 3D DNS of hydrogen auto-ignition [51], which was used as a validation case in the present work, was also performed for an increased turbulent intensity of 25% [52] for the same bulk mean velocity. DNS results showed that with an increase in the tur-

Table 6.3: Turbulent intensity parameter study boundary conditions

Case	Air Temperature [K]	Fuel Temperature [K]	U [m/s]	Lt [mm]	TI [%]
1	950	750	26	3	5
2	950	750	26	3	10
3	950	750	26	3	15
4	950	750	26	3	25

bulence intensity from 15 to 25 %, the autoignition location increased by 7-8%. This supports the observations from the experiments and the LES results that turbulence delays autoignition. But, these observations are made for turbulent time scales that are much smaller than the minimum ignition delay. Whether this trend continues in the region with turbulent time scales larger than the ignition delay time and what might be the driving mechanisms behind the trends, will be investigated in the next section.

6.2 Impact of turbulence on autoignition

Turbulence can be described by two quantities: turbulence intensity and integral length scales of the large eddies. Turbulence intensity describes the fluctuation of velocity perturbation over the bulk mean velocity, whereas the integral length scale describes the size of the largest energy containing eddies. In the following, the two parameters are varied separately in LES. The ETH hydrogen autoignition DNS test case described in section 5.2.1 is considered. The final subsection discusses the possible interactions between turbulence, mixing and autoignition.

6.2.1 Impact of turbulent intensity

Table 6.3 shows the boundary conditions for the turbulent intensity parameter study. All the boundary conditions except the turbulent intensity have been kept constant. With an increase in the turbulent intensity, faster mixing be-

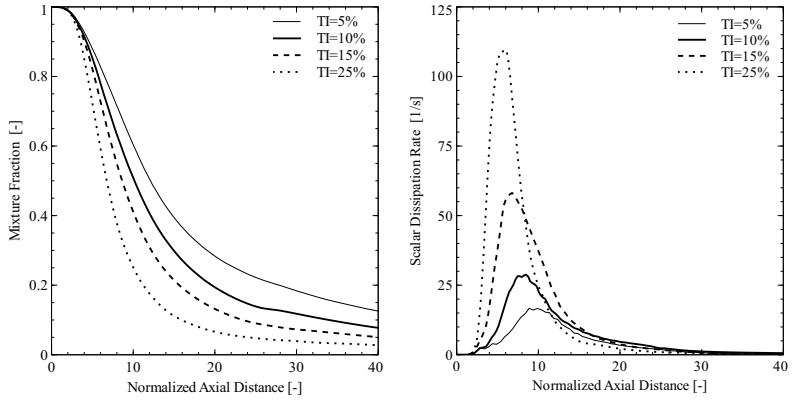

Figure 6.5: Left: Mixture fraction distribution along the axis. Right: Scalar dissipation rate distribution along the axis.

tween fuel and oxidizer is expected. Figure 6.5 shows the axial distribution of time averaged resolved mixture fraction. Higher velocity fluctuations lead indeed to more rapid mixing at the micro-mixing scales. This effect is included in LES through the increased sub-grid viscosity, also termed as modeled or eddy viscosity. The turbulent diffusivity of the mixture fraction is related to this viscosity by the Schmidt number.

Figure 6.6 compares the OH mass fraction for the turbulent intensity parameter study. The magnitude of maximum OH fraction decreases with higher turbulent intensity. The isoline in the contour plot shows the OH criteria of 1e-4. Although there is a radial distribution of the OH mass fraction, the peak OH mass fraction is close to the axis. Therefore, the minimum ignition location can be considered to be along the centerline. The center-line distribution of OH mass fraction along with the OH criterion line is shown on the left hand side of Fig. 6.6. The minimum autoignition length is observed for the 15% case, and maximum for 25%.

Figure 6.7 compares the scalar dissipation rate conditioned on the most reactive mixture fraction along the axis. It is interesting to observe that the conditioned scalar dissipation rate close to the injector (0-5 normalized nozzle radii) increases with the turbulent intensity. After about 15 injector radii the trend reverses. The reason for this behavior of scalar dissipation rate can be explained from the mixture fraction distribution in Fig. 6.5. The rate of mixture

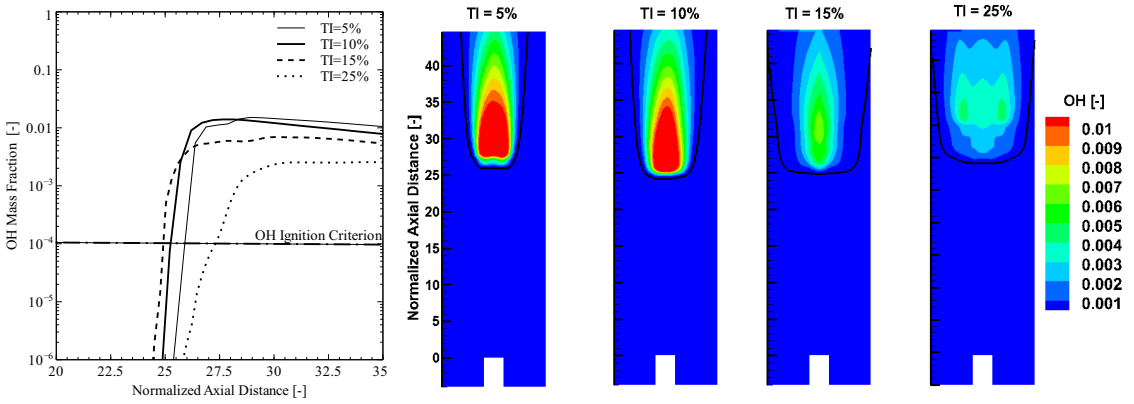

Figure 6.6: Left: LES axial distribution of OH mass fraction. Right: LES OH mass fraction contour with isoline indicating OH ignition criterion.

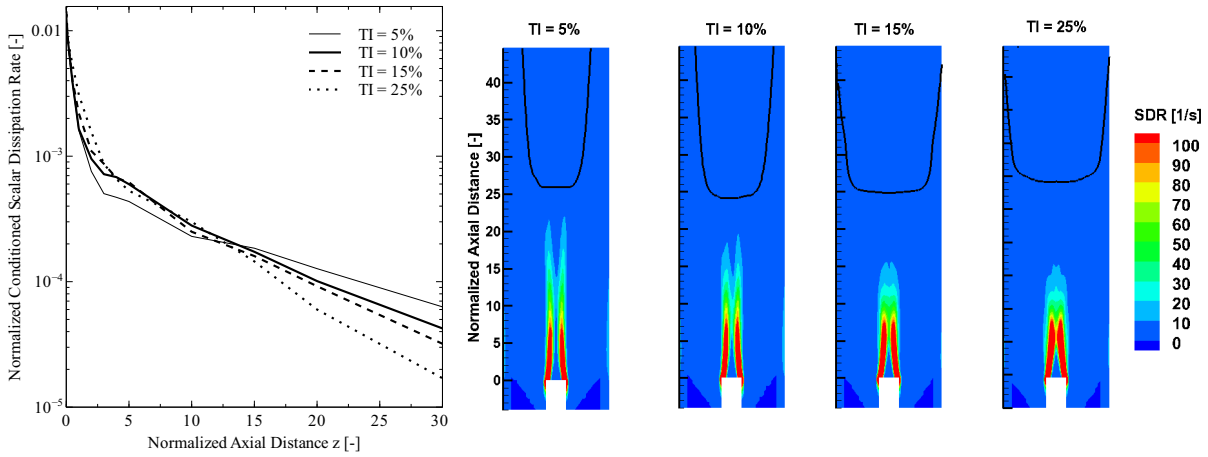

Figure 6.7: Left: LES axial distribution of scalar dissipation rate conditioned on the most reactive mixture fraction. Right: LES scalar dissipation rate contour with isoline indicating OH ignition criterion.

fraction decay increases with the turbulent intensity due to increased micromixing.

From the results, one can safely infer that the mixture fraction and scalar dissipation rate distributions are monotonic functions of the turbulent intensity. With the knowledge that an increase in the turbulence level will promote mixing between the fuel and oxidizer, it is expected that the autoignition length should decrease. This is true for the increase in the turbulent intensity from

5-10-15 % (refer Fig. 6.11). But, such a trend is not observed for a further increase in the turbulent intensity from 15 to 25 %, as was also confirmed by the 3D DNS [51, 52]. This non-monotonic dependence of auto-ignition length on turbulence is the topic of the discussion in section 6.3.

6.2.2 Impact of integral length scale

A non-monotonic dependence of autoignition location on turbulent intensity was observed in the previous section. In this section the integral length scale of the turbulent inlet boundary conditions is varied to study the dependence of autoignition location on the integral length scale.

The integral length scale describes the size of the large eddies. A smaller length scale would enhance the micro-scale mixing and hence increase the rate of fuel-oxidizer mixing which in turn will also affect the pre-ignition chemistry and, eventually, the autoignition length. In the present work integral length scales are varied between 2 mm and 7 mm for the 15% turbulent intensity in order to study their effect, separately from the turbulent intensity.

Table 6.4 shows the boundary conditions for the integral length study. All the boundary conditions except the integral length scale at the co-flow boundary conditions have been kept constant. The axial distribution of the mixture fraction and the scalar dissipation rate are compared in Fig. 6.8. At lower integral length scales, the mixture fraction decays faster. The reason for this is due to the smaller eddies that penetrate more easily into the fuel jet and enhance the micro-mixing. The corresponding scalar dissipation rate distribution shows a higher value and the peak is shifted towards the injector.

The scalar dissipation rate conditioned on the most reactive mixture fraction is shown in Fig. 6.10, and shows a monotonic behavior as for the turbulent intensity study. The scalar dissipation rate conditioned on the most reactive mixture fraction is larger close to the injector for smaller integral length scales. The faster rate of mixing causes the higher scalar dissipation rates.

From the two parameter studies made, one can conclude that the autoignition length shows a non-monotonic behavior with respect to turbulence charac-

Table 6.4: Integral length scale parameter study boundary conditions

Case	Air Temperature [K]	Fuel Temperature [K]	U [m/s]	Lt [mm]	TI [%]
1	950	750	26	2	15
2	950	750	26	3	15
3	950	750	26	4.5	15
4	950	750	26	7	15

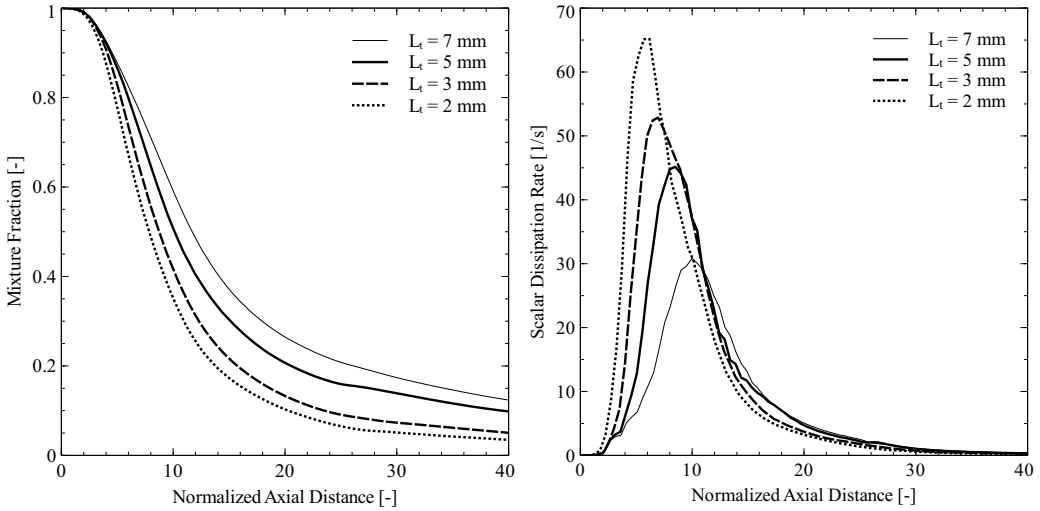

Figure 6.8: Left: Axial Mixture fraction distribution. Right: Axial scalar dissipation rate distribution.

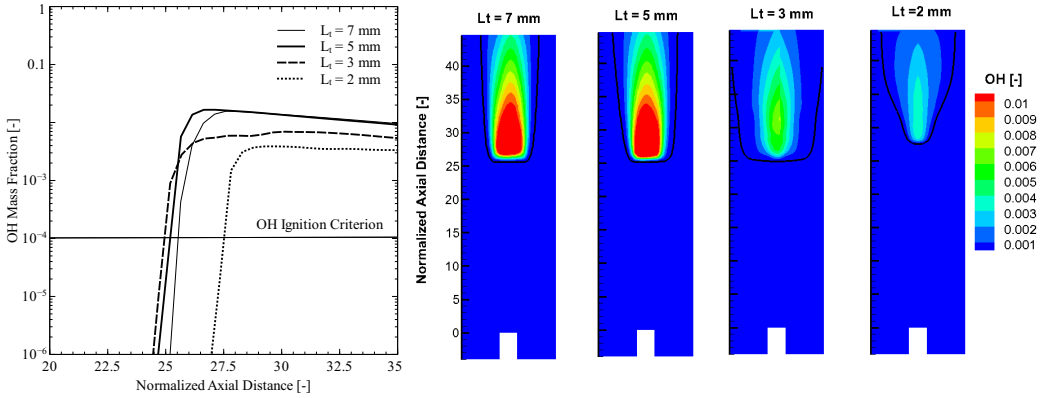

Figure 6.9: Left: LES axial distribution of OH mass fraction. Right: LES OH mass fraction contour with isoline indicating OH ignition criterion.

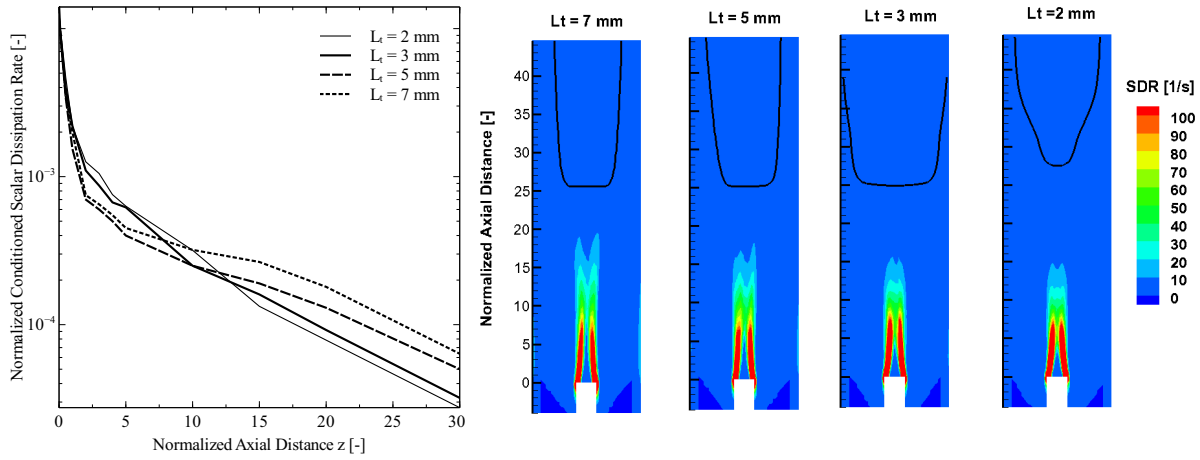

Figure 6.10: Left: Axial distribution of scalar dissipation rate conditioned on the most reactive mixture fraction. Right: Scalar dissipation rate contour with isoline indicating OH ignition criterion.

teristics. Interestingly, the effect can not be explained solely by considering the evolutions of the scalar dissipation rate, which shows a strictly monotonic behavior. Hence, the following section discusses the non-monotonic dependence on the basis of the most reactive mixture fraction surface and the scalar dissipation rate conditioned on it.

6.3 Discussion

Since the variations of turbulent intensity and length scale yielded similar results, the discussion would be focused on the general influence of turbulent time scale on auto-ignition location (refer Fig. 6.11 left). The OH mass fraction criteria of 1e-4 has been used here to be consistent with the DNS studies [51, 52]. Figure 6.11 compares the autoignition lengths for different turbulent intensities and integral length scales from LES. The 3D DNS autoignition lengths for 15% and 25% turbulent intensities are also included. The LES auto-ignition lengths are quite close to the DNS lengths and the trend of increasing autoignition length with turbulent intensity is observed for those two points. The simulated points are also shown in Fig. 6.11 on the right in

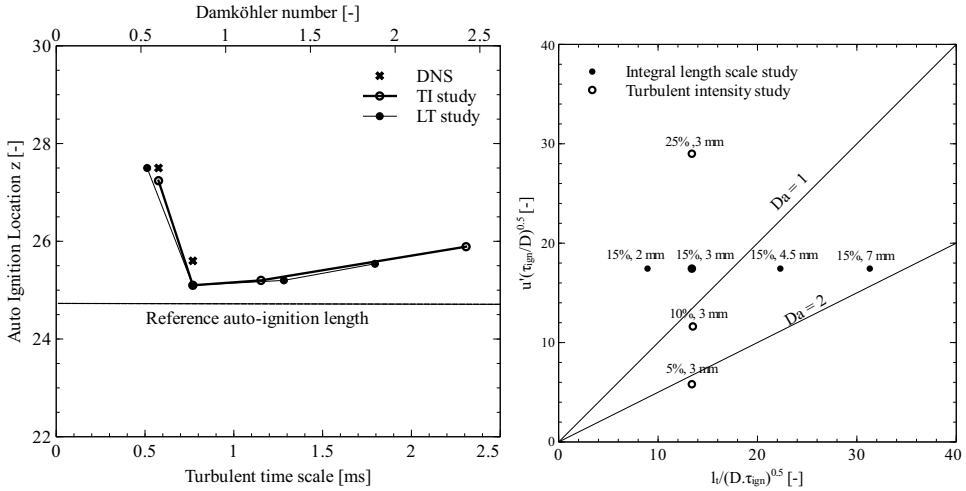

Figure 6.11: Left: Autoignition location for all the cases from the parametric study. Right: Simulated points on the Borghi diagram

a graphical representation similar to the Borghi diagram [11] used to describe the turbulence-flame interaction for premixed flame propagation. However, in our case it is used to describe the effects of turbulence intensities and length scales on mixing and subsequent auto-ignition.

For the axes, non-dimensional values of the turbulence parameters are used, scales with respect to the minimum ignition delay at most reactive mixture fraction and the molecular diffusivity of the mixture: Abscissa (length)= $l_t/(D\tau_{ign})^{0.5}$; Ordinate (intensity)=$u'(\tau_{ign}/D)^{0.5}$. For the present case, the non-dimensional Damköhler (Da) number is defined here as the ratio of the turbulent time scale and the autoignition delay. The constant Da lines are shown in Fig. 6.11. One can conclude from Fig. 6.11 that optimum ignition conditions are reached for Da $\approx$ 1.0 in the present case.

Figure 6.12 shows snapshots of the most reactive mixture fraction iso-line for the parameter studies. For large Da numbers, i.e. the points below the Da= 1 line in the regime diagram (6.11 right), the most reactive mixture fraction line is continuous. This region can be considered analogous to the "wrinkled and corrugated flame" regime. With a decrease in the Da number, i.e higher turbulent intensities (15 to 25%) or smaller integral length scales (3 to 2 mm), the iso-contour of the most reactive mixture fraction is not continuous any-

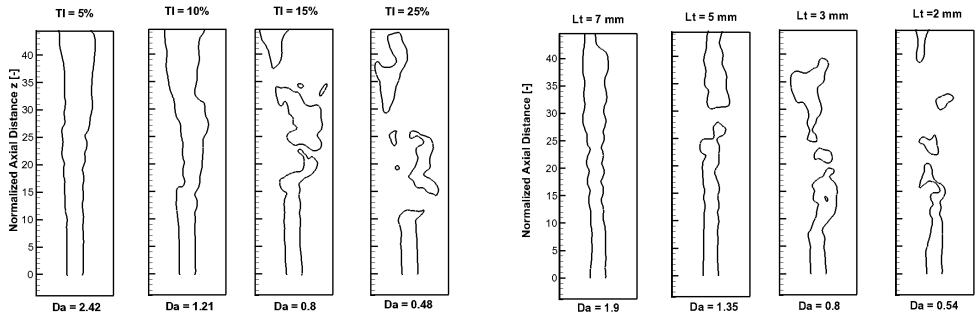

Figure 6.12: Left: Snapshots of the most reactive mixture fraction $Z_{MR} = 0.04$ for the turbulent intensity parameter study. Right: Snapshots of the most reactive mixture fraction $Z_{MR} = 0.04$ for the integral length parameter study.

more, but disrupted forming a sequence of rich mixture pockets convected along the stream. This leads to the so-called random ignition spots regime of auto-ignition. These points lie above the Da= 1 line in the equivalent Borghi diagram (6.11 right), which is equivalent to the ”broken reaction zone” regime.

Hence, two quantities act in competition depending upon the range of Da numbers:

1. Scalar dissipation rate conditioned on the most reactive mixture fraction $\chi|Z_{MR}$ (hindering effect), and

2: Most reactive mixture fraction Z_{MR} iso-surface (promoting effect).

Although all the LES simulations were carried out in 3D, the post processing was done on a cross sectional plane of the computational domain. Hence, in the present work, the most reactive mixture fraction iso-line length L_{MR} on the central cross section, shown in Fig. 6.12, represents the Z_{MR} iso-surface. The time averaged lengths of the most reactive mixture fraction iso-line and the scalar dissipation rate conditioned on it at the central cross-section of the geometry are plotted in Fig. 6.13 on the left and right, respectively.

Figure 6.13 shows that the $\chi|Z_{MR}$ increases steadily with decreasing turbulent time scale, whereas the averaged L_{MR} curve appears to reach a limit at lower values of the turbulent time scale. Due to the non-parallel increase in L_{MR} and

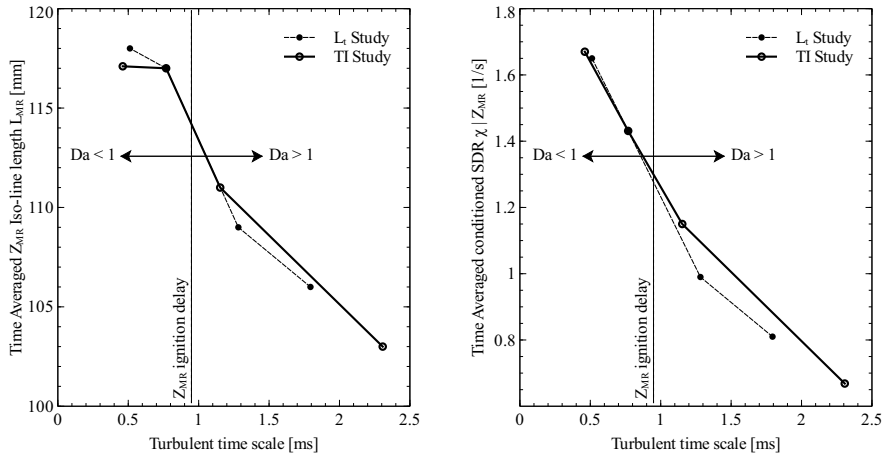

Figure 6.13: Left: Time averaged integral most reactive mixture fraction length. Right: Time averaged integral scalar dissipation rate conditioned on the most reactive mixture fraction

$\chi|Z_{MR}$, the non-monotonic behavior of the ignition length can be explained as follows:

1. At larger turbulent time scales (Da> 1): With a decrease in turbulent time scale, the mixing between fuel and oxidizer is enhanced and the surface area of the Z_{MR} is increased. This increase can be seen in the snapshots of Fig. 6.12 due to wrinkling of the Z_{MR} iso-surface. An increase in Z_{MR} iso-surface would promote the pre-ignition chemistry. The scalar dissipation rate, which inhibits chemical reactions due to heat and radical transport away from the most reactive surface, also increases simultaneously, but at a slower rate. The increase in most reactive mixture fraction zone dominates the increase in scalar dissipation rate, which altogether promotes the auto-ignition chemistry and leads to a shorter auto-ignition length.

2. At smaller time scales (Da < 1): With further decrease in the turbulent time scale, the rate of increase in the most reactive mixture fraction iso-surface is low. At the same time, the scalar dissipation rate increases at a faster rate and dominates over the promoting effect of the increase in Z_{MR} iso-surface. Moreover, transient effects, i.e. a highly perturbed mixing history of the fuel particles, additionally inhibit the auto-ignition pre-reactions. Indeed, when looking at the plots of Fig. 6.14, one can observe that the temporal fluctua-

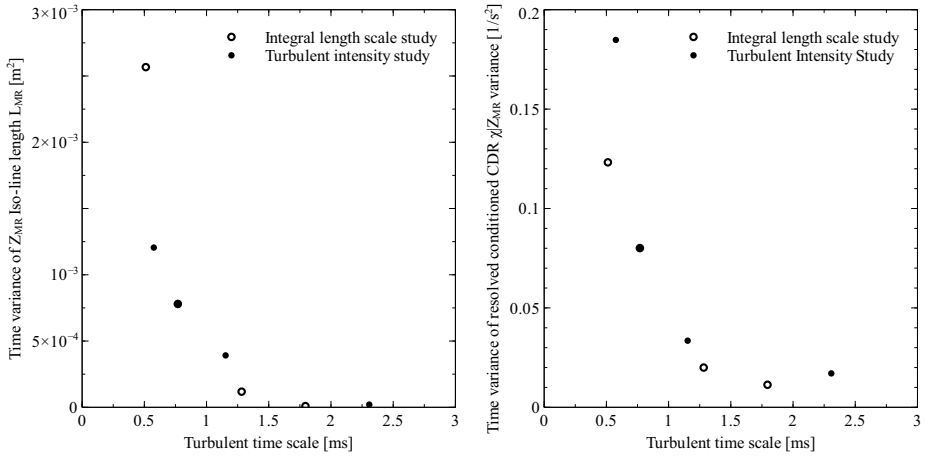

Figure 6.14: Left: Variance of the most reactive mixture fraction iso-line. Right: Variance of the conditioned scalar dissipation rate (SDR) on the most reactive mixture fraction.

tions of both conditioned scalar dissipation and Z_{MR} iso-line length start to increase in this range. Hence, for short turbulent time scales, the inhibiting effects dominate over the promoting ones and the autoignition length increases.

3. For intermediate time scales with Da close to unity, an optimum is reached between the different competing effects and a minimum autoignition length can be observed.

To study these effect more extensively, DNS studies or experiments need to be performed at a broader range of turbulent time scales and fuels.

7 Conclusion and outlook

The present dissertation conceptualized a novel turbulent combustion model for autoignition in LES. Apart from being capable of predicting autoignition with an accuracy within measurement tolerances, the major advantage of the model is the capability of its extension to complex multi-stream mixing problems at low computational cost and modeling complexity. The model is based on tabulated chemistry and stochastic fields turbulence-chemistry interaction model. As the present work concentrated on autoignition modeling, a tabulation method based on homogeneous plug flow reactors has been used. The model uses a transported probability density approach, thus the chemical source term is found in closed form. The model avoids the modeling complexities and errors that are unavoidable with the presumed PDF approach for multi-stream mixing. The model does not presume independence between the mixture fraction and the progress variable. Also, the fluctuations of the progress variable are considered, which makes the model potentially applicable to extinction and reignition.

The model was validated against four laboratory scale experiments on autoignition with various fuels (hydrogen, nHeptane and methane). The model was shown to be capable of capturing the effects of temperature, velocity (Reynolds number), and turbulence intensity variations with excellent qualitative and satisfactory quantitative agreement with the experimental measurements and DNS results. The model was also validated for the MILD (Mild or Intensely Low oxygen Dilution) combustion regime, which has recently been a topic of interest, due to its higher efficiency and lower pollutant emissions. The model moreover has the potential to be applied for premixed and diffusion flames with a suitable tabulation technique.

The LES combustion model was also validated for reheat combustor in Alstom GT 24/26 engine with quaternary (four-stream) mixing, although no re-

sults have been included in the disseration due to confidentiality reasons. The model performed satisfactorily and gave encouraging results for complex reheat combustor geometries. With the grid size of about 10 million cells, the model was capable to deliver results for 5 residence times in a time frame of two weeks. The simulations were run using 32 processors. With increasing computational power and efficient computation codes, the model shows promise to be a part of main-stream combustor development.

A parameter study on the impact of turbulence on hydrogen-air mixing and autoignition in a jet-in-hot-coflow configuration showed a non-trivial dependency of autoignition on turbulence parameters. Although the increased turbulent fluctuations enhanced mixing, the autoignition length behaves nonmonotonically. The nonmonotonic dependence of autoignition is due to the competing effects of improved mixing on the one hand, and the scalar dissipation on the other hand. Improved mixing creates larger most reactive mixture fraction regions, which enhance autoignition chemistry at turbulent scales larger than the ignition delays. For turbulent time scales smaller than the ignition delays, the enhanced scalar dissipation rate transports the radicals at a faster rate away from the most reactive mixture fraction zone, which dominates the effect of larger most reactive mixture fraction regions. This results in a trend reversal and increases the autoignition length. For industrial applications, which generally have smaller turbulent time scale than the autoignition delay, an increase in the Reynolds number (turbulence level) will move the autoignition disproportionately to the one predicted by simple scaling based on the velocities. The autoignition length will be longer than the one scaled using velocity ratios.

7.1 Outlook

The combustion model proposed in this work is suitable for autoignition in single phase flows, but has potential to be extended to include many physical phenomena important for industrial applications. Some of the important features that can be incorporated into the model are briefly discussed here.

As the combustion model is based on transported probability density function model, all the potential for the development of the approach also apply to the proposed model. For the micromixing, the basic IEM (Interaction by Exchange with the Mean) is used in the present work. This term is crucial for performance of the model. The performance of the SF-PV model with more advanced mixing models must be investigated.

The performance of the model for premixed (propagating) and diffusion flames needs validation. The larger gradients in those flames might require a large number of stochastic fields, which is an open question in LES context.

The potential of the model to multi-phase flows with autoignition needs to be investigated. From the modeling point of view a source term in the mixture fraction equations need to be included to consider the vaporization of the fuel droplets.

The model can be extended to include radiation and wall heat losses with an inclusion of an enthalpy dimension to the look-up table.

A more detailed study on the impact of turbulence on autoignition is necessary using experiments and DNS to validate the mechanisms that are proposed in the present work that describe the interaction between turbulence, mixing, and autoignition. The studied need to be carried out for various fuels, before any conclusions can be made.

Bibliography

[1] ANSYS FLUENT academic research, release 6.3 (2006). Technical report, 2012.

[2] J. Baldyga and J.R. Bourne. *Turbulent Mixing and Chemical Reactions*. John Wiley, 1999.

[3] R. A. Baurle and S. S Girimaji. Assumed pdf turbulence-chemistry closure with temperature-composition correlations. *Combust. Flame*, 134:131–148, 2003.

[4] A. C. Benim and K. J. Syed. Laminar flamelet modelling of turbulent premixed combustion. *Applied Mathematical Modelling*, 22:113–136, 1998.

[5] G. Bikas. *Kinetic Mechanism for Hydrocarbon Ignition*. PhD thesis, RWTH Aachen, 2001.

[6] R. W. Bilger. Turbulent flows with nonpremixed reactants. *Comb. Sci. Technol.*, 13(155), 1980.

[7] R. W. Bilger. Conditional moment closure for turbulent reacting flows. *Phys. Fluids*, A5(436), 1993.

[8] F. Bisetti and J. Y. Chen. Numerical issues of Monte Carlo PDF for large eddy simulations of turbulent flames. *Joint Central and Western States Combustion Institute*, 2005.

[9] J.D. Blouch and C.K. Law. Effects of turbulence one-point non-premixed ignition of hydrogen in heated counterflow. *Combust. Flame*, 132:512–522, 2003.

[10] J.D. Blouch, C.J. Sung, C.D. Fotache, and C.K. Law. Turbulent ignition of nonpremixed hydrogen by heated counter flowing atmospheric air. *Proc Combust Inst*, 27:1221–1228, 1998.

[11] R. Borghi. On the structure and morphology of turbulent premixed flames. *C. Bruno, S. Casci (Eds.), Recent advances in aerospace science*, Plenum, New York:117–138, 1985.

[12] D. Bradley, L. K. Kwa, A. K. C. Lau, and Missaghi M. Laminar flamelet modelling of recirculating premixed methane and propane-air combustion. *Combust. Flame*, 71:109–122, 1998.

[13] D. Bradley and A.K.C. Lau. The mathematical modelling of premixed turbulent combustion. *Pure & Appl. Chem.*, 62 (5):803–814, 1990.

[14] M. Brandt, W. Polifke, and P. Flohr. Approximation of joint PDFs by discrete distributions generated with Monte-Carlo methods. *Combust. Theor. Model.*, 10:535–558, 2006.

[15] M. Brandt, W. Polifke, B. Ivancic, P. Flohr, and Paikert B. Auto-ignition in a gas turbine burner at elevated temperature. In *International Gas Turbine and Aeroengine Congress & Exposition, ASME (2003-GT-38224), Atlanta, GA, U.S.A. (2003)*, 2003.

[16] R. Cabra, J. Y. Chen, A. N. Dibble, and R. S. Barlow. Lifted methane air jet flames in a vitiated coflow. *Combust. Flame*, 143:491–506, 2005.

[17] R. Cabra, T Myhrvold, J.Y. Chen, Dible R.W., A.N. Karpetis, and R.S. Barlow. Simultaneous laser Raman-Rayleigh-LIF measurements and numerical modeling results of a lifted turbulent h2/n2 jet flame in a vitiated coflow. *Proc. Combust. Inst.*, 29:1A03:1–20, 2002.

[18] A Cavaliere and Mara de Jaonnon. Mild combustion. *Progress in Energy and Combustion Science*, 30:329–366, 2004.

[19] I.B. Celik, Z.N. Cehreli, and I. Yavuz. Index of resolution quality for large eddy simulations. *J. Fluids Eng.*, 127:949–958, 2005.

[20] C.S. Chang, K. N. Zhang, K.N.C. Bray, and B. Rogg. Modelling and simulation and autoignition under simulated diesel engine conditions. *Combust. Sci. Technol.*, 113-114:205–219, 1996.

[21] M.J. Cleary, J.H. Kent, and R.W. Bilger. Prediction of carbon monoxide in fires by conditional moment closure. *Proc. Combust. Inst.*, 29(1):273–279, 2002.

[22] P.J. Coelho and N. Peters. Numerical simulation of a MILD combustion burner. *Combustion and Flame*, 124 (3):503–518, 2001.

[23] B.B. Dally, A.N. Karpetis, and R.S. Barlow. Structure of turbulent nonpremixed jet flames in a diluted hot coflow. *Proc. Combust. Inst.*, 29:1147–1154, 2002.

[24] A. De, E. Oldenhof, P. Sathiah, and D. Roekaerts. Numerical simulation of Delft-Jet-in-Hot-Coflow (DJHC) flames using the eddy dissipation concept model for turbulence-chemistry interaction. *Flow, Turbulence an Combustion*, 1386-6184:1–31, 2011.

[25] LPH De Goey and JHM ten Thije Boonkkamp. A flamelet description of premixed laminar flames and the relation with flame stretch. *Combust. Flame*, 119(3):253–271, 1999.

[26] G. De Paola, I.S. Kim, and Mastorakos E. Second-order conditional moment closure simulations of autoignition of an n-heptane plume in a turbulent coflow of heated air. *Flow Turbul. Combust.*, 82:455–475, 2009.

[27] P. Domingo, L. Vervisch, and Bray K. Partially premixed flamelets in LES of nonpremixed turbulent combustion. *Combust. Theor. Model.*, 6(4):529–551, 2002.

[28] P. Domingo, L. Vervisch, and D. Veynante. Large-eddy simulation of a lifted methane jet flame in a vitiated coflow. *Combust. Flame*, 152:415–432, 2008.

[29] C. Dopazo and E. O'Brien. Functional formulation of non-isothermal turbulent reactive flows. *Phys. Fluids*, 17, 1974.

[30] T. Echekki and J.H. Chen. Direct Numerical Simulations of auto-ignition in non-homogeneous hydrogen-air mixtures. *Combust. Flame*, 134:169–191, 2003.

[31] M. Frenklach, T. Bowman, G. Smith, and B. Gardiner. Gri methane chemical mechanism ver 3.0.

[32] J. Galpin, C. Angelberger, A. Naudin, and L. Vervisch. Large-eddy simulation of H2 air auto-ignition using tabulated detailed chemistry. *J. Turbul.*, 13:1–21, 2008.

[33] A. Gamory. *Micromixing Effects in Atmospheric Reacting Flows*. PhD thesis, University of Cambridge, 2007.

[34] A. Garmory, E.S. Richardsona, and E. Mastorakos. Effects on strain rate on high-pressure nonpremixed n-Heptane autoignition in counterflow. *Comb.Flame*, 137:320–339, 2004.

[35] A. Garmory, E.S. Richardsona, and E. Mastorakos. Micromixing effects in a reacting plume by the stochastic fields method. *Atmos. Environ.*, 40(6):1078–1091, 2006.

[36] M. Germano, U. Piomelli, P. Moin, and W.H. Cabot. A dynamic subgrid-scale eddy viscosity model. *Physics of Fluids*, 3:1760–1765, 1991.

[37] O. Gicquel, N. Darabiha, , and D. Roku Thevenin. Laminar premixed hyrogen/air counterflow flame simulations using flame prolongation of ildm with differential diffusion. *Proc Combust Inst*, 28:1901â€“1908, 2000.

[38] D. G. Goodwin. Cantera: Object-oriented software for reacting flows, california institute of technology. Technical report, web site: http://blue.caltech.edu/cantera/index.html, 2002.

[39] R.L. Gordon, A.R. Masri, and E. Mastorakos. Simultaneous rayleigh temperature, OH- and CH2O- LIF imaging of methane jets in a vitiated coflow. *Combust. Flame*, 155:181–195, 2008.

[40] M. Ihme, C.M. Cha, and H. Pitsch. Prediction of local extinction and re-ignition effects in non-premixed turbulent combustion using a flamelet/progress variable approach. *Proc Combust Inst*, 30(1):793–800, 2005.

[41] M. Ihme and H. Pitsch. Prediction of extinction and reignition in non-premixed turbulent flames using a flamelet/progress variable model: 1 a priori study of presumed pdf closure. *Combust. Flame*, 155:70–89, 2008.

[42] M. Ihme and H. Pitsch. Prediction of extinction and reignition in non-premixed turbulent flames using a flamelet/progress variable model 2. application in LES of Sandia flames D and E. *Combust. Flame*, 155:90–107, 2008.

[43] M. Ihme and Y.C. See. Prediction of autoignition in a lifted methane/air flame using an unsteady flamelet/progress variable model. *Combust. Flame*, 157:1850–1862, 2010.

[44] M. Ihme and Y.C. See. LES flamelet modeling of a three-stream MILD combustor: Analysis of flame sensitivity to scalar inflow conditions. *Proc. Combust. Inst*, 33:1309–1317, 2011.

[45] H. G. Im, J. H. Chen, and C. K. Law. Ignition of hydrogen/air mixing layer in turbulent flows. *Symposium (International) on Combustion*, 27:1047–1056, 1998.

[46] B. Ivancic, P. Flohr, B. Paikert, M. Brandt, and W Polifke. Auto-ignition and heat release in a gas turbine burner at elevated temperature. In *International Gas Turbine and Aeroengine Congress & Exposition, ASME GT-2004-53339, Vienna, Austria*, 2004.

[47] W.P. Jones and S. Navarro-Martinez. Large eddy simulation of autoignition with a subgrid probability density function method. *Combust. Flame*, 150:170–187, 2007.

[48] W.P. Jones and S. Navarro-Martinez. Study of hydrogen auto-ignition in a turbulent air co-flow using a Large Eddy Simulation approach. *Computers and Fluids*, 37:802–808, 2008.

[49] W.P. Jones, S. Navarro-Martinez, and O. Röhl. Large eddy simulation of hydrogen auto-ignition with a probability density function method. *Proc. Combust. Inst.*, 31(2):1765–1771, 2007.

[50] W.P. Jones and S. Prasad. Large eddy simulation of the sandia flame series (D - F) using the eulerian stochastic field method. *Combust. Flame*, 157, Issue 9:1621–1636, 2010.

[51] S.G. Kerkemeier. *Direct Numerical Simulation of Combustion on Peta-Scale Formats: Application to Non-premixed Hydrogen Autoignition*. PhD thesis, ETH Zürich, 2010.

[52] S.G. Kerkemeier, C.E. Frouzakis, K. Boulouchos, and E. Mastorakos. Numerical simulation of autoignition of a diluted hydrogen plume in coflowing turbulent hot air. In *AIAA Aerospace Sciences Meeting Including the New Horizons Forum and Aerospace Exposition*, pages 1–12, 2010.

[53] S. H. Kim and K.Y. Huh. Second-order conditional moment closure modeling of turbulent piloted jet diffusion flames. *Combust. and Flame*, 138:336–352, 2004.

[54] S. H. Kim, K.Y. Huh, and B.B. Dally. Conditional moment closure modeling of turbulent nonpremixed combustion in diluted hot coflow. *Proceedings of the Combustion Institute*, 30:751–757, 2005.

[55] S.H. Kim, K.Y. Huh, and R.W. Bilger. Conditional moment closure (CMC) predictions of a turbulent methane-air jet flame. *Combust. Flame*, 125(3):1176–1195, 2001.

[56] M. Klein, A. Sadiki, and J. Janicka. A digital filter based generation of inflow data for spatially developing direct numerical or large eddy simulations. *J. Comput. Chem. Phys.*, 2:652–665, 2003.

[57] A.Y. Klimenko. Multicomponent diffusion of various admixtures in turbulent flow. *Phys. Fluids*, 25(3):327–334, 1990.

[58] A.Y. Klimenko and R.W. Bilger. Conditional moment closure for turbulent combustion. *Prog. Energy Combust. Sci.*, 186(6):595–687, 1999.

[59] A. Kronenburg, R.W. Bilger, and J.H. Kent. Second-order conditional moment closure for turbulent jet diffusion flames. *Symposium (International) on Combustion*, 27(1):1097–1104, 1998.

[60] A. Kronenburg and M. Kostka. Modeling extinction and reignition in turbulent flames. *Combust. Flame*, 143(4):342–356, 2005.

[61] A. Kronenburg and A.E. Papoutsakis. Conditional moment closure modeling of extinction and re-ignition in turbulent non-premixed flames. *Proc. Combust. Inst.*, 30(1):759–766, 2005.

[62] R.M. Kulkarni and W. Polifke. Large eddy simulation of auto-ignition in a turbulent hydrogen jet flame using a progress variable approach. *Journal of Combustion,*, Special Issue: Turbulent Combustion Modeling 2012, 2012.

[63] R.M. Kulkarni and W Polifke. LES of Delft-Jet-In-Hot-Coflow (DJHC) with tabulated chemistry and stochastic fields combustion model. *Fuel Process. Technol.*, Special Issue: The Eleventh International Conference on Combustion and Energy Utilization:1–10, 2012.

[64] J. Li, Z. Zhao, A. Kazokov, and F.L. Dryer. An updated comprehensive kinetic model of hydrogen combustion. *Int. J. Chem. Kinet.*, 36:566–575, 2004.

[65] U. Maas and S.B. Pope. Simplifying chemical kinetics: Intrinsic low-dimensional manifolds in composition space. *Combust. Flame*, 88(3-4):239–264, 1992.

[66] U. Maas and S.B. Pope. Laminar flame calculations using simplified chemical kinetics based on intrinsic low-dimensional manifolds. *Proc.Comb.Inst.*, 25:1349–1356, 1994.

[67] B.F. Magnussen and B.H. Hjertager. On mathematcal modeling of turbulent combustion with special emphasis on soot formation and combustion. *Proc. Combust. Inst.*, pages 719–729, 1976.

[68] C.N. Markides. *Autoignition in Turbulent Flows*. PhD thesis, University of Cambridge, 2005.

[69] C.N. Markides, G. De Paola, and E Mastorakos. Measurements and simulations of mixing and autoignition of an n-heptane plume in a turbulent flow of heated air. *Exp. Therm Fluid Sci.*, 31:393–401, 2007.

[70] C.N. Markides and E. Mastorakos. An experimental study of hydrogen autoignition in a turbulent co-flow of heated air. *Proc Combust Inst*, 30(1):883–891, 2005.

[71] C.N. Markides and E. Mastorakos. Expetimental investigation of the effects of turbulence and mixing on auto-ignition chemistry. *Flow Turbul. Combust.*, 86:585–608, 2010.

[72] E. Mastorakos. Ignition of turbulent non-premixed flames. *Prog. Energy Combust. Sci.*, 35:57–97, 2009.

[73] E. Mastorakos, T.A. Baritaud, and T.J. Poinsot. Numerical simulations of autoignition in turbulent mixing flows. *Combust. Flame*, 109:198–223, 1997.

[74] F. Mathey, D. Cokljat, J. P. Bertoglio, , and E. Sergent. Assessment of the vortex method for large eddy simulation inlet conditions. *Progr. Comput. Fluid. Dyn.*, 6 (1/2/3):58–67, 2006.

[75] H. Möbus, P. Gerlinger, and D. Brüggemann. A probability density function method for turbulent mixing and combustion on three-dimensional unstructured deforming meshes. *Proc. Combust. Inst.*, 124(3):519–534, 2001.

[76] M. Muradoglu. A consistent hybrid finite-volume/particle method for the pdf equations of turbulent reactive flow. *J. Comput. Chem. Phys.*, 154:342–371, 1999.

[77] R. Mustata, L. Valino, C. Jim‘enez, W.P. Jones, and S. Bondi. A probability density function eulerian monte carlo field method for large eddy simulations: Application to a turbulent piloted methane/air diffusion flame (Sandia D). *Combust. Flame*, 145(1-2):88–104, 2005.

[78] A.T. Norris and S.B. Pope. Modeling of extinction in turbulent diffusion flames by the velocity-dissipation-composition pdf method. *Combust. Flame*, 100:211–220, 1995.

[79] E. Oldenhof, M.J. Tummers, E.H. van Veen, and D.J.E.M. Roekaerts. Ignition kernel formation and lift-off behaviour of jet-in-hot-coflow flames. *Combust. and Flame*, 157:1167–1178, 2011.

[80] E. Oldenhof, M.J. Tummers, E.H. vanVeen, and D.J.E.M. Roekaerts. Role of entrainment in the stabilisation of jet-in-hot-coflow flames. *Combust. Flame*, 158:1553–1563, 2011.

[81] N. Peters. Local quenching due to flame stretch and non-premixed turbulent combustion. *Combust. Sci. Technol.*, 30:1–7, 1983.

[82] N. Peters. *Turbulent Combustion.* Cambridge University Press, 2000.

[83] C.D. Pierce and P. Moin. Progress-variable approach for large-eddy simulation of turbulent combustion. *Tech. Report CTR*, 2001.

[84] C.D. Pierce and P. Moin. Progress-variable approach for large-eddy simulation of non-premixed turbulent combustion. *J. Fluid Mech.*, 504(1):73–97, 2004.

[85] H. Pitsch. Large eddy simulation of turbulent combustion. *The Annual Review of Fluid Mechanics*, 38(453-482):544–547, 2006.

[86] H. Pitsch, M. Chen, and N. Peters. Unsteady flamelet modeling of turbulent hydrogen-air diffusion flames. *Symposium (International) on Combustion*, 27(1):1057–1064, 1998.

[87] H. Pitsch and M. Ihme. An unsteady flamelet progress varibale method for LES of nonpremixed turbulent combustion. In *AIAA Aerospace Science Meeting*, 2005.

[88] T. Plessing, N. Peters, and J. G. Wünning. Laseroptical investigation of highly preheated combustion with strong exhaust gas recirculation. *Proceedings of the Combustion Institute*, 27:503–518, 1998.

[89] T. Poinsot and D. Veynante. *Theoritical and Numerical Combustion.* Plenum Press, 2005.

[90] W. Polifke, M. Bettelini, W. Geng, Müller U. C., W. Weisenstein, and P.vA. Jansohn. Comparison of combustion models for industrial applications. In *Eccomas 98, Athens, Greece*, 1998.

[91] S.B. Pope. A rational method of determining probability distributions in turbulent reacting flows. *Jnl. Non-Equil. Thermod*, 4(1):309–323, 1979.

[92] S.B. Pope. A Monte Carlo method for the PDF equations of turbulent reactive flow. *Combust. Sci. Technol.*, 25(1784):159–174, 1981.

[93] S.B. Pope. *Turbulent Flows.* Cambridge University Press, 2000.

[94] V.N. Prasad. *Large Eddy Simulation of partially premixed turbulent combustion.* PhD thesis, Imperial College, University of London, 2011.

[95] Kulkarni R., Zellhuber M., and Polifke W. LES based investigation of autoignition in turbulent co-flow configurations. In *European Combustion Meeting 2011*, pages 1–36, Cardiff, UK, June 29 – Juli 1 2011. British section of the Combustion Institute.

[96] Kulkarni R., Zellhuber M., and Polifke W. LES based investigation of autoignition in turbulent co-flow configurations. *Combust. Theor. Model.*, pages 0–21, 2012.

[97] V. Raman, H. Pitsch, and R.O. Fox. Hybrid large-eddy simulation/lagrangian filtered-density-function approach for simulating turbulent combustion. *Combust. Flame*, 143(1-2):56–78, 2005.

[98] G.A. Rao, Y. Levy, and E.J. Gutmark. Chemical kinetic analysis of a flameless gas turbine combustor. In *ASME Turbo Expo, Berlin, Germany GT2007-27766.*, 2008.

[99] N. Rott. Note on the history of the reynolds number. *Annual Review of Fluid Mechanics*, 22:1–11, 1990.

[100] V. Sabelnikov and O. Soulard. Rapidly decorrelating velocity field model as a tool for solving one point fokker planck equations for probability density functions of turbulent reactive scalars. *Physical Review E*, 72:016301, 2005.

[101] S. Sreedhara and K. N. Lakshmisha. Direct Numerical simulation of autoignition in a nonpremixed, turbulent medium. *Proc Combust Inst*, 28:25–33, 2000.

[102] S. Sreedhara and K. N. Lakshmisha. Direct Numerical Simulation of scalar mixing and autoignition in a turbulent medium. *Journal of Aeronautical Society of India*, 53 (2):65, 2001.

[103] I. Stanković, A. Triantafyllidis, E. Mastorakos, C. Lacor, and B. Merci. Simulation of hydrogen auto-ignition in a turbulent co-flow of heated air with LES and CMC approach. *Flow Turbul. Combust.*, 86:689–710, 2011.

[104] S. Subramaniam and D.C. Haworth. Comparison of eulerian and lagrangian monte carlo pdf methods for turbulent diffusion flames. *Int. J. of Engine Res.*, 1(2):519–534, 2000.

[105] G. Taylor. Dispersion of soluble matter in solvent flowing slowly through a tube. *Proc. R. Soc. London, Ser. A*, 219:186–203, 1953.

[106] L. Valino. A field monte carlo formulation for calculating the probability density function of a single scalar in a turbulent flow. *Flow Turbul. Combust.*, 60(2):157–172, 1998.

[107] J.A. van Oijen, F.A. Lammers, and L.P.H. DeGoey. Modeling of Complex Premixed Burner Systems by Using Flamelet-Generated Manifolds. *Combust. Flame*, 127:2124–2134, 2001.

[108] L. Vervisch, R. Hauguel, P. Domingo, and M. Rullaud. Three facets of turbulent combustion modelling: DNS of premixed v-flame, LES of lifted nonpremixed flame and RANS of jet-flame. *J. Turbul.*, 5:1–36, 2004.

[109] A.W. Vreman, J.A. van Oijen, LPH de Geoy, and RJM Bastian. Premixed and non-premixed generated manifolds in large-eddy simulation of sandia flame D and F. *Combust. Flame*, 153:394–416, 2008.

[110] J.A. Wünning and J.G. Wünning. Flameless oxidation to reduce thermalNO-formation. *Progress in Energy and Combustion Science*, 23:81–94, 1997.

[111] K. Xiao, D. Schmidt, and U. Maas. Implementation of reduced kinetic models in turbulent flame calculations. In *SFB568-Workshop: Trends in numerical and physical modeling for turbulent processes in gas turbine combustors*, 1994.

[112] B. Yang and S.B. Pope. An investigation of the accuracy of manifold methods and splitting schemes in the computational implementation of combustion chemistry. *Combust. Flame*, 112:16–32, 1998.

[113] R.A. Yetter, F.L. Dryer, and H. Rabitz. A comprehensive reaction mechanism for carbon monoxide/hydrogen/oxygen kinetics. *Combust. Sci. Technol.*, 79:97–129, 1991.

[114] R.A. Yetter, F.L. Dryer, and H. Rabitz. Triple flames and partially premixed combustion in autoignition of nonpremixed turbulent mixtures. *Proc. Combust. Inst.*, 26:233–240, 1996.

A Appendix 1

A.1 SF-PV Combustion model implementation

The SF-PV model described in chapter 4 for multi-stream mixing is implemented in Fluent v12 [1] to consider up to 5 stream mixing. This appendix describes the method that was used for the implementation. There are two major aspects in the model:

1. Look-up table generation
2. Turbulence-chemistry interaction in LES

These tabulation is done in a pre-processing step using open-source chemical kinetics code Cantera [38]. The table is then coupled to the LES solver (Fluent) through the combustion model transport equations described in chapter 4.3.4.The description in this appendix is split into two sections. The first section describes the tabulation method and the second describes the implementation of the turbulence-chemistry interaction model in Fluent and the coupling of the look-up table.

A.1.1 Look-up table generation

The look-up table generation is done in a pre-processing step. The look-up table is generated using reactor networks available in Cantera. The table needs all the boundary conditions, which are the thermo-chemical (species composition, temperature/enthalpy) properties of the streams (N_s) that are to be simulated. For the tabulation, depending on the number of streams, an array of tabulation points in the mixture fraction dimension is created. It is recommended to distribute the points non-uniformly along the mixture fraction

dimension with more points clustered close to the most reactive mixture fraction. Reactors are set up using the following initial conditions:

$$Y_{\alpha}^{t=0} = Z_1 * Y_{\alpha,1} + Z_2 * Y_{\alpha,2} + ... + Z_{N_s} * Y_{\alpha,N_s} \tag{A.1}$$

where $Y_{\alpha,N}$ is the species composition or enthalpy for stream N and $Z_1, Z_2, ...Z_{Ns}$ are the mixture fractions of the streams. The reactors are initialized for the points in the mixture fraction matrix one after another and are run (time marching) from the initial state to equilibrium. During their evolution, the chemical source terms, i.e. the rate of change in mass fraction, of the progress variable species, heat release and the species of interest are tabulated as a function of the progress variable and the mixture fractions. Other species or quantities of interest that are not transported in LES can also be tabulated. The value of the source term or any tabulated quantity can be read through interpolation. In the present work, linear interpolation has been used. This method should be sufficient, provided that the distribution of the mixture fraction and progress variable tabulation points is carefully done.

Another important setting in the tabulation methods is the definition of the progress variable. The definition has to be changed depending on the type of fuel. The choice of the progress variable is important. An incorrect choice of the progress variable will lead to failure of the model.

A.1.2 Turbulence-chemistry interaction

The stochastic PDE equations described in section 4.3.4 are solved using the UDS (User defined scalars). Each scalar on a field corresponds to a UDS. As eight stochastic fields are considered in the present work, altogether $8*(N_s-1)$ UDS are needed for the mixture fractions, where N_s is the number of streams. Additional 8 fields are necessary for the progress variable. Altogether N_s*8 number of UDS are used. There is a limitation of number of UDS in Fluent v12. Fluent v12 allows only 50 UDS. Therefore, there is a restriction on the number of fields that can be used, depending on the number of streams. If N_f represents the number of fields, then $N_s * N_f < 50$ is the restriction. For e.g.,

with 8 fields, one can use 7 streams, or for a binary case, up to 25 fields can be used.

The stochastic fields method used in the present work is based in Ito formulation of Valino [106]. One of the requirements of the formulation is that for implicit time schemes, the Wiener term ($\frac{dW_i^n}{dt}$ term in Eq. 4.12,4.13) should be evaluated only once at the beginning of the time step and should remain constant for that throughout the step. The Wiener process is modeled by $dW_i^n = R_i^n dt^{(1/2)}$, where R_i^n is the random dichotmic random number $[-1,+1]$. The dichotmic random number is different for each field, but is independent of space.

The stochastic term (third on the right-hand-side of Eq. 4.12 4.13), micro-mixing term (fourth term), and the chemical source term (only for the progress variable) are included as user defined source UDF (DEFINE SOURCE). The filtered density, gradients, and the scalar values are available from Fluent in the UDF. The average of a scalar over all the fields, which is needed to calculate the micro-mixing term, is evaluated at every time step in DEFINE ADJUST UDF ans stored in UDM (User defined memory). The chemical source term is read directly from the look-up table as a function of the mixture fractions and the progress variable for a particular field.

In LES, major chemical species (reactants and combustion products) and sensible enthalpy are transported. Chemical source terms for the species and energy equation is calculated using the following equation:

$$\widetilde{\dot{\omega}_\alpha} = \bar{\rho}\frac{1}{N_f}\sum_{n=1}^{N_f}\dot{\omega}_\alpha^n(Z_1^n, Z_2^n, ..., Z_{N_s}^n, Y_c^n) \tag{A.2}$$

The average is done over all the fields N_f. Other species of interest that are not transported in LES are read directly from the table using the same equation.

B Appendix 2

B.1 Mesh quality study

B.1.1 Hydrogen and heptane autoignition test cases

To study the LES mesh quality, two meshes with different sizes were used. Mesh 1 comprises 150x70x48 nodes in axial, radial and azimuthal directions respectively. The corresponding number of nodes for a finer mesh, Mesh 2, are 200x90x56. The mesh was clustered towards the central axis in order to resolve the mixing layer between the fuel and the air stream. Case 0 boundary conditions were used for this study.

The following LES quality index suggested by [19] based on the viscosity ratio has been used for the study:

$$LES\_IQ = \frac{1}{1 + 0.05\left(\frac{\nu_{t,eff}}{\nu}\right)^{0.53}} \tag{B.1}$$

In equation B.1, $\nu_{t,eff}$ is the effective viscosity (laminar+turbulent) and ν is the laminar viscosity. According to [19], the LES quality index should be above 0.8 for quality LES mesh.

The contour plots on the left hand side of Fig. B.1 show snapshots the LES quality index for both the meshes. The LES quality criteria based on the above index has been satisfied by both meshes. Mesh 2 has higher values of the index suggesting a better quality due to the more refined mesh.

The right hand side of Fig. B.1 shows the time averaged axial distribution of

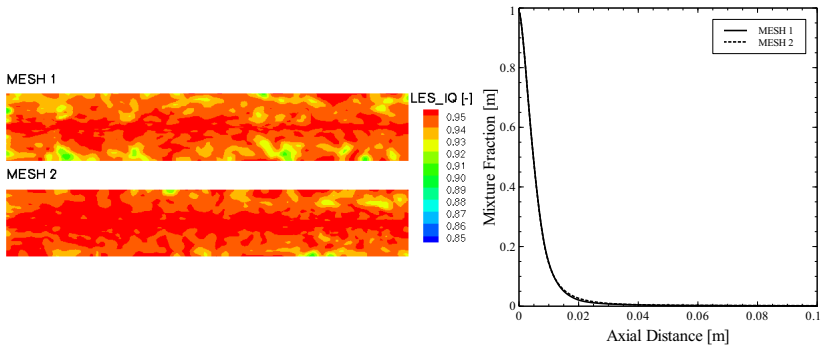

Figure B.1: LES quality criteria (left) and the time averaged resolved axial mixture fraction distribution(right) Mesh1: 150x70x48 and Mesh2: 200x90x56 nodes in axial, radial and azimuthal directions, respectively.

the resolved mixture fraction. No significant difference between the curves for the two meshes is observed. This shows that there is no further refinement necessary and that the Mesh1 is a good quality LES mesh for the test case. Due to this reason, the relatively coarser Mesh 1 is used for the model validation in the following sections.

B.1.2 Delft Jet in Hot Coflow mesh

In partially- or non-premixed cases the flow field and mixing between different streams is extremely important, as the chemical reactions strongly depend on the mixing processes. In the MILD combustion regime, where the Da number is low, combustion is kinetically controlled. Auto-ignition takes place at very lean conditions due to reduced oxygen content in the co-flow. The chemical reactions are strongly affected by the turbulent co-flow. The turbulence-chemistry interaction plays a major role in MILD combustion regime. Therefore, proper prediction of flow and mixing is an absolute necessity for successful combustion simulation.

The test case with Re= 8800 has been considered as a representative for the grid independence study, due to its highest jet velocity (Reynolds number).

A coarse mesh with 750 thousand and a fine mesh with 1 million cells was considered. The simulations were carried out with the combustion model described above.

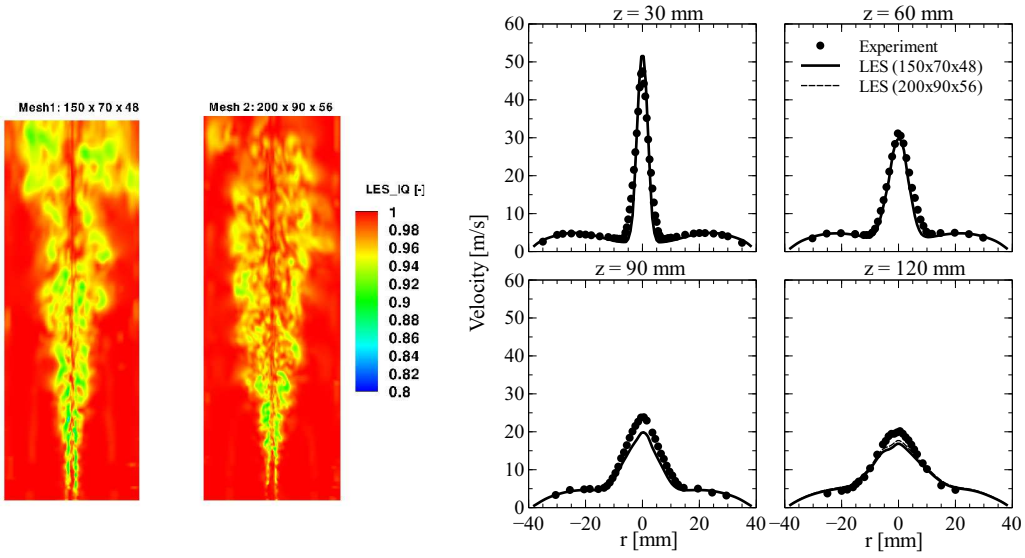

Figure B.2: LES quality criteria (left) and the time averaged resolved velocity (right) Mesh1: 150x70x48 and Mesh2: 200x90x56 nodes in axial, radial and azimuthal directions, respectively.

The LES quality factor is satisfied by both meshes. The quality of the finer mesh is obviously better. From the velocity profiles for the meshes at various downstream locations, shown in Fig. B.2, it can be safely said that both he meshes are good for LES. The coarser mesh with 0.75 million cells is used for the simulations of this test case.

B.2 Sensitivity of auto-ignition prediction to the progress variable definition

The progress variable is not a physical quantity, but a helping variable that describes the progress of the reactions. The definition of the progress variable is important for the success of the combustion model. $CO+CO_2$ is generally

used as a progress variable [28, 43] for hydrocarbons. The curves in Fig. 2.8 show that a significant amount of CH_2O is produced before CO in the initial stages of a reactor evolution. Figure B.3 displays the sensitivity of the LES combustion model to the progress variable definition will be investigated. The OH mass fraction contour for three different definitions of the progress variable are shown at the cross-section of the experiment for DJHC-I case at Re=4100 from table 5.3.

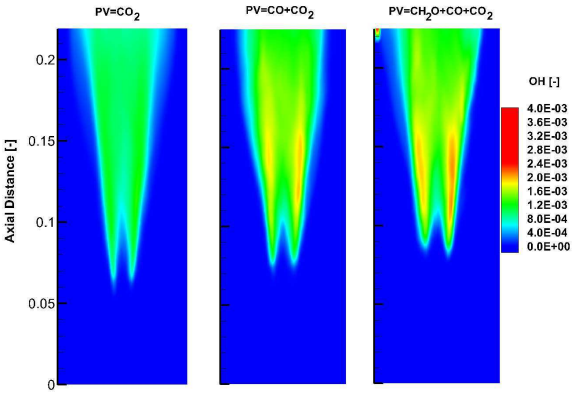

Figure B.3: Time averaged OH mass fraction distribution for three different progress variables.

The difference in the lift-off heights predicted by the model with different progress variable definition can be seen clearly. The lift-off length of about 85 mm can be seen with the inclusion of CH_2O in the progress variable definition, which is close to the experimental value. The error in the lift-off height using CO_2 as a progress variable is significant. There is also a considerable difference between the progress variable with and without CH_2O. The error is expected to increase with still lower temperatures or oxygen content. The reason for this, as described earlier, is due to the reduced pre-ignition chemical reactions that lead to a considerable difference in the CH_2O and CO evolution (refer fig. B.3). Therefore, for hydrocarbon combustion, a composite progress variable consisting of CH_2O+CO+CO_2 is recommended.